DEPARTMENT OF COMMERCE
SINCLAIR WEEKS, Secretary

WEATHER BUREAU
F. W. REICHELDERFER, Chief

MONTHLY WEATHER REVIEW

JAMES E. CASKEY, JR., Editor

Volume 86
Number 4

APRIL 1958

Closed June 15, 1958
Issued July 15, 1958

A NOTE ON THE GAMMA DISTRIBUTION

H. C. S. THOM

Office of Climatology, U. S. Weather Bureau, Washington, D. C.

[Manuscript received March 7, 1958; revised April 15, 1958]

ABSTRACT

The general properties of the gamma distribution, which has several applications in meteorology, are discussed. A short review of the general properties of good statistical estimators is given. This is applied to the gamma distribution to show that the maximum likelihood estimators are jointly sufficient. A new, simple approximation of the likelihood solutions is given, and the efficiency of the fitting procedure is computed.

1. INTRODUCTION

In 1947, the writer [1] developed approximate solutions of the maximum likelihood (M.L.) equations for the incomplete gamma distribution commonly called the gamma distribution. The purpose of this note is to give the development of the estimates which have since been widely employed. The first application of the methods was to rainfall data [2]; later it was found that the gamma distribution has wide application in meteorology to problems where the climatological variable has a physical lower bound of zero but no nonstatistical upper bound.

The gamma distribution is a special case of the Pearson Type III distribution where the locus parameter is zero. Fisher [3] first gave the M. L. equations for this distribution; however, as is often the case with M. L. estimation the equations are not conveniently solved. Our approximations make the estimation of the distribution parameters hardly more difficult than the estimation of the mean and standard deviation of the normal distribution.

2. THE GAMMA DISTRIBUTION AND PROPERTIES

The gamma distribution is a 2-parameter frequency distribution given by the equation

$$f(x)=\frac{1}{\beta^{\gamma}\Gamma(\gamma)}x^{\gamma-1}e^{-x/\beta};\quad \begin{matrix}\beta>0\\ \gamma>0\end{matrix}. \tag{1}$$

Here x is the random variable, β scales x and is therefore the scale parameter, γ is the shape parameter, Γ is the usual gamma function, and $f(x)=0$ for $x<0$. It will be noted that the distribution has a zero lower bound and is unlimited on the right. It is positively skewed, the amount of skew depending inversely on the shape factor γ. The mode of the distribution is at $\beta\ (\gamma-1)$ if $\gamma>1$ and at zero if $0<\gamma\leq 1$. In the latter case, the distribution is J-shaped. For $\gamma=1$ the distribution is exponential with ordinate $1/\beta$ at $x=0$; for $\gamma<1$ the ordinate at $x=0$ is infinite. The gamma distribution is closely related to the chi square distribution, for $\chi^2/2$ is a gamma variate with $\gamma=\frac{1}{2}n$ and $\beta=1$.

The moments about zero of the gamma distribution are given by the relation

$$\mu_r'=\beta^r\gamma(\gamma+1)\ \ldots\ (\gamma+r-1), \tag{2}$$

from which it follows immediately that the mean is

$$\mu_1'=\beta\gamma. \tag{3}$$

From the moment relationships the second, third, and fourth moments about the mean are easily found to be

$$\mu_2=\sigma^2=\beta^2\gamma \tag{4}$$

$$\mu_3=2\ \beta^3\gamma \tag{5}$$

$$\mu_4=3\beta^4\gamma(\gamma+2). \tag{6}$$

Since the skewness statistic is $\sqrt{b_1}=\mu_3/\sigma^3$, we have from (4) and (5) that

$$\sqrt{b_1}=\frac{2}{\sqrt{\gamma}}. \tag{7}$$

Hence, the skewness goes to zero with increasing γ showing that the gamma distribution becomes symmetrical for large γ; in fact, it may be shown that the distribution approaches normality slowly as γ increases. For $\gamma>100$ it is approximately normal for climatological applications.

The main interest in applications to climatological analysis is not in equation (1) but in its integral which gives probability. This cannot be found except as an expansion in series or continued fractions. The integral from 0 to any value of the variate has been tabulated by Pearson [4], and this of course gives the probability that any value of the variate is less than the tabulated value.

Pearson used the moments for fitting the Type III frequency curve, so the arguments of his table are u and p. The variate u is scaled in terms of the standard deviation instead of β. Hence, $u=x/(\beta\sqrt{\gamma})$ or $x/\beta=u\sqrt{\gamma}$ in our notation. Also, his $p=\gamma-1$. To use Pearson's table we find $\gamma=p+1$ and multiply the u value by $\sqrt{\gamma}$. For certain purposes it may be more convenient to convert the x's to u values.

3. STATISTICAL ESTIMATORS

The main statistical problem in the application of the gamma distribution to climatological data is the estimation of the parameters β and γ from a sample record. The estimation problem is one of three basic problems in statistical analysis, and it will serve our present purpose to discuss the general problem briefly.

It has long been known that there are many ways to estimate the parameters in a statistical equation from a sample of data. Two of the more common methods are least squares and moments. It was found by Fisher [3] that the various methods of estimation do not give equally good results in the sense that some estimates or statistics are more variable than others. Clearly, the best estimates are those which have the smallest variability. For example, in samples of 10 from a normal population the mean or expected value could be estimated by averaging the smallest and the largest value, or it could be estimated by averaging all the observations. Obviously, the latter statistic using all the observations should be better than that using only two of the observations. In fact, it has been shown that the variability from sample to sample for sample size 10 as measured by the variance is twice as large when only the extreme observations are averaged. The median, which is also an estimate of mean, has a variance about one-third greater than the mean for sample size 10. From this it may be inferred that if we use the mean range as an estimate, we in effect discard half of our data; if we use the median we discard one-third of it. In climatology, where data are scarce, the use of inefficient estimators is clearly to be avoided.

Fisher [3] made a remarkable contribution to statistical analysis by developing a method of estimation originally due to Gauss which he called the method of maximum likelihood (M. L.). This method consists of maximizing what he calls the likelihood or the product of the frequency functions of a sample. If $f(x;\beta,\gamma)$ is any frequency function, the likelihood is defined to be

$$M=\prod_{i=1}^{n} f(x_i;\beta,\gamma). \tag{8}$$

where x_i is the ith value in a sample of n. To maximize this it is simplest to take logarithms before differentiating and setting to zero. This gives

$$L=\sum_{i=1}^{n}\log f(x_i;\beta,\gamma). \tag{9}$$

Differentiating partially with respect to β and γ gives the M. L. differential equations

$$\left.\begin{aligned}\frac{\partial L}{\partial\beta}&=0,\\ \frac{\partial L}{\partial\gamma}&=0,\end{aligned}\right\} \tag{10}$$

Solving these gives the M. L. estimates commonly written as $\hat{\beta}$ and $\hat{\gamma}$. The M. L. estimates have certain remarkable advantages not always possessed by other estimates which will now be discussed.

In order to assess the quality of estimators in general, Fisher defined three desirable properties of statistics; viz., consistency, efficiency, and sufficiency. These may be defined as follows:

1. If an estimator or statistic is consistent it converges in probability to its population or parameter value. This may be expressed in symbols by

$$P(|T_n-\theta|<\epsilon)>1-\eta;\ n>N. \tag{11}$$

T_n is an estimate of the parameter θ based on sample size n, ϵ and η are arbitrarily small quantities, and N is any integer. This means that $T_n=\theta$ when T_n is calculated from the whole population.

2. A consistent estimate T_1 is said to be more efficient than another consistent estimate T_2 if $v(T_1)<v(T_2)$; i. e., if the variance of T_1 is less than the variance T_2. An estimate is said to be efficient if it has the smallest variance of a class of consistent estimates. The efficiency of an estimate is defined as $v(\hat{T})/v(T)$ where $\hat{T}$ is M. L. estimate.

3. An estimate T is said to be sufficient if it exhausts all possible information on θ from a sample of any size. If T_1 and T_2 are two different estimates of θ not functionally related, an estimate T_1 of θ is sufficient if the joint distribution of T_1 and T_2 has the form

$$f=f_1(T_1, \theta)f_2(T_2|T_1) \tag{12}$$

where f_1 is the frequency distribution of T_1 and f_2 is the distribution of T_2 given a sample value of T_1. Once T_1 is known the probability of any range of values for T_2 is the same for all θ; hence, T_2 cannot give any information on θ which is not already available from T_1. Sufficiency is the most desirable property of an estimate, and such estimates are said to be optimum.

The superiority of M. L. estimates was demonstrated by Fisher and others when they proved that M. L. estimates are consistent and efficient and if a sufficient estimate exists, it will be given by the M. L. method.

4. MAXIMUM LIKELIHOOD ESTIMATES

Applying (9) to the gamma distribution equation (1) gives

$$L=-n\gamma \log \beta - n\log\Gamma(\gamma)+(\gamma-1)\Sigma \log x-\frac{1}{\beta}\Sigma x \tag{13}$$

where the summation is over the n sample values. Differentiating as indicated in equations (10) we find the M. L. equations

$$\bar{x}/\hat{\beta}-\hat{\gamma}=0 \tag{14}$$

$$\log \hat{\beta}+\frac{\partial}{\partial \hat{\gamma}} \log \Gamma(\hat{\gamma})-\frac{1}{n}\Sigma \log x=0. \tag{15}$$

Since $\frac{\partial}{\partial \hat{\gamma}} \log \Gamma(\hat{\gamma})$ is the digamma function, $\psi(\hat{\gamma})$, we may write (15) in the simplified form

$$\log \hat{\beta}+\psi(\hat{\gamma})-\frac{1}{n}\Sigma \log x=0. \tag{16}$$

Taking logarithms of (14) and substituting for $\log \hat{\beta}$ in (16) gives

$$\log \hat{\gamma}-\psi(\hat{\gamma})=\log \bar{x}-\frac{1}{n}\Sigma \log x. \tag{17}$$

This equation is implicit in $\hat{\gamma}$ but may be solved with some difficulty using the Davis [5] tables of the ψ-functions. Masuyama and Kuroiwa [6] prepared tables of $\log \hat{\gamma}-\psi(\hat{\gamma})$ from tables of logarithms and tables of the digamma functions.

We developed the application of the gamma distribution to precipitation before Masuyama and Kuroiwa's tables were available although, of course, we had also followed the equivalent procedure of using the Davis tables. To simplify the technique of fitting we developed an approximation to $\log \hat{\gamma}-\psi(\hat{\gamma})$ as follows: Nörlund [7] shows that

$$\psi(\gamma)=\log \gamma-1/(2\gamma)-\sum_{k=1}^{m}(-1)^{k-1}B_k/(2k\gamma^{2k})+R_m \tag{18}$$

is an asymptotic expansion in which B_k are the Bernoulli numbers, $B_1=1/6$, $B_2=1/30$, etc., and R_m is the remainder after m terms. For $\gamma \geq 1$ we may write the inequality

$$|R_m|<\frac{B_{m+1}}{(2m+2)\gamma^{2m+2}}. \tag{19}$$

For only $m=1$ and $\gamma=1$, $|R_m|<0.00833$ which is less than 1.5 percent of the table value $\psi(1)=-0.57722$ given by Davis [5]. The approximation, of course, increases in accuracy with γ. At $\gamma=2$ it is within 0.1 percent of table value. We are not, however, interested in approximating ψ but in approximating γ.

From (18) for $m=1$ we find

$$\psi(\gamma)=\log \gamma-1/(2\gamma)-1/(12\gamma^2). \tag{20}$$

Substituting in (17) we find

$$12\left(\log \bar{x}-\frac{1}{n}\Sigma \log x\right)\hat{\gamma}^2-6\hat{\gamma}-1=0.$$

Simplifying by letting $A=\log \bar{x}-\frac{1}{n}\Sigma \log x$ we have

$$12A\hat{\gamma}^2-6\hat{\gamma}-1=0, \tag{21}$$

which is a quadratic equation whose only pertinent root is

$$\hat{\gamma}=\frac{1+\sqrt{1+4A/3}}{4A}. \tag{22}$$

This together with equation (14) gives the M. L. estimates for the gamma distribution. It is only necessary to sum the natural logarithms of x and take the natural logarithm of the mean of x to provide the basic data for equations (14) and (21). Common logarithms may, of course, also be used by multiplying by the proper conversion factor.

The error in $\hat{\gamma}$ resulting from using only one term of equation (18) is not readily expressed in mathematical form; hence, we have computed the following table for correcting the estimate obtained from equation (22).

$\hat{\gamma}$	$\Delta\hat{\gamma}$	$\hat{\gamma}$	$\Delta\hat{\gamma}$	$\hat{\gamma}$	$\Delta\hat{\gamma}$	$\hat{\gamma}$	$\Delta\hat{\gamma}$
0.2	0.034	0.8	0.012	1.4	0.006	2.2	0.003
0.3	.029	0.9	.011	1.5	.005	2.3	.002
0.4	.025	1.0	.009	1.6	.005	3.1	.002
0.5	.021	1.1	.008	1.7	.004	3.2	.001
0.6	.017	1.2	.007	1.8	.004	5.5	.001
0.7	.014	1.3	.006	1.9	.003	5.6	.000

The value of $\Delta\hat{\gamma}$ is to be subtracted from the value of $\hat{\gamma}$ obtained from equation (22).

5. SUFFICIENCY OF THE ESTIMATES

Koopman [8] has given the necessary and sufficient conditions for a set of estimators to be jointly sufficient in the form

$$\log f=\sum_{k=1}^{p} A_k X_k+B+Y. \tag{23}$$

Here A_k and B are functions of the parameters of the distribution (β and γ in this case) and X_k and Y are functions of x. Taking logarithms of (1) we have

$$\log f=-x/\beta+(\gamma-1)\log x-\log \Gamma(\gamma)-\gamma \log \beta. \tag{24}$$

This is of the form (23) where $A_1=-1/\beta$, $A_2=\gamma-1$, $X_1=x$, $X_2=\log x$, $Y=0$, and $B=-(\log\Gamma(\gamma)+\gamma \log \beta)$. This shows that $\hat{\beta}$ and $\hat{\gamma}$ are jointly sufficient estimates of β and γ. Thus, no other estimates of β and γ can give more information on these parameters, and $\hat{\beta}$ and $\hat{\gamma}$ are optimum statistics and have, indeed, a highly desirable property. Fisher [3] has also shown that $\bar{x}$ is a 100 percent efficient estimate of the population mean. This is important in many applications of the gamma distribution.

6. VARIANCE OF THE ESTIMATORS

Fisher [3] has shown how to obtain the large sample variance of M. L. estimates in general and has demonstrated that M. L. estimates are normally distributed in large samples. Using matrix methods we define

$$\sigma^{ij}=-E\left[\frac{\partial^2}{\partial\theta_i\partial\theta_j}\log f\right], \tag{25}$$

where σ^{ij} is the ijth element of a matrix, the θ's are the parameters, and E is the expected value operator. If further we define the matrix equation

$$[\sigma_{ij}]=[\sigma^{ij}]^{-1} \tag{26}$$

the variance-covariance matrix is

$$C=\left[\frac{1}{n}\sigma_{ij}\right]. \tag{27}$$

Since θ takes on two values β and γ, we may write the second partial derivatives as L_{11}, L_{22}, and L_{12} where the subscripts refer to the parameters. Differentiating equation (24) partially with respect to β and γ we find

$$L_{11}=\frac{\gamma}{\beta^2}-\frac{2x}{\beta^3}, \tag{28}$$

$$L_{22}=-\psi'(\gamma), \tag{29}$$

$$L_{12}=L_{21}=-\frac{1}{\beta}, \tag{30}$$

where ψ' is the trigamma function.

We have seen above in equation (3) that $E(x)=\beta\gamma$; hence

$$\sigma^{11}=\frac{\gamma}{\beta^2}. \tag{31}$$

Since (29) and (30) do not involve the random variable x, we have simply

$$\sigma^{22}=\psi'(\gamma) \tag{32}$$

$$\sigma^{12}=\frac{1}{\beta}=\sigma^{21}. \tag{33}$$

We now may write the matrix

$$[\sigma^{ij}]=\begin{bmatrix}\frac{\gamma}{\beta^2} & \frac{1}{\beta}\\ \frac{1}{\beta} & \psi'(\gamma)\end{bmatrix}. \tag{34}$$

The inverse of this after multiplying each term by $1/n$ as required by (27) is

$$\left[\frac{1}{n}\sigma_{ij}\right]=\begin{bmatrix}\frac{\beta^2\psi'(\gamma)}{n(\gamma\psi'(\gamma)-1)} & \frac{-\beta}{n(\gamma\psi'(\gamma)-1)}\\ \frac{-\beta}{n(\gamma\psi'(\gamma)-1)} & \frac{\gamma}{n(\gamma\psi'(\gamma)-1)}\end{bmatrix} \tag{35}$$

which is the variance-covariance matrix. From this it immediately follows that the variances and covariance are

$$v(\hat{\beta})=\frac{\beta^2\psi'(\gamma)}{n(\gamma\psi'(\gamma)-1)} \tag{36}$$

$$v(\hat{\gamma})=\frac{\gamma}{n(\gamma\psi'(\gamma)-1)} \tag{37}$$

$$\text{cov}\ (\hat{\beta},\hat{\gamma})=\frac{-\beta}{n(\gamma\psi'(\gamma)-1)} \tag{38}$$

Since $\text{cov}\ (\hat{\beta},\hat{\gamma})=r\sqrt{v(\hat{\beta})v(\hat{\gamma})}$, we easily find the correlation r between $\hat{\beta}$ and $\hat{\gamma}$ to be

$$r=\frac{-1}{\sqrt{\gamma\psi'(\gamma)}}. \tag{39}$$

This is negative as it is seen it must be by equation (14), for if the mean is fixed, $\hat{\beta}$ and $\hat{\gamma}$ must vary inversely. The large sample variances were also given by Masuyama and Kuroiwa.

7. EFFICIENCY OF THE METHOD OF MOMENTS

Although the method of moments is widely used in fitting frequency distributions in climatology, it is the exceptional case when this method proves to be fully efficient in estimating climatological parameters. The most prominent exception is, of course, the normal distribution where the moment estimates are jointly sufficient and so are identical with the M. L. estimates. As we have seen the M. L. method of estimation is always superior to moments when they give different results.

It is of interest then to compute the efficiency of the moment estimates for the gamma distribution to evaluate

the superiority of M. L. estimates. We have seen that the efficiency of a moment estimate is the ratio of the variance of the M. L. estimate to that of the moment estimate. The M. L. variances are given by equations (36) and (37) and the variances of the moment estimates may be worked out as follows:

$$\beta_m=s^2/\bar{x} \tag{40}$$

$$\gamma_m=\bar{x}^2/s^2. \tag{41}$$

The problem now is to find the variance of these two estimates. This may be done using Taylor's formula. Taking the total differential of (40) with respect to $\bar{x}$ and s^2 gives

$$\Delta\beta_m=\frac{1}{\bar{x}}\Delta s^2-\frac{s^2}{\bar{x}^2}\Delta\bar{x} \tag{42}$$

in which the coefficients of the delta increments are the partial derivatives and the increments of higher order are ignored. Squaring and taking expected values we find

$$E(\Delta\beta_m)^2=\frac{1}{\bar{x}^2}E(\Delta s^2)^2+\frac{s^4}{\bar{x}^4}E(\Delta\bar{x})^2-\frac{2s^2}{\bar{x}^3}E(\Delta\bar{x}\Delta s^2). \tag{43}$$

Since the expected value of the square of an error is the variance, and the expected value of an error product is the covariance, we have

$$v(\beta_m)=\frac{1}{\bar{x}^2}v(s^2)+\frac{s^4}{\bar{x}^4}v(\bar{x})-\frac{2s^2}{\bar{x}^3}\operatorname{cov}(\bar{x},s^2). \tag{44}$$

Now the variances of s^2, $\bar{x}$, and cov $(\bar{x}, s^2)$ are known in large samples to be [9]

$$v(s^2)=(\mu_4-\mu_2^2)/n \tag{45}$$

$$v(\bar{x})=\mu_2/n \tag{46}$$

$$\operatorname{cov}(\bar{x}, s^2)=(n-1)\ \mu_3/n^2. \tag{47}$$

Substituting values of the moments of the gamma distribution given by equations (3), (4), (5), and (6) for the moments in (45), (46), and (47) and then for the sample moments, variances, and covariance in (44) we find after some simplification

$$v(\beta_m)=\frac{\beta^2}{n\gamma}[2\gamma+7-4(n-1)/n] \tag{48}$$

which for large n becomes

$$v(\beta_m)=\frac{\beta^2}{n\gamma}(2\gamma+3). \tag{49}$$

Performing similar operations on equation (41) we find for large samples

$$v(\gamma_m)=\frac{2\gamma}{n}(\gamma+1). \tag{50}$$

If we assume $\beta=1$, a common value for climatological data, we find for $\gamma=1$

$$v(\beta_m)=5/n;\ v(\gamma_m)=4/n. \tag{51}$$

and for $\gamma=10$,

$$v(\beta_m)=2.3/n;\ v(\gamma_m)=220/n. \tag{52}$$

Using the Davis tables [5] we find the M. L. variances from (36) and (37) for $\gamma=1$

$$v(\hat{\beta})=2.55/n;\ v(\hat{\gamma})=1.55/n \tag{53}$$

and for $\gamma=10$,

$$v(\hat{\beta})=2.04/n;\ v(\hat{\gamma})=193.6/n. \tag{54}$$

According to our definition of efficiency we must take the ratio of the variance of the M. L. estimate to the moment estimate. This gives from equation (51) and (53) for $\gamma=1$,

Eff $(\beta_m)=51$ percent

Eff $(\gamma_m)=39$ percent

and for $\gamma=10$

Eff $(\beta_m)=89$ percent

Eff $(\gamma_m)=88$ percent

We see that for $\gamma<10$ the method of moments produces unacceptable estimates for both β and γ. For γ near 1 the moment estimates use only 50 percent of the information in the sample for estimating β and only 40 percent for γ. Thus, for β the M. L. estimator would do as well with half the length of record as the moment estimate and for γ with two-fifths the record length. Hence, use of the moment estimates in effect results in discarding half the record in estimating β and three-fifths of the record in estimating γ. For $\gamma=10$ the efficiencies of β_m and γ_m both approach satisfactory values. In view of the difficulty in obtaining homogeneous climatological data series, it seems at least a questionable procedure to employ inefficient estimators which do not make the best use of the available climatological samples.

REFERENCES

1. H. C. S. Thom, "A Note on the Gamma Distribution" Statistical Laboratory, Iowa State College, 1947 (Manuscript).
2. G. L. Barger and H. C. S. Thom, "Evaluation of Drought Hazard," *Agronomy Journal* vol. 41, No. 11, Nov. 1949, pp. 519–526
3. R. A. Fisher, "On the Mathematical Foundations of Theoretical Statistics," *Philosophical Transactions Royal Society*, Series A, vol. 222, 1941, pp. 309–368.
4. K. Pearson et al., *Tables of the Incomplete Γ-function*, Cambridge University Press. Reissue 1951.

5. H. T. Davis, *Tables of Higher Mathematical Functions*, vol. I and II, Principia Press, Bloomington, 1933.
6. M. Masuyama and Y. Kuroiwa, "Table of the Likelihood Solutions of Gamma Distribution and its Medical Applications," *Statistical Application Research*, vol. 1, No. 1, 1951.
7. N. E. Nörlund, *Vorlesungen über Differenzenrechnung*, Springer, Berlin, 1924, p. 101, 106.
8. B. O. Koopman, "Distributions Admitting a Sufficient Statistic", *Transactions, American Mathematical Society*, vol. 39, 1936, p. 399.
9. H. Cramér, *Mathematical Methods of Statistics*, Princeton University Press, 1946, p. 348.

A GRAPHICAL TECHNIQUE FOR DETERMINING EVAPOTRANSPIRATION BY THE THORNTHWAITE METHOD

WAYNE C. PALMER
U. S. Weather Bureau, Washington, D. C.

and

A. VAUGHN HAVENS
Department of Meteorology, Rutgers University, New Brunswick, N. J.

[Manuscript received December 4, 1957; revised March 6, 1958]

ABSTRACT

Generalized diagrams for the determination of evapotranspiration and potential evapotranspiration in accordance with the empirical equations of Thornthwaite are presented.

1. INTRODUCTION

The loss of water from the earth to the atmosphere by transpiration from vegetation and by direct evaporation constitutes an important part of the water balance problem. However, direct measurement of these factors has proved to be extremely difficult, and this inherent difficulty has led to the development of a number of formulas designed to estimate water loss directly from meteorological data.

It is not the purpose of this article to review or evaluate the various methods which have been developed, but it would appear that some mention of the various approaches to the problem is in order. A detailed and excellent review has been published by van Wijk and de Vries [1]; and an enlightening analysis of the problems involved was presented by Penman [2].

The list of references following this article includes some of the principal publications devoted to the problem of estimating soil moisture loss directly from meteorological data and will suffice to indicate the nature of the various approaches used. They fall into three groups: (1) Those involving the flux of water vapor; (2) those utilizing the heat balance of the evaporating or transpiring surface; and (3) those which use an empirically determined relationship between evapotranspiration and one or more of the meteorological factors involved.

None of these methods provides a completely adequate solution to the problems of evaporimetry because none is free from assumptions, arbitrary constants, or technical difficulties of observation and measurement. In spite of the shortcomings, a number of workers have surmised that these methods enable the climatologist to estimate *total* evapotranspiration from a sizable field more accurately than a soil scientist can measure it.

The Thornthwaite method [3] was developed from rainfall and runoff data for several drainage basins. The result is basically an empirical relationship between potential evapotranspiration and mean air temperature. In spite of the inherent simplicity and obvious limitations of the method, it does surprisingly well. It is not necessarily the most accurate method, nor does it have the soundest theoretical basis. On the contrary, these distinctions probably belong to one of the vapor flux or heat balance methods. Among the more obvious shortcomings of Thornthwaite's empirical relationship is the inherent assumption that a high correlation exists between mean temperature and some of the other pertinent parameters such as radiation, atmospheric moisture, and wind. While such limitations may be relatively unimportant under certain circumstances, they are at times of the utmost importance; and Thornthwaite and Mather [4], recognizing that solar radiation and atmospheric turbulence are the important factors in natural evaporation, have stated that the problem of developing a formula for potential evapotranspiration remains unsolved.

Although ease of application is not a suitable criterion of adequacy, it is often a primary consideration for use. The vapor flux and heat balance methods require meteorological data which are either not observed or are observed only at a few widely separated points. On the other hand, Thornthwaite's empirical formula can be used for any location at which daily maximum and minimum temperatures are recorded. It is this simple universal applicability rather than any claim to outstanding accuracy which has led to the widespread use of this method.

It is not the purpose of this paper to make a case either for or against this or any other method. Rather, recognizing the widespread interest in computing and testing

results of Thornthwaite's method, it is the purpose to present a graphical solution which will make such computations easier.

2. GRAPHICAL SOLUTION OF THORNTHWAITE METHOD

Thornthwaite's basic formula in the form for computing monthly potential evapotranspiration is

$$e=1.6\ (10T/I)^a$$

where e=monthly potential evapotranspiration (cm.)
T=monthly mean temperature (° C.)
I=a heat index which is a constant for a given location and is the sum of 12 monthly index values i, where i is a function of the monthly normal temperatures. (See table 1.)
a=an empirically determined exponent which is a function of I, $a=6.75\times10^{-7}\ I^3-7.71\times10^{-5}I^2+1.79\times10^{-2}\ I+0.49$.

Arithmetic solution of the equation becomes an extremely laborious procedure primarily because of the complexity of the exponent a. Therefore, extensive use of the method for many locations over a long period of time requires the use of a tabular or graphical solution to the equation. Thornthwaite and Mather [4] have published such tables for only one location, Seabrook, N. J. Their publication includes a diagram for the graphical determination of unadjusted potential evapotranspiration in metric units. However, the day-length correction, depending on date and latitude, appears in a separate table. It was thought that a generalized and complete graphical solution in English units would be useful. Such a solution is presented here. It includes the adjustment for day length and provides a means whereby tables or graphs for use at any particular place can be readily prepared. In addition diagrams are provided for the conversion of weekly rates to daily rates of potential evapotranspiration and for a correction due to soil dryness.

Weekly rates of unadjusted potential evapotranspiration may be obtained from figure 1, using only the mean temperature for the period and the heat index (I) for the location concerned. The graph also provides the adjustment for day-length required to convert unadjusted potential evapotranspiration to adjusted potential evapotranspiration.

Figure 2 is a simple graph for converting weekly rates of adjusted potential evapotranspiration (PE) to daily rates. For certain purposes, daily rates may be desirable, although some evidence has been obtained which indicates that weekly rates of PE correlate better with measured evapotranspiration than do daily rates. A monthly rate can of course be obtained by simply multiplying the daily rate by the number of days in the month.

There is considerable evidence that during long dry periods the rate of evapotranspiration decreases as the soil dries. Thornthwaite and Mather [4] suggested one method of correcting for this effect. It is shown graphically in figure 3.

Listed below is the step-by-step procedure to be followed in the use of these graphs.

A. To obtain potential evapotranspiration, PE:

1. Using monthly normal or long-term mean temperatures (F.°) for the station or area concerned, obtain from table 1 the monthly heat index, i, corresponding to the normal temperature for each of the 12 months.
2. Add these 12 i-values to obtain I, the heat index.
3. Enter figure 1 at the bottom with the mean temperature (F.°) for the period concerned. (The length of the period is immaterial at this point; it may be of any length from 1 day to 1 month.)
4. Follow vertically up the appropriate mean temperature line until it intersects the horizontal heat index line equal to the heat index determined in step A-2 above. At this intersection determine unadjusted PE (inches) from the slanting lines. This is the potential moisture loss for a 7-day period, each day having a length of 12 hours.
5. Enter the bottom (or top) of the upper-right portion of figure 1 with the unadjusted PE value found in step A-4. This determines the appropriate vertical line to follow in this portion of the figure.
6. Enter the upper-left portion of figure 1 according to the north latitude of the station or area under consideration and proceed vertically downward to the intersection with the "month" line corresponding to the month under consideration. This intersection determines the appropriate horizontal line to follow into the upper-right portion of figure 1. (The climatological week numbers and the day-length correction are discussed in Appendix 1.)
7. At the intersection of the vertical line determined in step A-5 and the horizontal line determined in step A-6 read the final PE in inches per week from the curved lines.
8. If daily values are required, the daily mean temperature would be used in step A-3. The adjusted weekly PE rate obtained from step A-7 would then be converted to daily PE by dividing by 7 or by using figure 2.
9. If monthly PE is desired, monthly mean temperature would be used in step A-3 proceeding through step A-8 to obtain the mean daily rate for the month. This may be multiplied by the number of days in the month to obtain total PE for the month.

B. To correct PE to account for soil moisture depletion:

1. From actual measurement or from water balance tabulations, obtain the soil moisture content. This should be expressed as a percentage of the

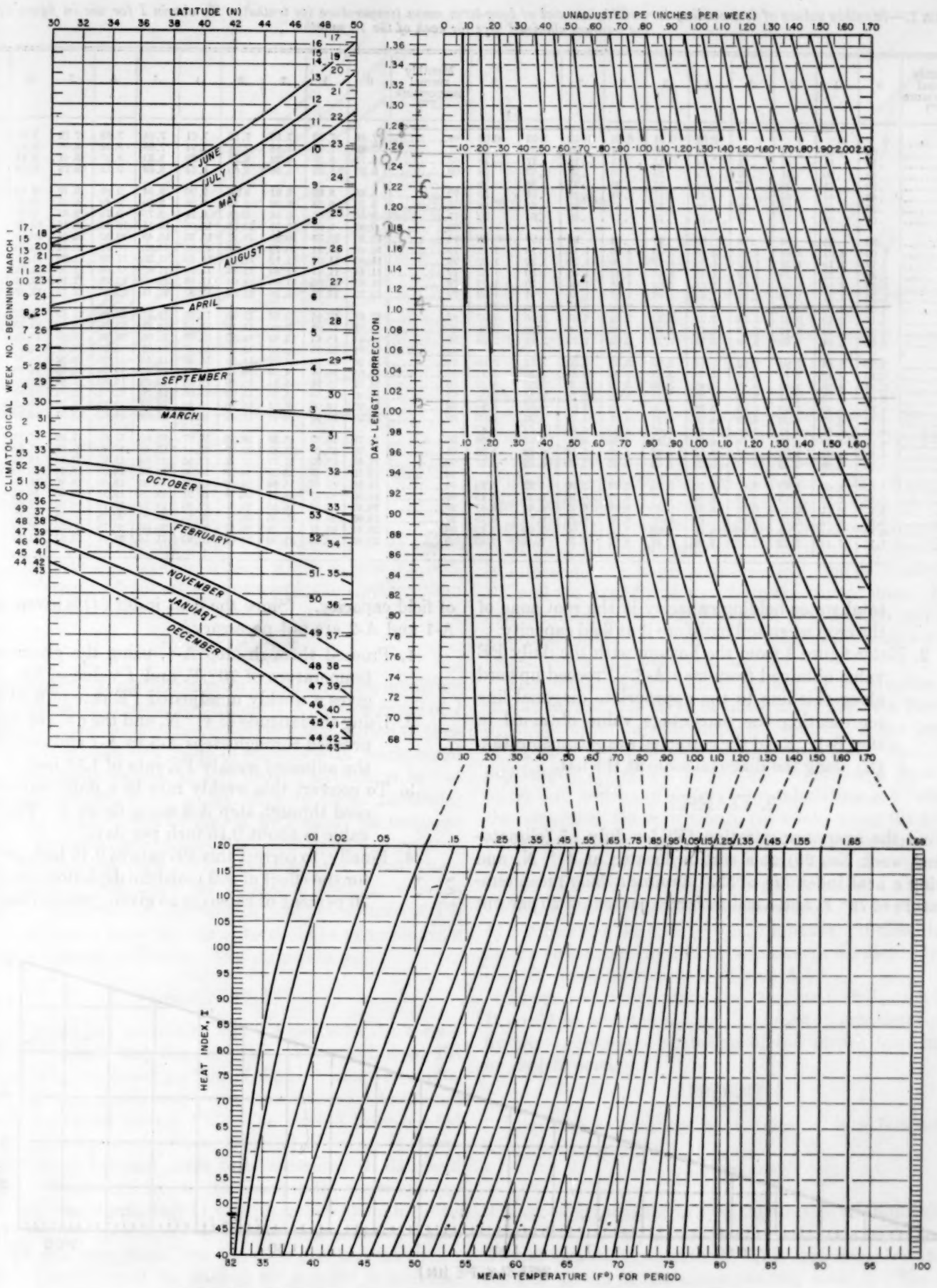

FIGURE 1.—Nomogram for computation of potential evapotranspiration (PE).

TABLE 1.—*Monthly values of i, according to monthly normal or long-term mean temperature (to tenths). To obtain I for use in figure 1, add the i-values obtained here for each of the 12 months.*

Monthly normal temperature (F°)	0	.1	.2	.3	.4	.5	.6	.7	.8	.9
32	0	0	0	0	0.01	0.01	0.01	0.02	0.02	0.03
33	0.03	0.04	0.04	0.05	.06	.06	.07	.08	.09	.09
34	.10	.11	.12	.13	.14	.15	.15	.16	.17	.18
35	.19	.20	.21	.22	.23	.24	.25	.26	.27	.28
36	.29	.31	.32	.33	.34	.35	.36	.37	.38	.39
37	.42	.43	.44	.45	.46	.47	.48	.49	.51	.53
38	.55	.56	.57	.58	.59	.61	.62	.63	.66	.68
39	.69	.70	.71	.72	.74	.75	.77	.80	.81	.82
40	.83	.85	.86	.88	.89	.91	.94	.95	.97	.98
41	1.00	1.01	1.03	1.04	1.06	1.09	1.10	1.12	1.14	1.16
42	1.17	1.19	1.20	1.22	1.25	1.27	1.29	1.30	1.32	1.33
43	1.35	1.37	1.39	1.42	1.43	1.45	1.47	1.49	1.50	1.52
44	1.54	1.56	1.59	1.61	1.63	1.64	1.66	1.68	1.70	1.72
45	1.74	1.77	1.79	1.81	1.83	1.85	1.87	1.89	1.91	1.93
46	1.96	1.98	2.00	2.02	2.04	2.06	2.08	2.10	2.12	2.15
47	2.17	2.19	2.21	2.23	2.25	2.27	2.29	2.31	2.35	2.37
48	2.39	2.41	2.44	2.46	2.48	2.50	2.52	2.56	2.58	2.60
49	2.62	2.64	2.66	2.69	2.71	2.73	2.76	2.79	2.81	2.83
50	2.86	2.88	2.90	2.92	2.94	2.99	3.01	3.03	3.05	3.08
51	3.10	3.12	3.14	3.17	3.20	3.23	3.25	3.27	3.30	3.32
52	3.34	3.36	3.39	3.42	3.45	3.48	3.50	3.53	3.55	3.58
53	3.60	3.62	3.67	3.69	3.72	3.74	3.76	3.78	3.81	3.83
54	3.86	3.90	3.93	3.96	3.98	4.00	4.02	4.05	4.07	4.10
55	4.14	4.17	4.20	4.22	4.25	4.27	4.30	4.32	4.35	4.39
56	4.42	4.45	4.47	4.50	4.52	4.55	4.57	4.60	4.64	4.67
57	4.70	4.72	4.75	4.79	4.81	4.83	4.86	4.90	4.93	4.96
58	4.98	5.01	5.04	5.07	5.09	5.12	5.16	5.19	5.22	5.25
59	5.28	5.30	5.33	5.35	5.39	5.43	5.46	5.49	5.52	5.55
60	5.57	5.60	5.63	5.66	5.70	5.73	5.76	5.79	5.82	5.84
61	5.87	5.90	5.93	5.98	6.01	6.04	6.07	6.10	6.12	6.15
62	6.17	6.21	6.26	6.29	6.32	6.35	6.38	6.41	6.44	6.47
63	6.50	6.54	6.57	6.60	6.63	6.66	6.69	6.72	6.75	6.78
64	6.84	6.81	6.90	6.92	6.95	6.98	7.01	7.04	7.08	7.12
65	7.15	7.19	7.22	7.25	7.28	7.31	7.34	7.38	7.42	7.45
66	7.49	7.52	7.55	7.58	7.61	7.64	7.68	7.72	7.75	7.79
67	7.82	7.85	7.88	7.91	7.94	7.98	8.02	8.06	8.10	8.13
68	8.16	8.19	8.22	8.25	8.29	8.33	8.37	8.41	8.44	8.47
69	8.50	8.53	8.56	8.60	8.64	8.68	8.72	8.75	8.78	8.81
70	8.85	8.88	8.91	8.96	9.00	9.04	9.07	9.10	9.13	9.17
71	9.20	9.23	9.28	9.32	9.36	9.39	9.42	9.45	9.49	9.52
72	9.56	9.60	9.64	9.68	9.71	9.75	9.78	9.82	9.85	9.88
73	9.93	9.97	10.01	10.04	10.08	10.11	10.15	10.18	10.22	10.26
74	10.30	10.35	10.38	10.41	10.44	10.48	10.52	10.56	10.60	10.64
75	10.68	10.71	10.75	10.78	10.82	10.85	10.89	10.94	10.98	11.02
76	11.05	11.09	11.12	11.16	11.19	11.23	11.28	11.32	11.37	11.40
77	11.44	11.47	11.50	11.54	11.58	11.62	11.66	11.70	11.74	11.78
78	11.82	11.86	11.90	11.94	11.98	12.02	12.06	12.10	12.14	12.18
79	12.22	12.26	12.30	12.34	12.37	12.41	12.45	12.49	12.53	12.57
80	12.61	12.65	12.69	12.73	12.77	12.81	12.85	12.89	12.93	12.97
81	13.01	13.05	13.09	13.13	13.17	13.21	13.25	13.29	13.33	13.37
82	13.41	13.45	13.49	13.53	13.57	13.61	13.65	13.69	13.73	13.77
83	13.81	13.85	13.89	13.93	13.97	14.01	14.05	14.09	14.14	14.19
84	14.24	14.28	14.32	14.36	14.40	14.44	14.48	14.52	14.57	14.61
85	14.65	14.69	14.73	14.77	14.81	14.85	14.90	14.95	14.99	15.03
86	15.07	15.11	15.15	15.19	15.23	15.28	15.33	15.38	15.42	15.46
87	15.50	15.54	15.58	15.62	15.66	15.70	15.75	15.79	15.84	15.88
88	15.92	15.96	16.01	16.06	16.10	16.15	16.19	16.23	16.27	16.31
89	16.35	16.39	16.44	16.49	16.54	16.58	16.62	16.66	16.70	16.74
90	16.78	16.83	16.88	16.93	16.97	17.01	17.05	17.09	17.13	17.18
91	17.23	17.28	17.33	17.37	17.41	17.45	17.49	17.53	17.58	17.63
92	17.68	17.73	17.77	17.81	17.85	17.89	17.93	17.98	18.03	18.08
93	18.13	18.17	18.22	18.26	18.30	18.34	18.39	18.44	18.49	18.54
94	18.58	18.62	18.66	18.70	18.75	18.80	18.85	18.90	18.95	18.99
95	19.03	19.07	19.11	19.16	19.21	19.26	19.31	19.36	19.41	19.45
96	19.49	19.53	19.58	19.63	19.68	19.73	19.78	19.82	19.86	19.90
97	19.95	20.00	20.05	20.10	20.15	20.20	20.24	20.28	20.32	20.37
98	20.42	20.47	20.52	20.57	20.62	20.66	20.70	20.75	20.80	20.85
99	20.90	20.95	21.00	21.04	21.09	21.13	21.17	21.21	21.25	21.30

total water-holding capacity in the root zone of the crop when soil moisture is at field capacity.

2. Enter figure 3 from the bottom with the daily PE value obtained from step A-8. Proceed upward along this line to the appropriate diagonal line representing the percentage value obtained in step B-1. Read the corrected evapotranspiration (E) along the diagonal scale at the left.

3. EXAMPLE

Find the evapotranspiration (E) for July 15 (climatological week No. 20) at a station located at 41° N. and having a heat index (I) of 52. Assume a daily mean temperature of 70° F. and a soil moisture content of 70 percent of field capacity. (Since the heat index (I) is given, steps A-1 and A-2 are not necessary.)

1. Proceed through step A-4, using the given mean temperature of 70° F. and I value of 52. This gives a weekly unadjusted PE rate of 0.92 inch.
2. Using the latitude of 41° N. and the date of July 15 proceed through steps A-5 to A-7 and determine the adjusted weekly PE rate of 1.13 inches.
3. To convert this weekly rate to a daily value proceed through step A-8 using figure 2. The final value is about 0.16 inch per day.
4. Finally, to correct this PE rate of 0.16 inch per day for the effect of soil moisture depletion, using the 70 percent of capacity as given, proceed through

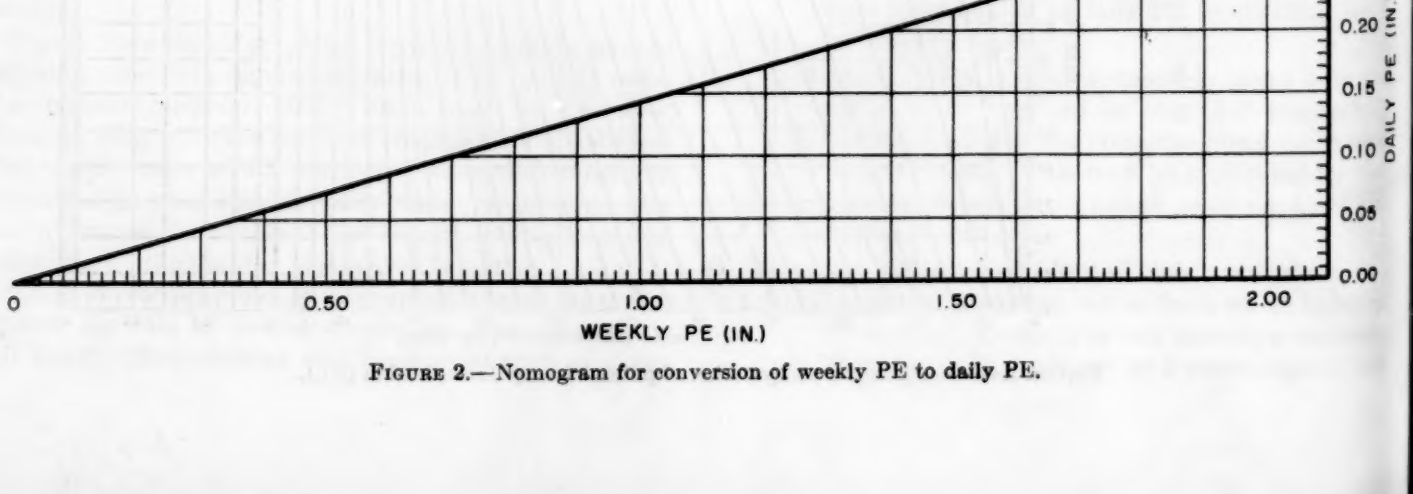

FIGURE 2.—Nomogram for conversion of weekly PE to daily PE.

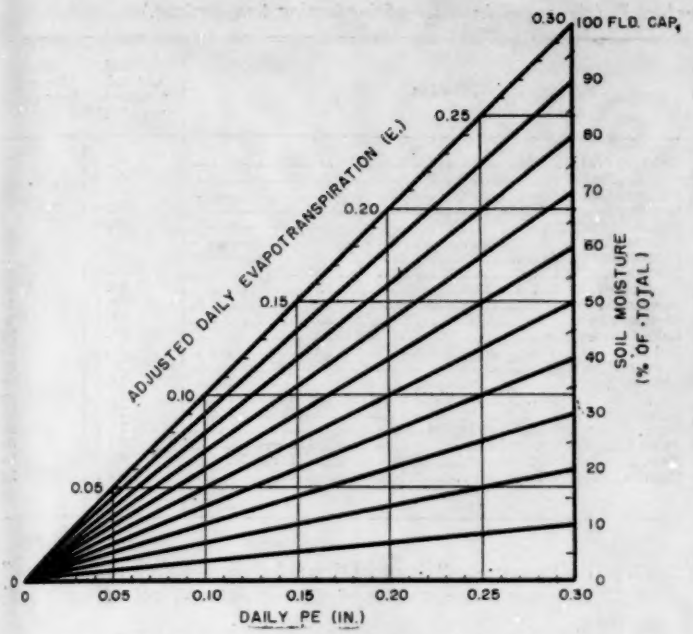

FIGURE 3.—Nomogram for adjustment of PE for soil moisture depletion.

step B-2 using figure 3. A daily rate of about 0.11 inch is determined, which is now an estimate of actual evapotranspiration rather than potential.

4. CONCLUSIONS

This graphical method is most useful for work involving a wide range of climatic conditions (i. e., a wide range of I values.) For computations covering a long period of time at a single station or a group of stations with nearly equal I and latitude values, it will usually save time to use tables or graphs which apply only to those particular stations. Such tables or graphs may easily be prepared using the diagrams presented here over a suitable range of temperature and time. For example, at a given place, latitude and heat index are constants and PE depends only on temperature and time of year; so a table of PE as a function of these two variables could be prepared from figure 1 without difficulty. (See Appendix 1.)

APPENDIX 1

The upper-left portion of figure 1 concerns the correction for latitude and time of year. The unadjusted PE obtained in the lower portion of figure 1 must be multiplied by this day-length correction in order to obtain adjusted rate of weekly PE. The curved lines labeled by months represent mid-month, and for most purposes interpolation between these lines according to date will suffice. However, for a more accurate determination one may use climatological week number (March 1–7= week No. 1, 8–14=No. 2, etc.) rather than month. These lines are not reproduced, but the week numbers are shown for the middle day of the week at 30° and 50° N. latitude. With an appropriate drafting curve one can construct the

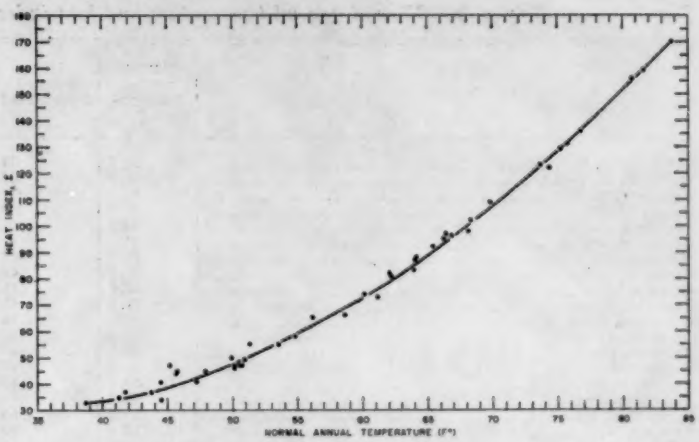

FIGURE 4.—Relation of heat index, I, to normal annual temperature.

lines for week number. For example, the curve for week No. 10 (May 3–9) would have approximately the same shape as the May line, whereas week No. 24 (Aug. 16–22) would approximate the August curvature.

It is not necessary that the numerical value of the day-length correction be determined; the adjustment is accomplished graphically when the appropriate horizontal line of day-length correction is followed to the right until it intersects the appropriate vertical line of unadjusted PE and the final PE is read from the curved lines. However, in order to facilitate the work of those who may wish to prepare tables for a particular station, the scale for day-length correction has been included.

The preparation of tables for any given location is a simple matter. A table of unadjusted PE as a function of temperature can be prepared from the lower portion of figure 1 along the appropriate heat index line. The day-length correction table can be prepared from the upper-left portion of figure 1 by tabulating the value of the correction for each month (or week) along the appropriate latitude line. The final PE for any particular week is then the product of the appropriate two values from the tables. Another convenient device for use at a particular station is a set of tables or graphs of final PE as a function of temperature for each of the 12 months. If these tables are made for monthly PE, an adjustment for month length must be made as indicated in step A-9.

Figure 1 as drawn applies to the Northern Hemisphere. It could be adapted for use in the Southern Hemisphere by the appropriate relabeling of the month lines in the upper-left portion.

APPENDIX 2

Inasmuch as monthly heat index, i, is a function of temperature only [3]

$$i=(T/5)^{1.514},$$

it seemed reasonable to investigate the relationship between heat index, I, as determined from table 1, and normal annual temperature. This was done for the 43 stations shown in the accompanying table 2. The only criterion for the selection of these stations was that a

TABLE 2.—*Normal annual temperature and heat index value, I. (Arranged in order of increasing temperature.)*

Station	Normal annual temperature (°F.)	Heat index, *I*, from table 1	Station	Normal annual temperature (°F.)	Heat index *I*, from table 1
Devils Lake, N. Dak.	38.7	33	Raleigh, N. C.	61.1	73
Williston, N. Dak.	41.3	35	Fort Smith, Ark.	62.0	82
Bismarck, N. Dak.	41.7	37	Atlanta, Ga.	62.2	81
Havre, Mont.	43.7	37	Los Angeles, Calif.	63.9	83
Portland, Maine	44.5	34	Augusta, Ga.	64.0	87
Rochester, Minn.	44.5	41	Abilene, Tex.	64.1	88
Minneapolis, Minn.	45.6	44	Montgomery, Ala.	65.4	92
Huron, S. Dak.	45.7	45	San Angelo, Tex.	66.2	95
Billings, Mont.	47.2	41	Shreveport, La.	66.4	97
Valentine, Nebr.	47.9	45	Savannah, Ga.	66.8	96
Goodland, Kans.	49.9	50	Mobile, Ala.	68.1	98
Scranton, Pa.	50.1	46	Lake Charles, La.	68.3	102
Hartford, Conn.	50.1	47	Del Rio, Tex.	69.8	109
Bridgeport, Conn.	50.5	47	Brownsville, Tex.	73.6	123
Boston, Mass.	50.7	47	Laredo, Tex.	74.3	122
Allentown, Pa.	50.9	49	Honolulu, Hawaii	75.2	129
Burlington, Iowa	51.3	55	Miami, Fla.	75.7	131
Trenton, N. J.	53.5	55	Ponce Santa Isobel, West Indies	76.7	136
Baltimore, Md.	54.7	58	Swan Island, West Indies	80.7	156
Kansas City, Mo.	56.1	65	Yap, Caroline Islands	81.6	159
Richmond, Va.	58.6	66	Canton, Phoenix Islands	83.7	170
Nashville, Tenn.	60.1	74			

wide and uninterrupted range of normal annual temperatures should be represented. As a consequence a number of climatic types are represented but not equally so.

Figure 4 shows heat index plotted as a function of normal annual temperature for these 43 points. The curve was drawn by eye. The relationship is surprisingly good and suggests that heat index, I, can be quickly estimated from normal annual temperature with a maximum error of $\pm$ 4 or 5. This amount of error in the heat index would introduce an error in PE of no more than .03 or .04 inch per week, which is very likely well within the limits of accuracy of the entire empirical procedure. Of course, this result suggests that the heat index scale in figure 1 could be replaced by a scale of normal annual temperature without significant loss of accuracy.

REFERENCES

1. W. R. van Wijk and D. A. de Vries, "Evapotranspiration," *Netherlands Journal of Agricultural Science*, vol. 2, pp. 105–119, 1954.
2. H. L. Penman, "Evaporation: An Introductory Survey," *Netherlands Journal of Agricultural Science*, vol. 4, pp. 9–29, 1956.
3. C. W. Thornthwaite, "An Approach toward a Rational Classification of Climate," *Geographical Review*, vol. 38, pp. 55–94, 1948.
4. C. W. Thornthwaite and J. R. Mather, "The Water Balance," *Publications in Climatology*, vol. 8, No. 1, Drexel Institute of Technology, Laboratory of Climatology, Centerton, N. J., 1955.
5. H. F. Blaney and W. D. Criddle, *Determining Water Requirements in Irrigated Areas from Climatological and Irrigation Data*, U. S. Department of Agriculture, Soil Conservation Service, 1950.
6. C. H. M. van Bavel, *Estimating Soil Moisture Conditions and Time for Irrigation with the Evapotranspiration Method*, U. S. Department of Agriculture, Agricultural Research Service, 1956.
7. G. W. Robertson, *Latent Evaporation: Its Concept, Measurement, and Application*, Experimental Farms Service, Department of Agriculture, Ottawa, Canada, 1954.

RADIATIONAL INVERSIONS AND SURFACE TEMPERATURE CHANGES

SIGMUND FRITZ

U. S. Weather Bureau, Washington, D. C.

[Manuscript received March 12, 1958; revised April 24, 1958]

ABSTRACT

When air stagnates in dark polar regions, an inversion forms. The change of the inversion magnitude is studied under the assumption that the snow surface radiates about as much energy as it receives from the atmosphere. It turns out that the inversion magnitude may either decrease or increase as the surface temperature falls, depending on the rate of change of atmospheric "emissivity" with air temperature.

1. INTRODUCTION

Wexler [1, 2] has studied the formation of inversions during the long polar night. An examination of his papers shows that under some conditions the inversion magnitude, ΔT, decreases, and for other conditions ΔT increases as the surface temperature, T_s decreases. The inversion magnitude is given by

$$\Delta T = T_a - T_s \tag{1}$$

where T_a is the temperature of an isothermal layer of air which lies above a colder surface.

Actually, Wexler studied the following phenomenon. He assumed that during the long polar night a relatively unstable maritime airmass stagnated over a snow surface with initial surface temperature 273° K. He then tried to compute the future course of the air temperature, T_a, and surface temperature, T_s, assuming that only radiation was acting. The model he adopted stipulated that T_s falls very quickly to a quasi-equilibrium value determined by the downcoming radiation from the air. Thereafter, T_s decreases slowly. The air temperature then also falls slowly, forming an isothermal layer with temperature, T_a, above the ground; above the isothermal layer, the original maritime air temperature prevails. In his 1936 paper, with the aid of water vapor absorption coefficients measured by Weber and Randall [3], Wexler [1] found that ΔT decreased as T_s decreased, after T_s had reached the quasi-equilibrium value. Later, in 1941, Wexler [2] found that if he used the newly developed Elsasser diagram for saturated air ΔT increased as T_s decreased. Whether or not ΔT increases or decreases depends critically on the *rate of change* of the atmospheric radiation with air temperature.

It is the purpose of this paper to inquire under what conditions ΔT would *increase* with decreasing T_s, and under what conditions ΔT would *decrease* with decreasing T_s, in an individual mass of air cooling by radiation only.

2. EMISSIVITY AND RADIATION

From the assumed state of quasi-radiative equilibrium between the snow surface and the overlying air, we get

$$R = \sigma T_s^4 = k\sigma T_a^4 \tag{2}$$

$$T_s = k^{1/4} T_a \tag{3}$$

where k is an overall "emissivity" of the atmosphere, and we assume that the main part of the downward atmospheric radiation comes form the isothermal layer; σ is the Stefan-Boltzmann constant.

Since $\Delta T = T_a - T_s$, by substituting for T_s from equation (3), we get

$$\Delta T = T_a(1 - k^{1/4}) \tag{4}$$

The problem now is to find under what conditions of radiation, R, and therefore of atmospheric emissivity, k, ΔT increases with decreasing T_s, and when ΔT decreases with decreasing T_s. We can get the limiting condition by making ΔT constant.

Thus equation (4) becomes

$$T_a = \frac{\Delta_c T}{(1 - k^{1/4})} \tag{5}$$

where Δ_c denotes that ΔT is constant with variations in T_s or T_a.* Equation (5) shows the relation between the "emissivity", k, and isothermal air temperature, T_a, which is required in order for the inversion magnitude, ΔT, to remain constant as the surface temperature, T_s, drops. This relation of k vs. T_a is shown in figure 1 for a range of k and T_a which is found in Wexler's studies. Figure 1 shows that the emissivity of the isothermal air may decrease with decreasing air temperature even though the

*Under the conditions that ΔT = constant with T_s,

$$\frac{\delta \Delta T}{\delta T_s} = \frac{\delta \Delta T}{\delta T_a} = 0$$

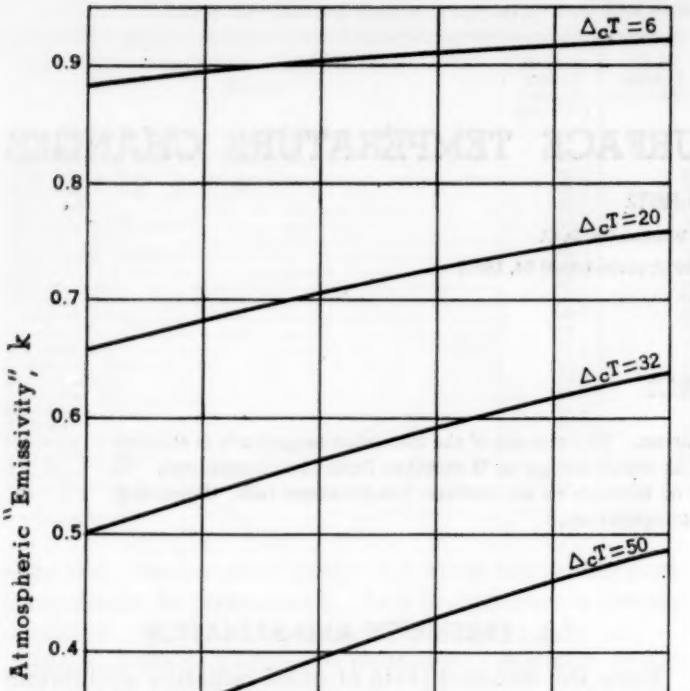

FIGURE 1.—Variations of atmospheric "emissivity," k, with inversion temperature, T_a, when the inversion magnitude, $\Delta_c T$, does not change with surface temperature, T_s.

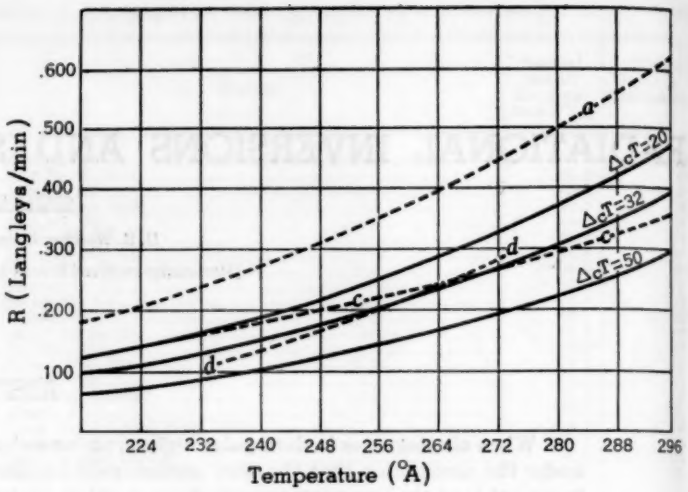

FIGURE 2.—Radiation, R, vs. temperature. Curve "a" refers to radiation of a black body, in langley/min., against surface temperature, T_s. Curves "c" and "d" refer to radiation from the atmosphere related to air temperature (see text). (Curves a, c, d from [2].) Curves labeled $\Delta_c T$ refer to radition from air when the inversion magnitude does not change with surface temperature.

inversion magnitude is not changing as surface temperature falls. However, if the slope of the k vs. T_a lines is steeper than those in figure 1 (that is, if k decreases faster with decreasing T_a), ΔT will increase as T_s decreases; if the slope is less steep, ΔT will decrease.

The conditions on the atmospheric radiation R, for ΔT=constant, can be readily found from equation (2). As background, however, we should look at R vs. T curves from Wexler's 1941 paper [2]. In figure 2, curves a, c, and d are taken from that paper. Curve a represents the black body radiation of a snow surface, plotted against T_s; curves c and d represent the downward atmospheric radiation computed in various ways and plotted against T_a. In curve c, T_a represents "the highest mean temperature of any layer of air containing 1 mm. of precipitable water and normal CO_2 content." In the computation of R for curve c the absorption coefficients of Weber and Randall [3] were used. Curve d was ". . . computed by use of the Elsasser diagram in the following way: the radiation coming from a saturated atmosphere in convective equilibrium with an ocean surface of 0° C. is designated by the ordinate of the extreme right hand point of curve (d), while the ordinates of other points of this curve refer to the radiation coming from atmospheres whose lower portions are isothermal at temperatures corresponding to the abscissae of the curve and whose upper portions follow the original convective equilibrium curve." The values of T_a and T_s, tabulated by Wexler [2] show that

$$\frac{\partial \Delta T}{\partial T_s} > 0 \text{ for curve c and less than zero for curve d.}^{**}$$

This result is to be expected. From the definition of $\Delta_c T$, by substituting for T_s in equation (2), we get

$$R = \sigma(T_a - \Delta_c T)^4$$

The values of R vs. T_a for several values of $\Delta_c T$ are plotted in figure 2. These curves, of course, apply only when ΔT is constant with changes in T_a or T_s. If any lines in figure (2) converge toward curve a, as T_a decreases, more rapidly than the $\Delta_c T$ curves, then $\frac{\partial \Delta T}{\partial T_s} > 0$; if such lines diverge from curve a more rapidly than the $\Delta_c T$ curves then $\frac{\partial \Delta T}{\partial T_s} < 0$. Thus, curves c and d represent the type of variation of $\frac{\partial \Delta T}{\partial T_s}$ to be expected; that is, for curve c the inversion decreases with decreasing surface temperature; the opposite is true for curve d. It is easy to verify from figure 2, that in curve c, k is very nearly constant. But for curve d, k decreases more rapidly with decreasing T_a than indicated by the curves in figure 1.

**Wexler's table shows this for $T_s < -40°$ C. However his curve d shows it for all values of T_s.

Thus, we might expect in our simplified model, the condition for $\frac{\partial \Delta T}{\partial T_s} < 0$ is that the "emissivity" of the atmosphere should decrease more rapidily with decreasing air temperature than the curves in figure 1.

3. DISCUSSION

Although curves c and d represent only computation with special assumptions and conditions, it is not hard to visualize that in actual atmospheres the emissivity may vary with T_a in the same way as implied in curve c or in curve d. For example, evaporation and condensation may do this. Therefore, it is not valid to generalize that the inversion magnitude either increases or decreases with decreasing surface temperature after quasi-equilibrium has been reached. What happens in any particular case depends on the radiation properties of the atmosphere and how they change with temperature.

Moreover comparison of T_s with ΔT with the aid of many different radio-soundings for many different meteorological conditions and airmasses, does not shed any light on the direction of change of ΔT with T_s in a single airmass. Nevertheless Belmont [4] has concluded from his own findings that his results conflict with Wexler's theoretical results. Belmont compiled measurements of inversions and found that, on the average, the magnitude of "radiation" inversions increases as T_s decreases, especially for low values of T_s. Since radiosonde data were used, the results do not refer to the history of a single mass of air during the time when the air and surface cool. The results compare, instead, the temperatures of many different masses of air with the simultaneous surface temperatures. Therefore, Belmont's results are, in any case, not comparable with Wexler's results since each was dealing with a different problem. But it should nevertheless be pointed out that Wexler's results include *both* the increase *and* decrease of ΔT with decreasing T_s, depending on the rate of change of atmospheric emissivity with air temperature.

ACKNOWLEDGMENTS

This problem was discussed on several occasions with Dr. H. Wexler. Mr. T. H. MacDonald suggested a simplification in the derivation of equation (5).

REFERENCES

1. H. Wexler, "Cooling in the Lower Atmosphere and the Structure of Polar Continental Air," *Monthly Weather Review*, vol. 64, No. 4, Apr. 1936, pp. 122–136.
2. H. Wexler, "Observations of Nocturnal Radiation at Fairbanks, Alaska, and Fargo, North Dakota," *Monthly Weather Review, Supplement* No. 46, 1941, 21 pp.
3. L. R. Weber and H. M. Randall, "Absorption Spectrum of Water Vapor beyond 10 μ," *Physical Review*, Series 2, vol. 40, No. 5, June 1, 1932, pp. 835–847.
4. A. D. Belmont, "Lower Tropospheric Inversions at Ice Island T-3," *Scientific Report* No. 2, Contract AF–19 (604)–1141, Arctic Meteorology Research Group, McGill University, Montreal, Canada, August 1955, 57 pp., 2 appendices.

THE WEATHER AND CIRCULATION OF APRIL 1958[1]

PAUL STARK

Extended Forecast Section U. S. Weather Bureau, Washington, D. C.

1. INTRODUCTORY REMARKS

Not since November 1957 has there been a monthly mean trough in the United States west of the Mississippi River, although in March 1958 a trough of moderate intensity was located along the west coast (fig. 4 of [1]). During April (fig. 1) that trough moved inland, perhaps as a result of the downstream dispersion of vorticity following the generation of increased westerlies and a new trough in the Pacific at middle latitudes. The increase in zonal winds in the Pacific followed the development of an Asiatic coastal trough in March, a feature conspicuously absent during the months of January and February 1958 [2, 3].

In April, on the average, there were remnants of blocking over northeastern Canada, but the complete collapse of that blocking near the end of the month and its replacement by a mean trough permitted a northerly displacement of mid-latitude westerlies. Retreat of Canadian blocking toward the west and entry of the west coast trough into the United States were responsible for considerable variability in weather and circulation patterns, not only from week to week but also on a bi-weekly basis. Many daily, monthly, and seasonal records of temperature and precipitation were broken, some of which are listed in table 1.

TABLE 1.—*April monthly weather records broken in 1958*

Station	Record
Precipitation	
Alpena, Mich.	Driest of record.
Greenville, S. C.	Wettest of record.
Jacksonville, Fla.	Do.
Mt. Shasta, Calif.	Greatest snowfall in 80 years.
Newark, N. J.	Wettest of record.
Providence, R. I.	Do.
San Francisco, Calif.	Wettest since 1884.
Worcester, Mass.	Wettest of record.
Temperature	
Cape Hatteras, N. C.	Coldest since 1907.
Ely, Nev.	Coldest of record.
Los Angeles, Calif.	Warmest of record.

2. MONTHLY MEAN CIRCULATION AND WEATHER

INDEX

The monthly mean circulation for April, shown in figure 1, represents a transition stage over North America from a low index state to one of a higher index. Of course, that is not apparent solely from the 700-mb. contours. One can see that there was a general zonal flow in the temperate westerlies of the Western Hemisphere, with the exception of the interruptions in the Gulf of Alaska and northwestern Canada. However, the departure from normal isopleths (hereafter called DN), shown as dotted lines in figure 1, give a more graphic representation of the state of the zonal westerlies. In this instance there was actually an easterly flow relative to normal north of 45° N. over most of North America. Thus, in spite of the apparently well-formed westerlies, there were some low index features, especially blocking, which persisted long enough to retain their identities and affect the month-long time-averaged mean.

The computed zonal index for temperate westerlies (35° N.—55° N. in the Western Hemisphere) for April was 7.9 m. p. s., only 0.4 m. p. s. below normal. But that represents a considerable recovery over the previous month whose index was 5.3 m. p. s., some 3.8 m. p. s. below normal. The rise of index in April is even more significant if one considers that the index normally decreases by 0.8 m. p. s. from March to April.

NORTHERN HEMISPHERE CIRCULATION

While our interest is centered principally on North America, it is worthwhile to examine the salient features of the general circulation of the whole Northern Hemisphere. In figure 1 there are three major troughs at high latitudes and six significant middle-to-low-latitude troughs. That wave number was supported to some extent by the existence of high-latitude blocking, which can be seen as positive DN centers over Alaska, northern Quebec, and the Norwegian Sea.

The outstanding feature of the DN pattern was the overall weakness of the gradient, except for the area from Scandinavia to northwestern Siberia, and another just east of Japan. In the latter region the abnormal strength of the subtropical ridge, which was longitudinally in phase with a deep polar trough, accounted for the fairly strong westerlies sweeping across the north-central Pacific. The DN gradient over the United States was especially weak and is not indicative of the variability within the month.

The subtropical ridging in the eastern Pacific was accompanied by a difluent area along the United States west coast, to the rear of the progressive trough in the central United States. The difluence was partially re-

[1] See Charts I-XVII following p. 148 for analyzed climatological data for the month.

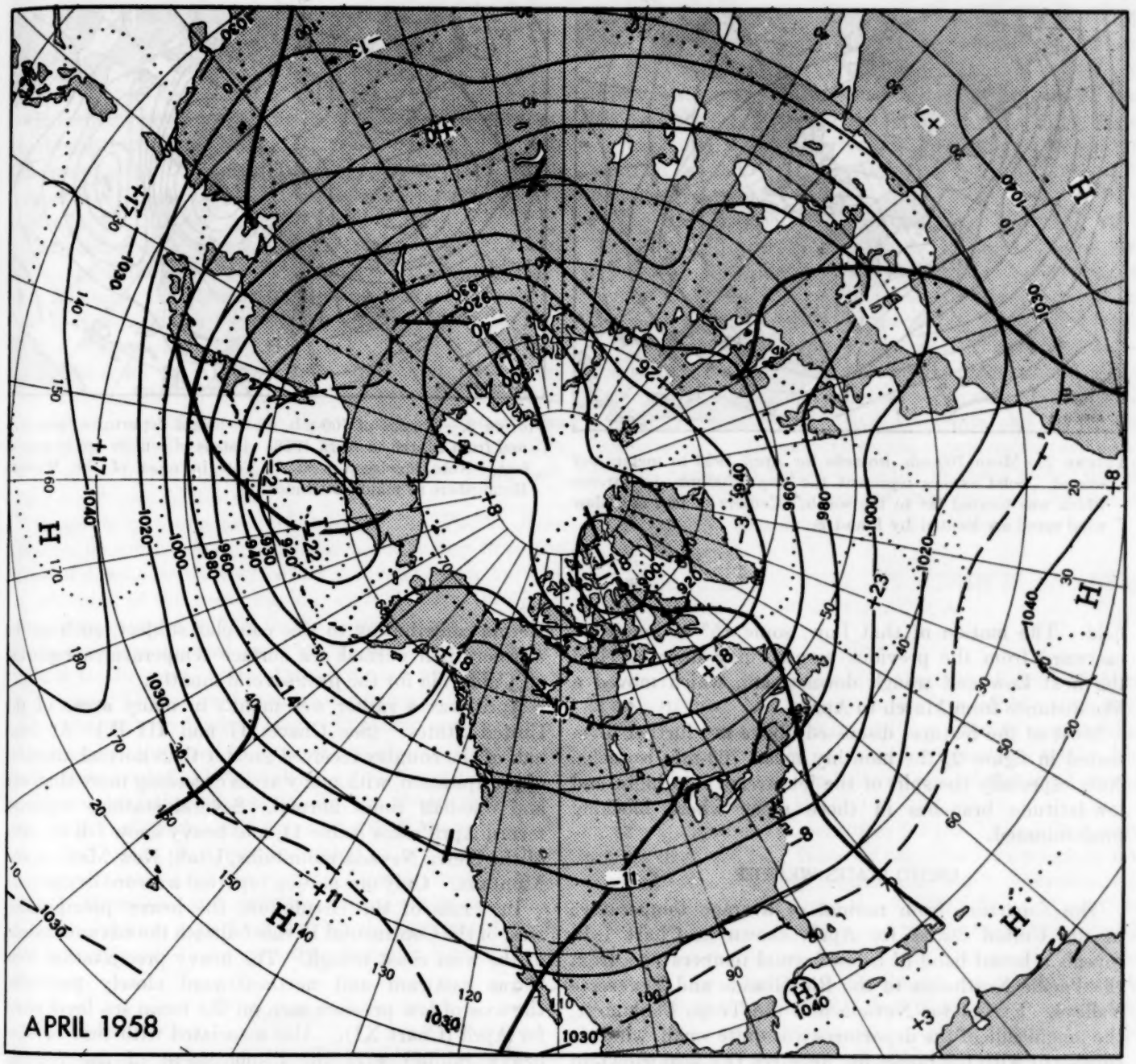

FIGURE 1.—Mean 700-mb. contours (solid) and height departures from normal (dotted) (both in tens of feet) for April 1958. High-latitude blocking over North America is defined by the positive height departures in the north and negative height departures to the south.

sponsible for lower than normal 700-mb. westerly wind speeds across the northern United States. The slight ridge in the eastern United States and the residual block in Quebec also contributed to the weaker than normal westerlies.

Most of North America was under the influence of cyclonic flow at the 700-mb. level as can be seen in figure 1, with Canada having a flow much more cyclonic than that in the United States. The short wave-spacing between the two United States troughs along 45° N. might have been incompatible had it not been supported by the block in Quebec.

The Atlantic was characterized by the normally sharp slope (vertically) of the Icelandic Low [4] and the presence of a strong ridge in the eastern portion. The DN field shows that there must have been some tendency toward bridging between the Canadian block and the intensifying Atlantic ridge. The European-African trough is normally sheared [4] with the middle-to-low-latitude segment west of Spain and Africa. Its position far inland this month, however, was favored by the building of the Atlantic ridge and the Scandinavian block.

To a great extent Asia was dominated by the deepening Low in north-central Siberia and its rather extensive DN

468423—58——2

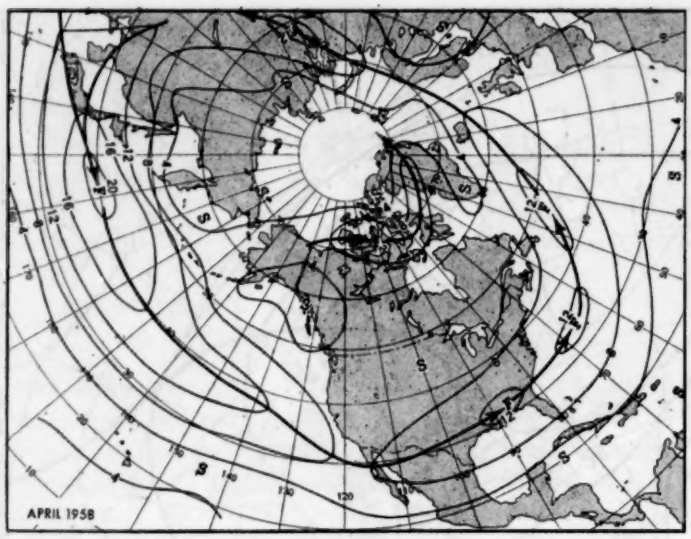

FIGURE 2.—Mean 700-mb. isotachs for April 1958 in meters per second. Solid arrows represent the mean 700-mb. jet stream which was located far to the south. Centers of fast and slow wind speed are located by F and S.

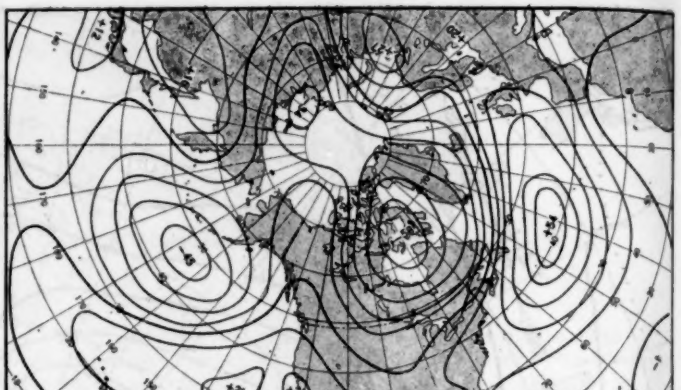

FIGURE 3.—Change of 700-mb. mean height departures from normal from March to April 1958. Labels of centers are in tens of feet. Note increased westerly flow in most of the Western Hemisphere at middle latitudes.

field. The motion of that Low, some 15° of longitude eastward from the previous month, may have repelled the next Low and trough downstream, which moved a like distance from March to April.

Most of the features discussed above are further illustrated in figure 2, the monthly mean 700-mb. isotachs. Note especially the split of the jet stream into high- and low-latitude branches in those areas where blocking predominated.

UNITED STATES WEATHER

The departure from normal of average temperature in the United States for April, shown in Chart I–B, reveals a broad band of below normal temperatures from the Pacific Northwest to the Rio Grande and Tennessee Valleys. Except for Nevada and the Texas Panhandle, the magnitude of the departures was quite small, which is consistent with the rather flat negative DN field shown in figure 1. The normal to above normal temperatures from eastern Montana to the Middle Atlantic States resulted from the persistent Canadian blocking (and resultant easterly DN flow) and above normal 700-mb. heights which extended from the Northern Plains States eastward. A further factor to consider is that the tracks of polar anticyclones (Chart IX) were principally north of the Canadian border.

The above normal temperatures observed in the California coastal belt cannot be explained in terms of DN flow. In fact, an onshore DN and contour flow would usually produce cooler than normal temperatures. However, cold air inland and its suppressing effect on the sea breeze usually does produce some warming along the coast. But since warmer than normal temperatures have been extremely persistent in this area, there may be other factors contributing to this complex subject, such as the warmer than normal sea surface temperatures reported off California for the past several months.

April was a rather wet month in many areas of the United States. (See Charts II and III–B.) At least half of the country received greater than normal amounts of precipitation, with many areas exceeding more than one and one-half times normal. Several stations reported record April rains (table 1), and heavy snow fell in parts of the Sierra Nevada mountains, Utah, New Mexico, and Montana. Only one station reported a record dry month.

In terms of the circulation, the heavy precipitation west of the Continental Divide fell with the advance inland of the west coast trough. The heavy precipitation from Texas eastward and northeastward closely paralleled the axis of low pressure seen on the mean sea level chart for April (Chart XI). Also associated with that band of heavy rainfall were the displacement of the 700-mb. jet stream far to the south (fig. 2) and the location of a secondary maximum of cyclone frequencies (shown only as tracks in Chart X) in the Gulf of Mexico, where cyclone frequency is normally low during April [5].

The area of below normal precipitation from southern Utah to Missouri is difficult to explain. Most qualitative considerations indicate the probability of heavy precipitation in that area, but a survey of daily sea level charts shows that there was considerable northerly flow which would have been discouraging to heavy precipitation. The mean southerly flow at sea level on Chart XI appears to have been too weak to permit the establishment of a pronounced moist tongue of Gulf air that far to the north. This and other features mentioned above may have more meaning after a discussion of the changes in circulation which took place from March to April.

3. MARCH TO APRIL CHANGES IN CIRCULATION AND WEATHER

CIRCULATION

Principal circulation changes from March to April can best be interpreted from figure 3, the 30-day mean 700-mb. anomalous height change from March to April. (The reader is referred to figure 4 of the preceding report of this series [1] for the March contour pattern.)

Excepting Asia, the overall decrease in DN at high latitudes, combined with the increased DN at middle and low latitudes, indicates: (1) a general increase in westerly winds (a rising index), and (2) a weakening of the blocking in the Western Hemisphere.

Blocking on the Asiatic side of the Pole in the Laptev Sea was transferred to the south of Novaya Zemlya in April, where a 270-foot positive anomalous change was centered. The increases over Manchuria were possibly a response to the upstream deepening of the mean Low over north-central Siberia.

Large height changes occurred in the Pacific from March to April. A ridge in March, extending from the Gulf of Alaska to Midway Island, was replaced in April by a flattening of the westerlies and cyclonic curvature. An extensive increase in DN in the eastern Pacific resulted. Consequently, the west coast trough of March was forced inland to the west-central United States where we see a decrease of DN extending northward to a 580-foot maximum change over Hudson Bay. This does not mean that blocking left that part of Canada completely, but it must have been eroded substantially.

In the Atlantic and western Europe the increased DN indicates that there was a great growth of the subtropical ridge. This, in turn, was associated with weakening and retrograde motion of the western Atlantic trough to the west of Greenland and along the United States east coast. Thus it became a part of the North American trough-ridge complex and consequently a factor in United States weather.

WEATHER

Changes in weather over the United States from March to April are most easily expressed in terms of temperature and precipitation classes. The reports from one hundred selected stations used routinely are summarized in table 2 in terms of class changes. (For example: a class change of +2 in temperature means that a particular station may have warmed in the mean from normal to much above or from much below to normal.) Table 2 shows that April was considerably warmer than March. Only 7 percent of the country had lower anomalous temperatures during April, while 55 percent of the stations were warmer than in March. The remaining 38 percent showed no change.

TABLE 2.—*Temperature and precipitation class changes from March to April 1958 in the United States (based on 100 selected stations).*

Temperature		Precipitation	
Class change	Percent of stations	Class change	Percent of stations
+3	2	+2	12
+2	20	+1	23
+1	33	0	44
0	38	−1	16
−1	7	−2	5
−2	0		
−3	0		

The class changes of precipitation from March to April, expressed in terms of three classes in table 2, show that April was somewhat wetter than March. Forty-five percent of the cities showed an increase of one or two classes, while 21 percent totaled less precipitation than in March.

The changes in circulation and weather described above did not proceed in a gradual manner during April. It is true that if one is given monthly mean charts at sea level and aloft, certain qualitative comments and deductions can be made. However, there was considerable variability during April, and therefore, many of the weather details can be more easily recognized and discussed by use of shorter-period time-means.

4. VARIABILITY WITHIN THE MONTH IN AND NEAR NORTH AMERICA

APRIL 1–15

The 700-mb. circulation for the first 15 days of April shown in figure 4a presents a picture of blocking over North America. The split in the westerlies approaching the continent not only provided for two storm tracks, but also left between the two belts an area of shattered trough and blocking ridge.

The anomalous temperatures for the United States are shown in figure 5a. Here we see a pattern which is not atypical of a blocking regime and which compares well with the DN flow in figure 4a. The DN flow derived from the blocking was easterly across the northern States, with heights above normal from North Dakota through the northern Great Lakes. Even though some of the heights were slightly below normal, that type of flow encourages warmer than normal temperatures since in April the cold source region is not in eastern but in western Canada.

The below normal temperatures in the southern two-thirds of the United States resulted almost exclusively from intrusions of relatively cold Pacific air in a moderately fast, low-latitude, carrying current along the mean jet axis (fig. 2). There were only two penetrations of continental polar air into the country in this period, and those were of short duration. (See Chart IX.) Most of the polar anticyclonic activity was concentrated in the Hudson Bay area, where Highs are frequent in April [5], and where they became the sea level counterpart of upper-level blocking.

A comparison of the 2 weeks comprising the first half of April [2] brings out some interesting occurrences. An

[2] It is not implied that the two 5-day means will total the 15-day mean shown. For convenience and economy of space only 4b and 4c were selected as representative of the first and second weeks of the month.

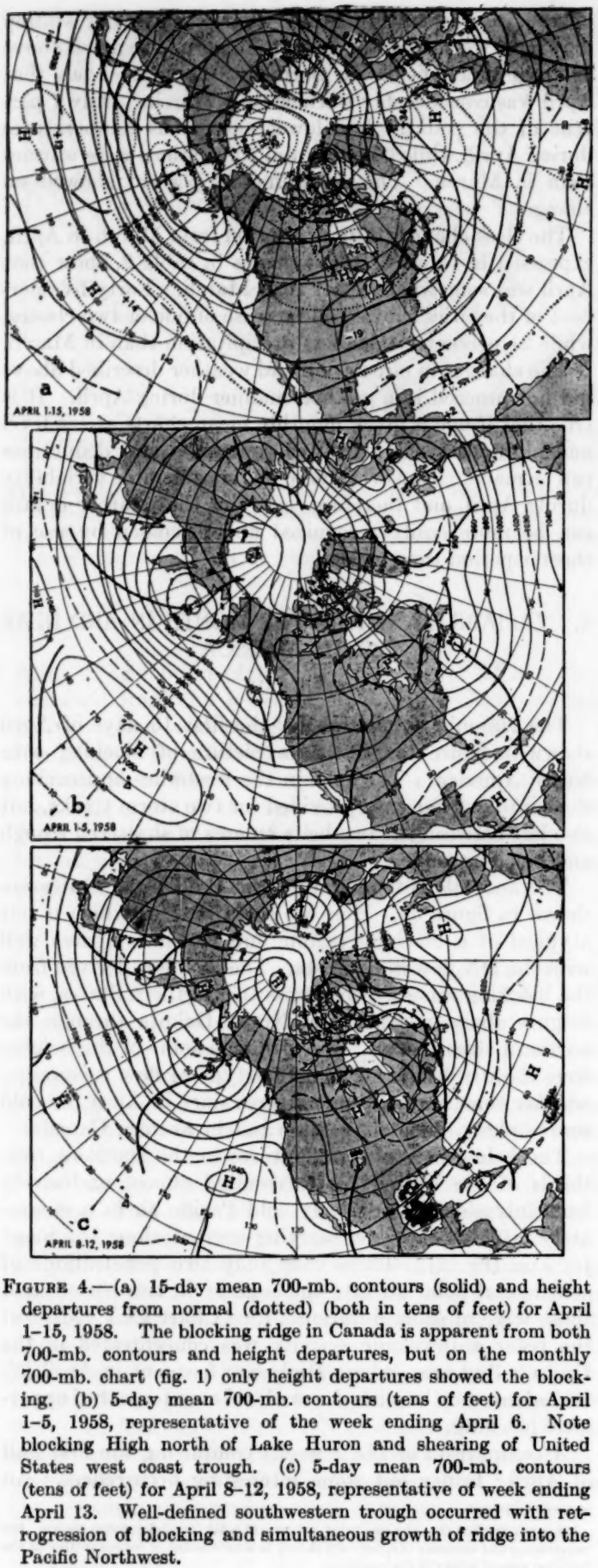

FIGURE 4.—(a) 15-day mean 700-mb. contours (solid) and height departures from normal (dotted) (both in tens of feet) for April 1–15, 1958. The blocking ridge in Canada is apparent from both 700-mb. contours and height departures, but on the monthly 700-mb. chart (fig. 1) only height departures showed the blocking. (b) 5-day mean 700-mb. contours (tens of feet) for April 1–5, 1958, representative of the week ending April 6. Note blocking High north of Lake Huron and shearing of United States west coast trough. (c) 5-day mean 700-mb. contours (tens of feet) for April 8–12, 1958, representative of week ending April 13. Well-defined southwestern trough occurred with retrogression of blocking and simultaneous growth of ridge into the Pacific Northwest.

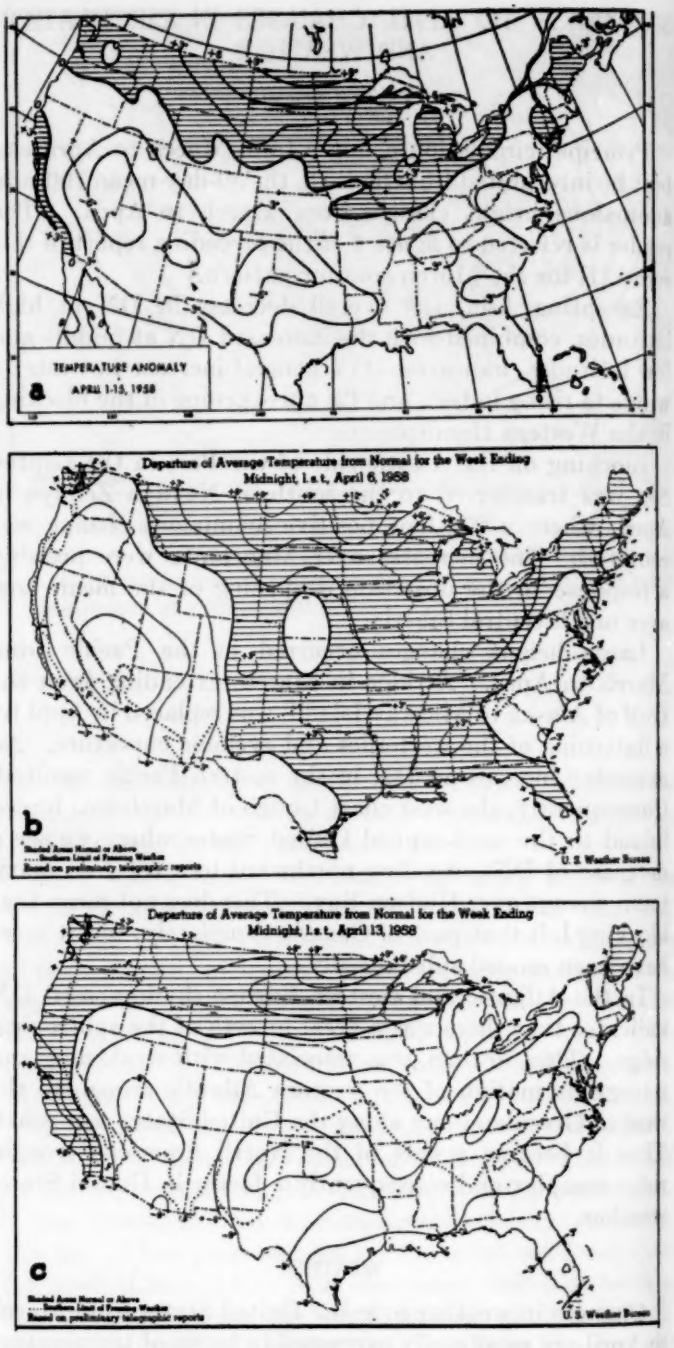
TEMPERATURE ANOMALY
APRIL 1-15, 1958
a
Departure of Average Temperature from Normal for the Week Ending
Midnight, l.s.t., April 6, 1958
b
U.S. Weather Bureau
Departure of Average Temperature from Normal for the Week Ending
Midnight, l.s.t., April 13, 1958
c
U.S. Weather Bureau

FIGURE 5.—Departure of average surface temperatures from normal (F. °) during the first half of April 1958. (a) April 1–15. This type of zonal pattern, warm in the north and cold in the south, represents the influence of blocking. (b) Week ending April 6. Cold air covered the West, but the central half of the country was warm as the west coast trough sheared and moved inland. (c) Week ending April 13. Cold air progressed to the east coast through the trough, and the west coast warmed as the 700-mb. ridge extended into the Pacific Northwest. (b and c from *Weekly Weather and Crop Bulletin, National Summary*, vol. XLV, Nos. 14 and 15, April 7 and 14, 1958.)

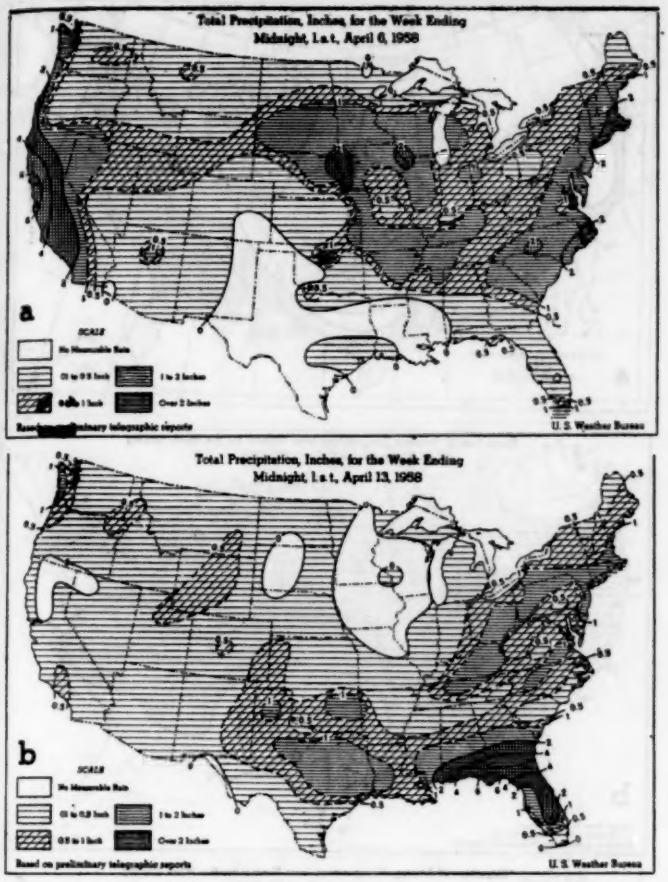
Total Precipitation, Inches, for the Week Ending
Midnight, l.s.t., April 6, 1958
a
Total Precipitation, Inches, for the Week Ending
Midnight, l.s.t., April 13, 1958
b

FIGURE 6.—Total precipitation, inches, for: (a) April 1–6, 1958. Amounts over 6 inches in the San Francisco region caused local flooding before the trough moved inland. (b) April 8–13, 1958. Northerly 5-day mean 700-mb. flow over the West inhibited rainfall as the trough moved inland. Cyclogenesis in the Gulf of Mexico early in the week was responsible for the heavy accumulation in the Southeast. (From *Weekly Weather and Crop Bulletin, National Summary*, vol. XLV, Nos. 14 and 15, April 7 and 14, 1958.)

inspection of figure 4b reveals a blocking High between James Bay and Lake Superior, in phase with a tropical ridge in the eastern Gulf States. The northern portion of the west coast trough stayed well offshore, while that segment below 40° N. sheared and moved rapidly inland.

Successive invasions of fairly cold maritime Pacific airmasses followed, and most of the West became much colder than normal, with temperatures averaging more than 9 F.° below normal over southern Nevada (fig. 5b). Meanwhile, the balance of the country was normal or above, except for below normal temperatures in the East which lagged the offshore trough.

Precipitation (fig. 6a) was most notable in California. Record amounts (table 1) accumulating in this first week of the month were accompanied by severe local flooding and mudslides and heavy snows in the mountains [6]. Only light amounts of rain fell near the trough in the southern Plains owing to the foehn drying effect and the absence of Gulf moisture.

The second week of April was quite different from the first. The remnants of the offshore west coast trough were replaced by strong ridging (fig. 4c) into the Pacific Northwest as the blocking High retrograded to North Dakota. Thus, as the western trough-ridge couplet became appreciably more meridional, a temperature reversal took place in the second week (fig. 5c).

As rapid cooling spread eastward from the Southwest, above normal temperatures in the South and Central States dropped to below normal. Temperatures as much as 14 F.° below normal were reported in the Texas Panhandle, a change of some 15F.° in the mean in a week's time. In the Pacific Coast States temperatures were above normal under the ridging aloft.

Precipitation in the West was generally less than one-half an inch (fig. 6b), with an inhibiting northerly flow aloft to the rear of the Southwest trough. As westerlies with broad cyclonic curvature swept over the Gulf States, rainfall amounts exceeding 7 inches were deposited in Florida with the development of two Gulf storms. (See Chart X.)

In general, then, as the week progressed, precipitation was most marked in the eastern and southern parts of the country, and average temperature anomalies assumed a zonal nature with warm air to the north and cold air to the south. Sudden changes followed, however, to give a sharply different picture of those elements.

APRIL 16–30

Changes in 700-mb. circulation during the last half of April were quite abrupt. Even a cursory comparison of the last 15 days of April (fig. 7a) with the first 15 days (fig. 4a) shows certain obvious gross differences in and near North America.

The amplification in the eastern Pacific was perhaps the most important areal change in the Western Hemisphere. In the Gulf of Alaska there were rises of some 800 feet from the previous 15-day period. That imposing block was probably related to the suppression of the High in the Arctic Ocean and the discontinuous retrogression of the Canadian block. Regardless of its evolution, however, its effect downstream was of great importance. One result was the consolidation of the multiple trough structure in the western United States of the first half of the month to an almost full-latitude trough in the central United States during the following 15 days. The change was reflected somewhat in the DN distribution (fig. 7a), but much more so in the changes in anomalous temperatures.

Temperature departures from normal for the last half of the month (fig. 8a) hardly resemble those of the first half of April. Significant warming in the Southwest and East, coupled with vigorous cooling in the Northwest, produced a pattern of anomalies which was dominantly meridional, in contrast to the zonal pattern of April 1–15.

The blocking ridge in the Gulf of Alaska and the accompanying northerly DN flow over western North America

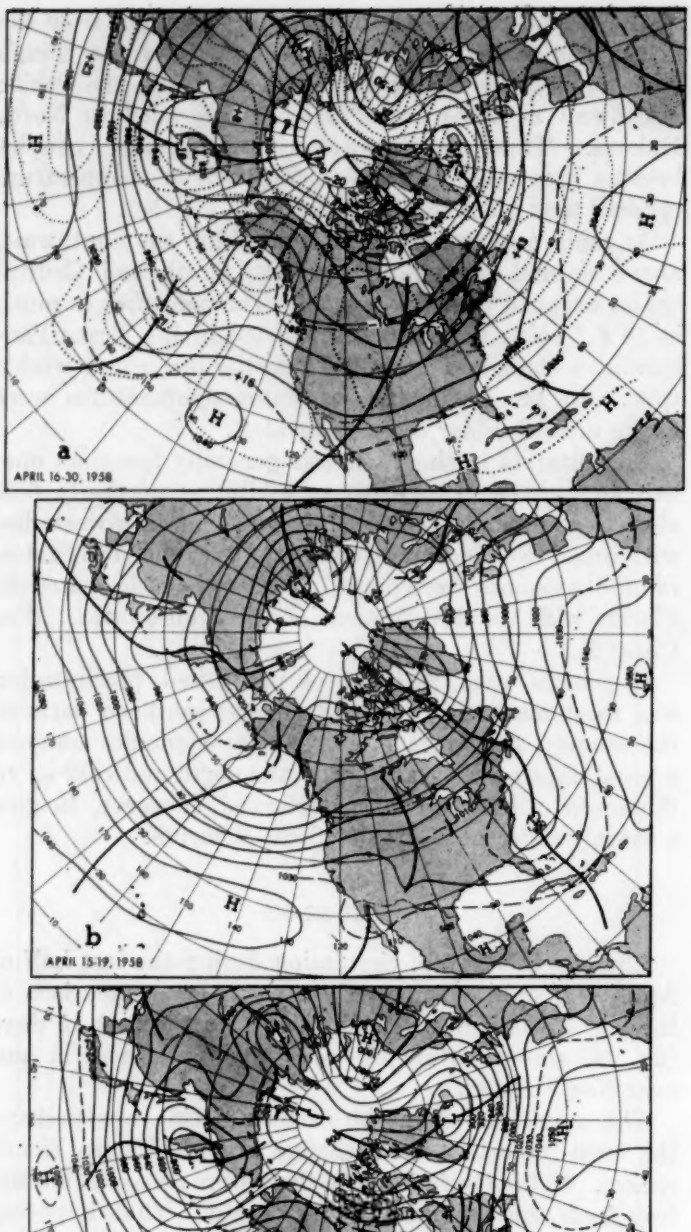

FIGURE 7.—(a) 15-day mean 700-mb. contours (solid) and height departures from normal (dotted) (both in tens of feet) for April 16–30, 1958. Well-defined United States trough replaced shattered troughs and blocking ridge of first half of month. Note the more meridional pattern of height departures from normal. (b) 5-day mean 700-mb. contours (tens of feet) for April 15–19, 1958, representative of week ending April 20. Compared with the previous week (fig. 5c), the westerlies strengthened considerably in higher latitudes over North America and weakened in lower latitudes. (c) 5-day mean 700-mb. contours (tens of feet), for April 22–26, 1958, representative of week ending April 27. This is an example of the extreme variability within the month, with change from a zonal to a meridional pattern in one week.

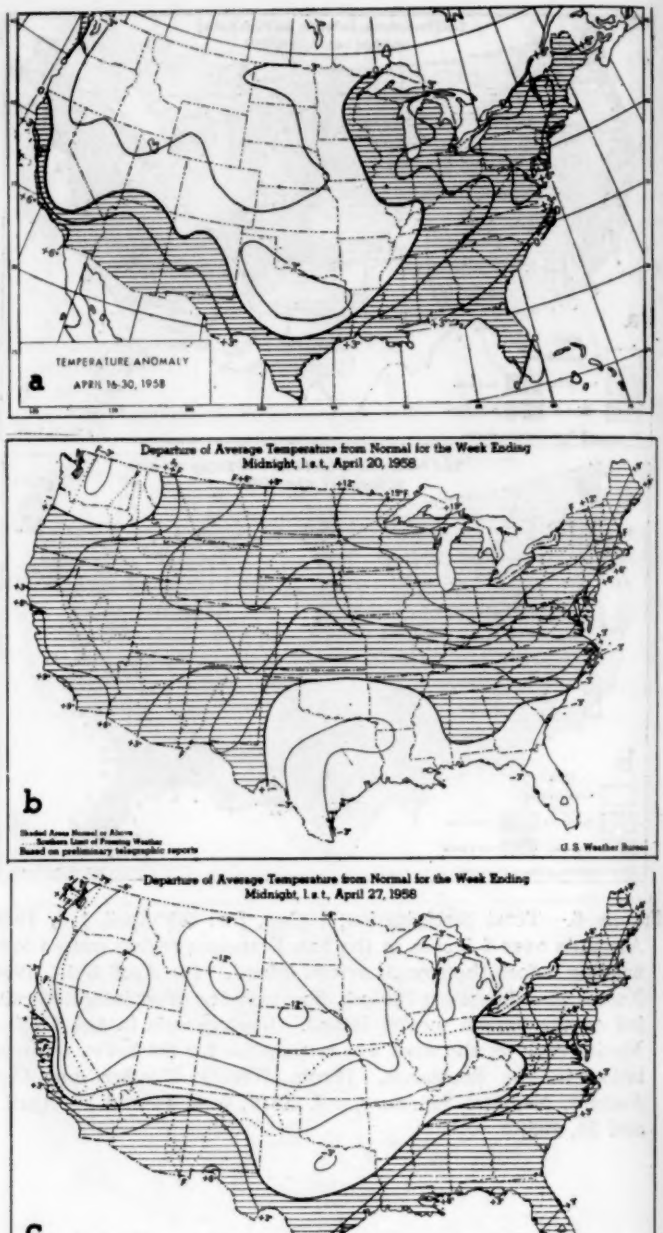
TEMPERATURE ANOMALY
APRIL 16-30, 1958
a
Departure of Average Temperature from Normal for the Week Ending
Midnight, l.s.t., April 20, 1958
b
U.S. Weather Bureau
Departure of Average Temperature from Normal for the Week Ending
Midnight, l.s.t., April 27, 1958
c
U.S. Weather Bureau

FIGURE 8.—Departure of average surface temperatures from normal (F. °) during the last half of April 1958. (a) April 16–30. This meridional distribution of temperature anomalies is in marked contrast to that of the previous 15-day period. (b) Week ending April 20. Normal or above normal temperatures over most of the country were a response to the northerly migration of westerlies during this week. (c) Week ending April 27. Here again is another reversal. During this week cold continental polar and maritime Pacific airmasses dominated the country as a result of the large amplification in the eastern Pacific Ocean.

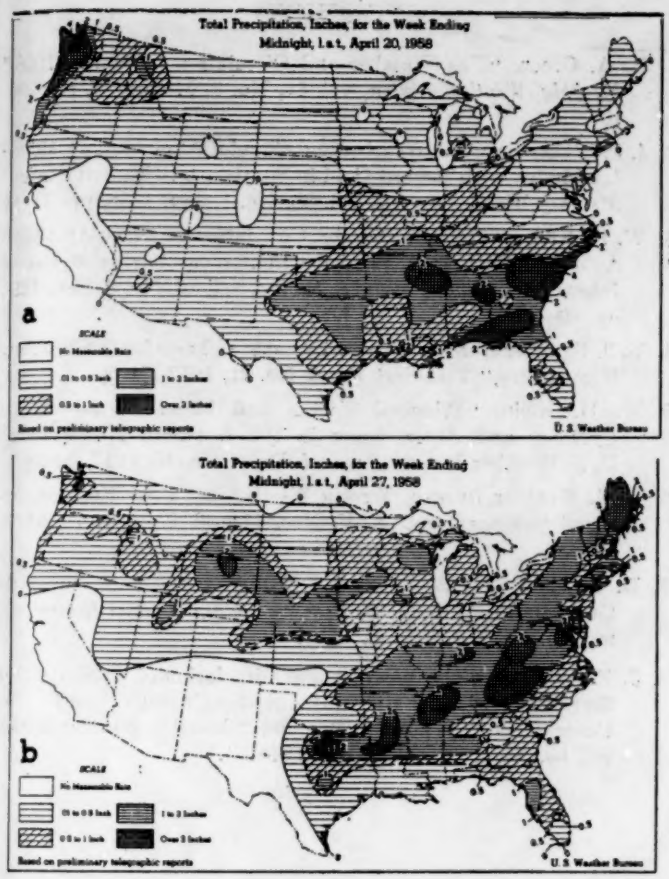

FIGURE 9.—Total precipitation, in inches, for: (a) April 15–21, 1958. Most of the precipitation was accounted for by one storm in the Gulf of Mexico early in the week and several frontal passages into the Pacific Northwest. (b) April 22–28, 1958. The pattern of areas of precipitation exceeding 1 inch has a fair correspondence with the areas of maximum cyclonic curvature on the 5-day mean chart for the same week (fig. 7c).

were basically responsible for the fairly strong advection of cold air into the northwestern third of the country. There must have been some dynamic cooling as the trough deepened, but this was probably of less significance than the advective cooling. Decreases in anomalous temperatures in the Northwest ranged as high as 16.3 F.° at Winnipeg, with changes in the 5°–10° category commonplace. The eastern third of the United States was dominated by widespread warming which was caused by the southerly DN flow and the advection of maritime tropical air in advance of the mean trough.

Further details of the circulation of April 16–30 can be seen by an examination of the weekly variability in that period. Figure 7b shows the 5-day mean 700-mb. circulation centered in the middle of the week ending April 21. In this instance the westerlies were quite strong north of 40° N., but rather flat and ill-defined in lower latitudes of the United States. The temperature pattern (fig. 8b) showed a remarkable reversal. About three-fourths of the country was flooded by normal and above normal temperatures with readings as high as 91° F. in South Dakota, while cooler air began to invade Washington. Residual cold air along the Gulf of Mexico kept temperatures there below normal, although less so than in the previous week.

Along with the general warming came a large area of light precipitation (fig. 9a). Heavy amounts were confined to the Pacific Northwest coast, following several frontal passages, and to the Southeast as a result of one Gulf storm early in the week.

Figure 7c is representative of the circulation for the last week of April. The change from the previous week's circulation was quite extreme. From the eastern Pacific to the central United States a strong meridional flow was observed, in contrast to the strong zonal flow of the previous week, as amplification in the eastern Pacific and western North America reached its maximum.

Explosive deepening in the Great Basin on the 22d and 23d was associated barotropically with the propagation of vorticity from the eastern Pacific and baroclinically with the strong thermal advection (for more details see [7]). It was followed by the coldest intrusion of Canadian air of the month. Some temperatures in the West fell as much as 12 F.° below normal (fig. 8c), where they had been as much as 9 F.° above normal the week before (fig. 8b). An example of the temperature gradient accompanying that storm, as reported by the *Weekly Weather and Crop Bulletin* [6], was the record high temperatures of 91° F. in eastern Kansas on the 23d, and a record minimum of 21° F. in northwestern Kansas on the 24th. Not as extreme, but indicative of the weekly variability, was the low of 31° F. at Roswell, N. Mex., on April 14 followed by a maximum of 91° F. on April 22 at the same city.

Cold air surging eastward as far as West Virginia toppled various minimum temperature records, while normal and above average temperatures were recorded in the East Coast States and in portions of the South and Southwest.

The week's precipitation is shown in figure 9b. Heavier accumulations were confined to the northern Rocky Mountain States and in a corridor extending from northern Texas to New England, while the Southwest was mostly dry. Rising flood stages were noted in parts of New England and the South, but serious flooding was not of major proportions this week.

The variability of temperature (and to some extent of precipitation) during the month was intimately related to the variability of the 700-mb. mean flow. The relationship of another group of phenomena, severe storms, will be considered next.

TORNADO ACTIVITY

The incidence of tornadoes in April 1958 (table 3) was significantly lower than that reported in April 1957. Since acceptable normals are not available, one cannot classify this month's tornado totals relative to normal. However, it may be of interest to briefly compare this year's April circulation (fig. 1) with that of April 1957 (fig. 8 of [8]). The positions of the central United States troughs were comparable, but the similarity ends there.

TABLE 3.—*Number of tornadoes and funnel clouds reported in the United States, January–April 1957 and 1958.**

Month	1957			1958		
	Tornadoes	Funnels	Total	Tornadoes	Funnels	Total
January	18	1	19	14	4	18
February	5	0	5	22	5	27
March	39	26	65	17	10	27
April	217	164	381	**85	**93	**178
Total	279	191	470	138	112	250

*Data tabulated by the U. S. Weather Bureau, Office of Climatology, Washington D.C.
**Preliminary totals.

In April 1957 a ridge some 200 feet above normal lay along the east coast. That ridge was accompanied by a strong southerly positive DN flow over the Midwest, a condition conducive to a mean influx of warm, moist, tropical air. The same area in April 1958 was dominated by below normal heights and did not have a southerly DN flow suggestive of extended intrusions of maritime tropical air into the Midwest.

It seems fairly clear that this year's decrease in tornado activity was effected by the persistent block in eastern Canada, a real deterrent to middle- and low-latitude ridging in the eastern United States.

REFERENCES

1. R. A. Green, "The Weather and Circulation of March 1958," *Monthly Weather Review*, vol. 86, No. 3, Mar. 1958, pp. 100–107.
2. J. F. O'Connor, "The Weather and Circulation of January 1958—Low Index with Record Cold in Southeastern United States," *Monthly Weather Review*, vol. 86, No. 1, Jan. 1958, pp. 11–18.
3. W. H. Klein, "The Weather and Circulation of February 1958—A Month With an Expanded Circumpolar Vortex of Record Intensity," *Monthly Weather Review*, vol. 86, No. 2, Feb. 1958, pp. 60–70.
4. U. S. Weather Bureau, "Normal Weather Charts for the Northern Hemisphere," *Technical Paper* No. 21, 1952, 74 pp.
5. W. H. Klein, "Principal Tracks and Mean Frequencies of Cyclones and Anticyclones in the Northern Hemisphere," U. S. Weather Bureau *Research Paper* No. 40, 1957, 60 pp.
6. U. S. Weather Bureau, *Weekly Weather and Crop Bulletin, National Summary*, vol. XLV, Nos. 14 and 17, Apr. 7 and 28, 1958.
7. R. F. Shaw and E. J. Joseph, "Rapid Cyclogenesis over the Great Basin, April 22–23, 1958," *Monthly Weather Review*, vol. 86, No. 4, Apr. 1958, pp. 141–146.
8. J. F. Andrews, "The Weather and Circulation of April 1957—A Stormy Month over the United States Characterized by Two Contrasting Temperature Regimes," *Monthly Weather Review*, vol. 85, No. 4, Apr. 1957, pp. 124–131.

RAPID CYCLOGENESIS OVER THE GREAT BASIN, APRIL 22–23, 1958

ROBERT F. SHAW AND ELLIS J. JOSEPH

National Weather Analysis Center, U. S. Weather Bureau, Washington, D. C.

1. INTRODUCTION

The 0000 GMT surface chart for April 22, 1958, gave the first indications of formation of a surface Low near Wendover, Utah, in the Great Basin. Just 12 hours later it was evident that a storm of major proportions was developing, for central pressure of the Low dropped 17 mb. and the circulation about the center extended over the entire western third of the Nation.

The variety of bad weather produced by this storm, particularly in its early stages, ranged from dust storms in the southern Great Plains to record-breaking snowstorms in the mountainous sections of Montana and Wyoming. Some details of the weather conditions and of record-breaking occurrences are given in section 5. The rapid development of the Low, however, was the most spectacular feature of this storm and this paper is primarily concerned with discussion of significant factors contributing to the cyclogenesis.

2. BROAD-SCALE FEATURES

Comparison of 500-mb. charts for 1200 GMT on April 20 and April 21 (figs. 1a, 1c) shows the remarkable change in the upper-air flow pattern over the eastern Pacific and Gulf of Alaska during one 24-hour period. The sequence of (1) essentially simple southwest flow, (2) a split in the westerlies with its resultant cutoff Low, and (3) repositioning of the major jet axis into a northwesterly current, is not uncommon in this area, but the brief period of time required for the complete transition is noteworthy. We shall show how the requisite factors for cyclogenesis in the western United States, though obscure at 1200 GMT on April 20, became apparent on the 1200 GMT charts of April 21.

Long-wave trough positions prior to April 20 were: (1) off the east coast of Asia, (2) near the 160° W. meridian, and (3) in the central United States. Average wavelength between troughs was 70° of longitude. A new long-wave trough position was established east of the Kamchatka Peninsula by the vigorous deepening of a short-wave trough which moved into that area. The resulting shorter wavelength between the Kamchatka trough and the trough at 160° W. necessitated readjustment of the long-wave trough positions downstream, with the Kamchatka trough acting as an "anchor trough."

Constant absolute vorticity trajectories were computed from points along the southwest flow on the east side of the Kamchatka trough. The average of these trajectories, when superimposed on the 500-mb. chart for 1200 GMT of the 20th (fig. 1a), suggested the "shear and reamalgamation" process for readjustment of the long-wave trough positions, with a new position established over the western United States in approximately 48 hours. This process has been discussed and illustrated by Namias [1]. "Overshooting" of the strong southwesterly winds from the Kamchatka trough [2] across the sharply curved contours of the central Pacific ridge produced an eastward shearing effect on the northern portion of the trough at 160° W. The northern branch of the westerlies consequently increased and cut off the lower portion of the trough. The southern branch of the westerlies weakened and eventually became restricted to circulation around the newly-formed cutoff Low. The 300-mb. jet-stream axes as shown in figures 1 and 2 clearly depict the changes in relative strength and position of the two branches of westerly flow.

The second half of the process, "reamalgamation," followed the breakthrough of the northern branch of the westerlies. The ridge over the Aleutians (fig. 1b) moved into the Gulf of Alaska in response to the advection of warmer air and anticylonic vorticity into this region, while similar advection occurred in southeasterly current which developed on the northeastern side of the cutoff Low (fig. 1d). Thus the two ridges, one from the west and the other from the south, combined to produce strong anticyclogenesis over the Gulf of Alaska.

With the elimination of the long-wave trough position at 160° W. through the process discussed above, the resulting wavelength between the Kamchatka long-wave trough and the long-wave trough in the central United States was in excess of the stationary value required by the Rossby wave formula, suggesting that a major readjustment of waves was necessary. This readjustment of the super-stationary wavelength was effected through what Cressman [3] terms "discontinuous retrogression." Comparison of the 0000 GMT 500-mb. charts for April 21, 22, and 23 (figs. 1b, 1d, and 2b) shows how the long-wave trough position, which was over the central United States, retrograded to the Plateau Region. The anticyclogenesis in the Gulf of Alaska, combined with the necessity for retrogression of the long-wave trough position from the central United States, provided a field of motion favorable for the plunging of a cyclonic vorticity maximum and associated pool of Arctic air from Alaska southeastward

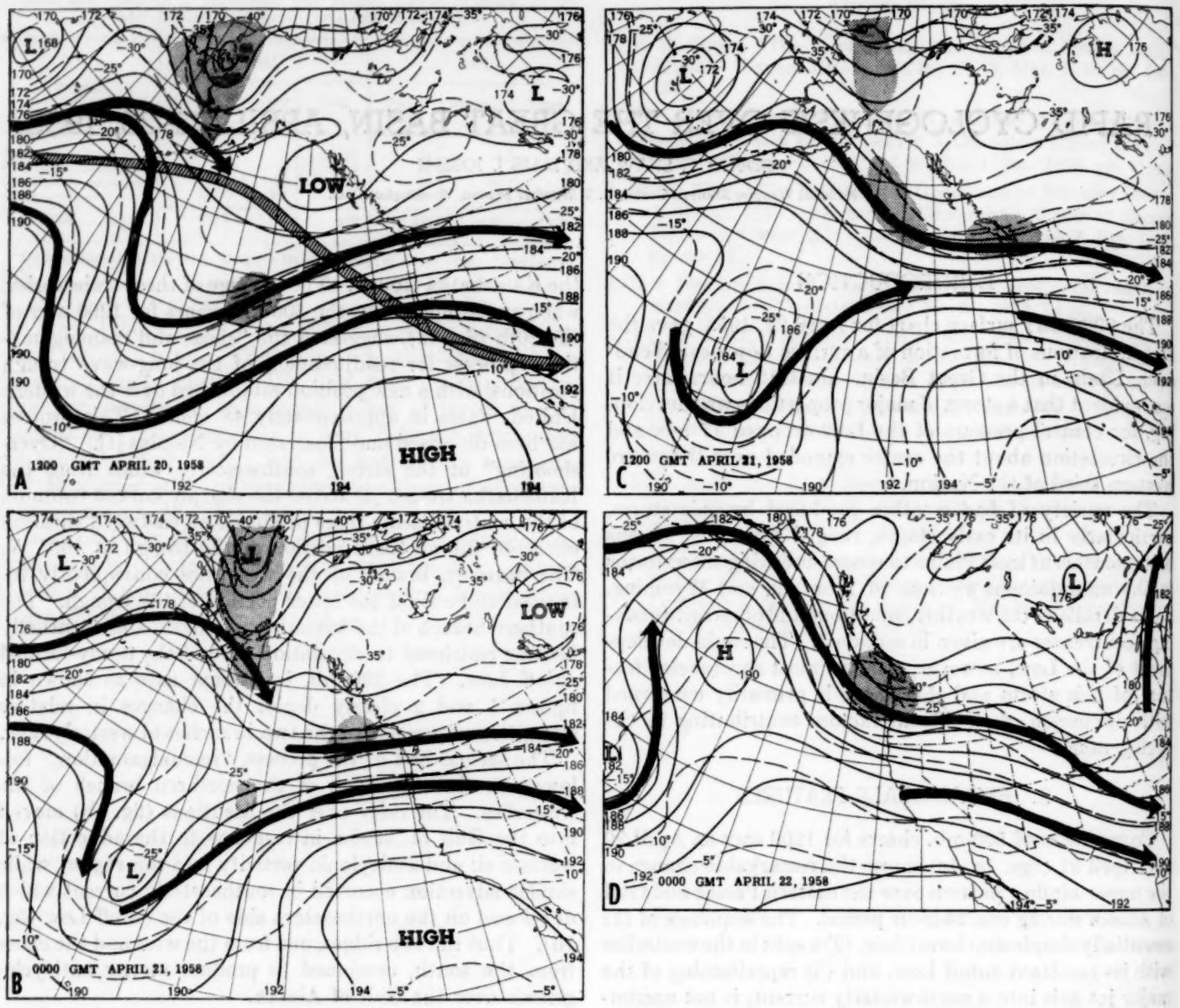

FIGURE 1.—500-mb. charts. (a) 1200 GMT, April 20, (b) 0000 GMT, April 21, (c) 1200 GMT, April 21, and (d) 0000 GMT, April 22, 1958. Contours (solid lines) at intervals of 200 geopotential feet; isotherms (dashed lines) at intervals of 5° C.; and areas of absolute vorticity (shaded) greater than 150 × 10^{-6} sec.$^{-1}$. 300-mb. jets denoted by heavy arrows. Hatched arrow in (a) represents average constant absolute vorticity trajectory.

into the Great Basin. In its broad-scale evolution, this situation was strikingly similar to the outbreak of Arctic air into the Pacific Northwest during November 1955 [4], [5].

3. VORTICITY CONSIDERATIONS

To show more clearly the source and development of the 500-mb. trough which preceded the surface development, the movement of areas of maximum cyclonic absolute vorticity at 500 mb. were tracked (fig. 3). Absolute vorticity charts were prepared by the Joint Numerical Weather Prediction Section of the National Meteorological Center for 12-hour intervals from 1200 GMT, April 20 through 0000 GMT, April 24. On the 500-mb. charts in figures 1 and 2, areas of absolute vorticity in excess of 150 x 10^{-6} sec. $^{-1}$ are shaded. The distribution of these vorticity maxima in the 500-mb. flow pattern shows quite plainly the movements and tendencies of the upper-air troughs associated with the surface cyclogenesis.

The apparent effect of the cyclonic vorticity maximum which moved northeastward out of the Pacific trough[1] was temporary retardation and flattening of the ridge building off the west coast. The short-wave trough in Alaska on April 21 moved southeastward into the portion

[1] In the following discussion the trough near 160° W. longitude will be referred to as the Pacific trough.

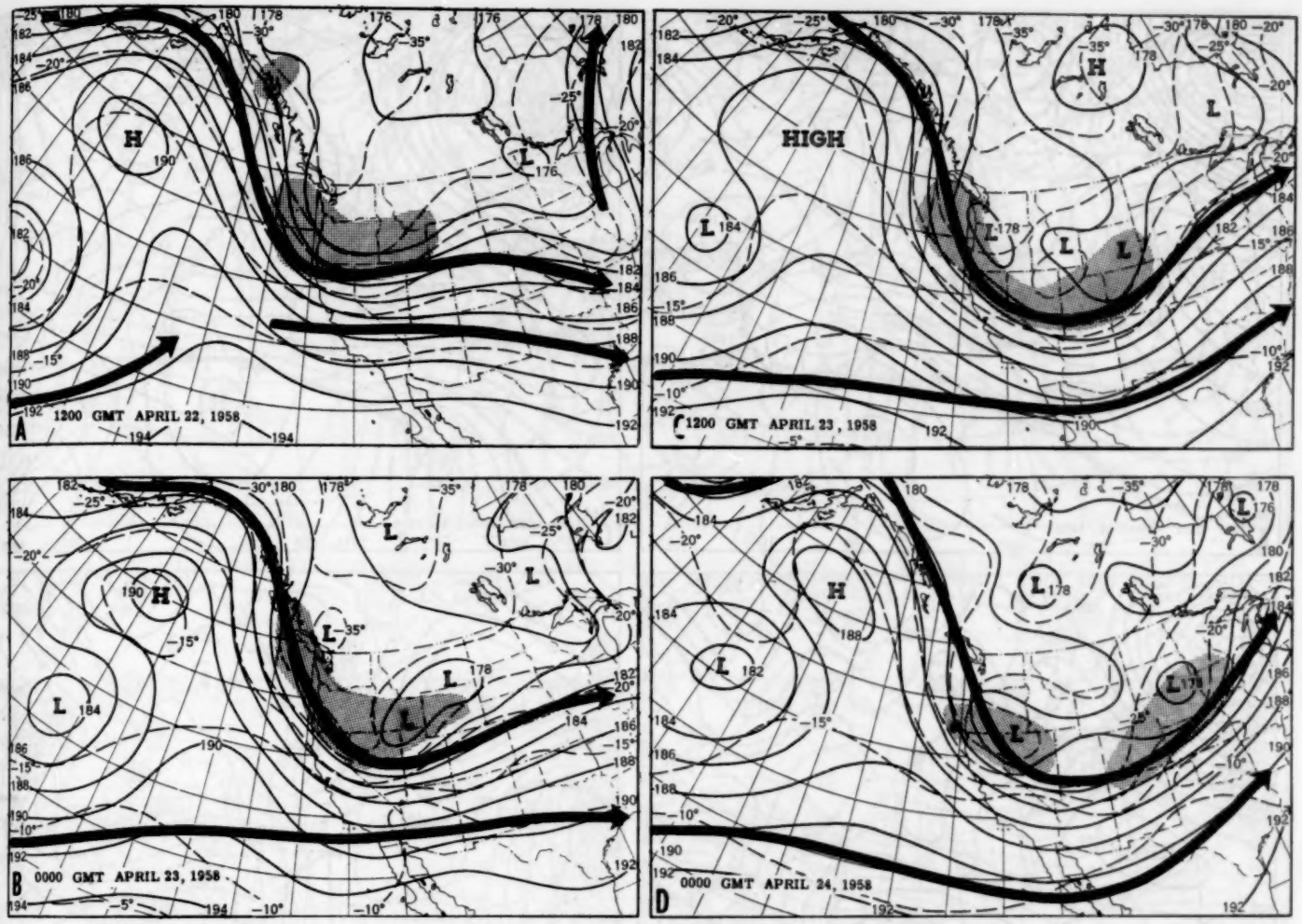

FIGURE 2.—500-mb. charts. (a) 1200 GMT, April 22, 1958. (b) 0000 GMT, April 23, (c) 1200 GMT, April 23, and (d) 0000 GMT, April 24. 300-mb. jets denoted by heavy arrows and areas of maximum absolute vorticity shaded.

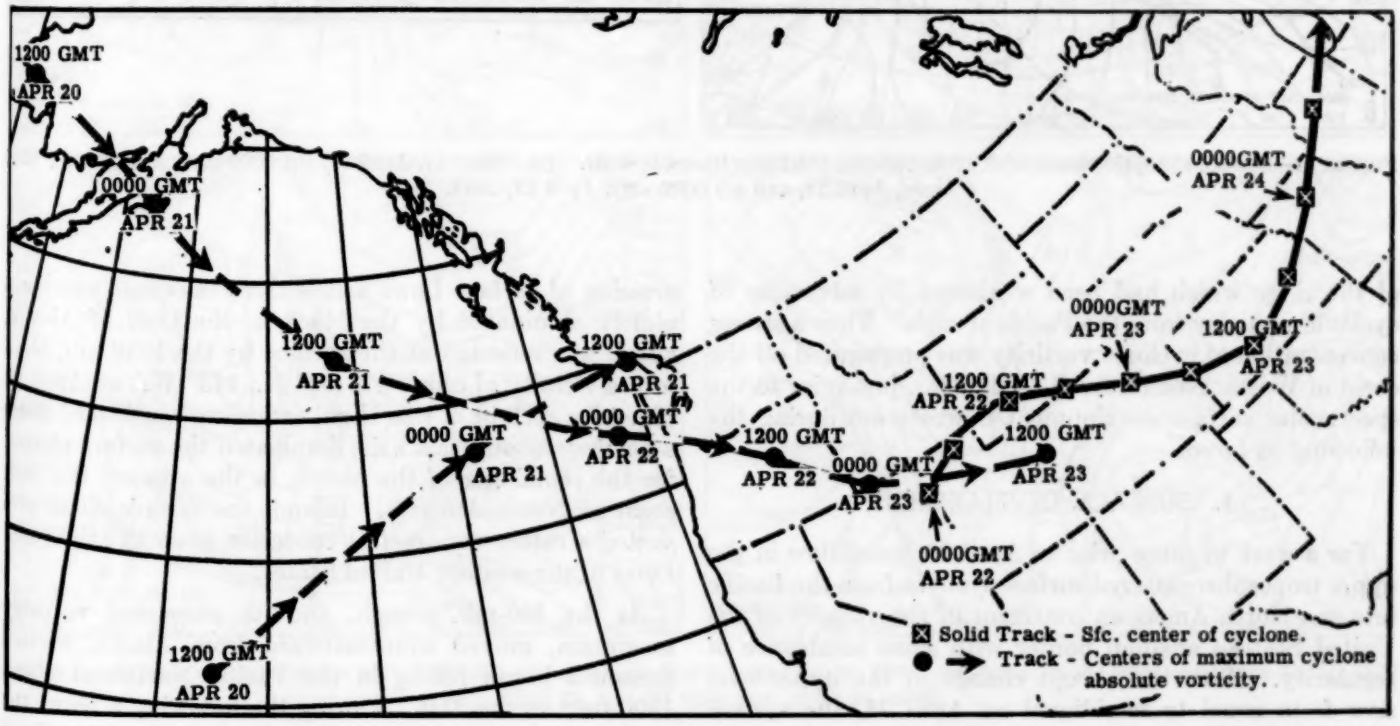
1200 GMT APR 20
0000 GMT APR 21
1200 GMT APR 21
0000 GMT APR 21
1200 GMT APR 21
0000 GMT APR 22
1200 GMT APR 22
0000 GMT APR 23
1200 GMT APR 20
0000GMT APR 24
0000GMT APR 23
1200 GMT APR 23
1200 GMT APR 22
1200 GMT APR 23
0000 GMT APR 23
0000GMT APR 22
Solid Track - Sfc. center of cyclone.
Track - Centers of maximum cyclone absolute vorticity.

FIGURE 3.—Tracks of centers of areas of maximum absolute vorticity (dashed lines), 1200 GMT, April 20 to 1200 GMT, April 23, 1958, and track of surface Low (solid line), 0000 GMT, April 22 to 0600 GMT, April 24, 1958.

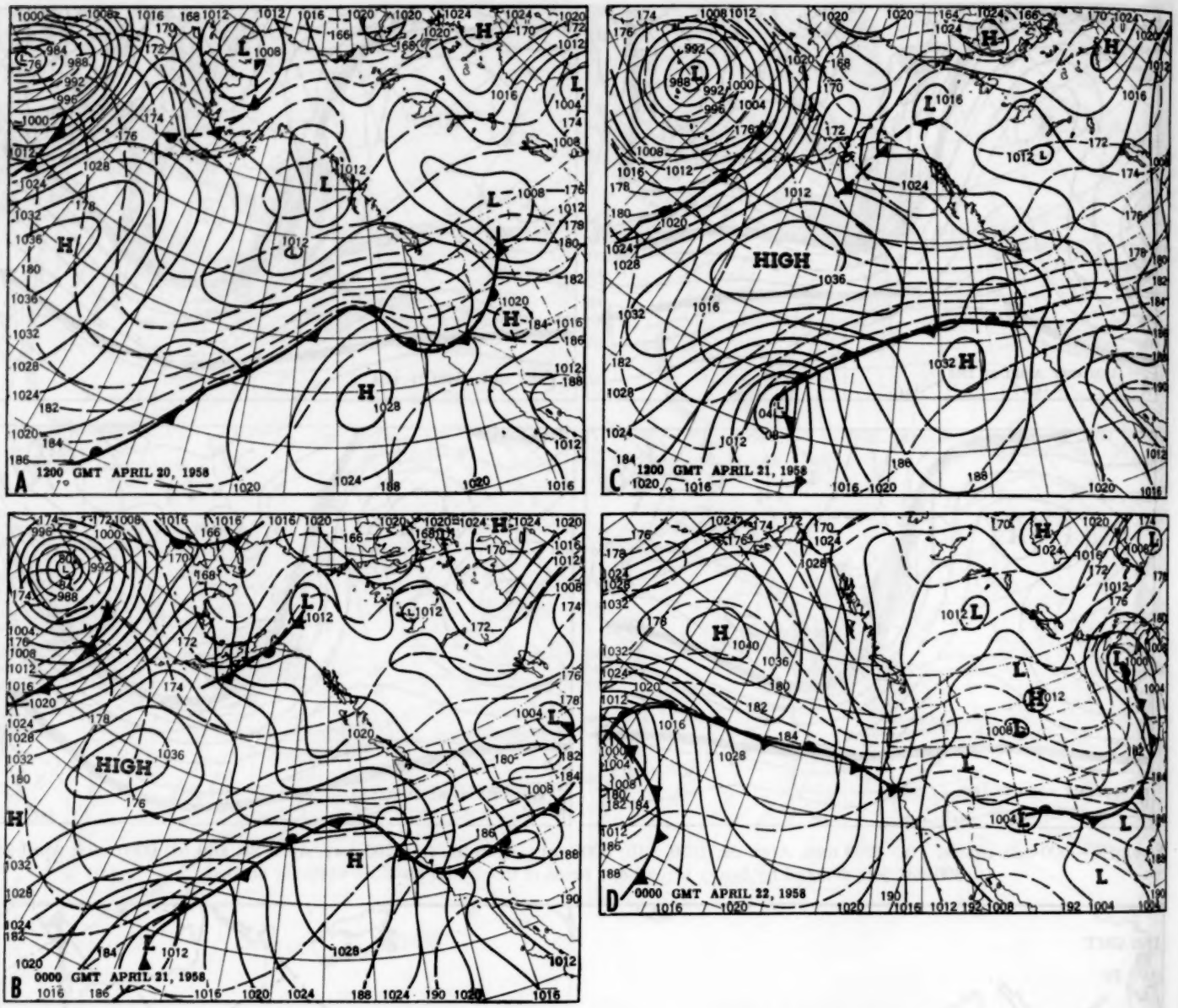

FIGURE 4.—Surface synoptic charts with 1000–500-mb. thickness lines (dashed). (a) 1200 GMT, April 20, (b) 0000 GMT, April 21, (c) 1200 GMT, April 21, and (d) 0000 GMT, April 22, 1958.

of the ridge which had been weakened by advection of cyclonic vorticity from the Pacific trough. Thus a strong concentration of cyclonic vorticity was propagated off the coast of Washington on April 22 (fig. 2a), just prior to the spectacular surface development downstream during the following 24 hours.

4. SURFACE DEVELOPMENT

For a week or more prior to April 20, zonal flow in the upper troposphere steered surface systems from the Pacific into the North American continent in the vicinity of the United States-Canadian border with some semblance of regularity. With the abrupt change in the upper-level flow from zonal to meridional on April 21, the surface picture also changed quite markedly (fig. 4). The progression of surface Lows across the west coast was completely eliminated by the block in the Gulf of Alaska, which was reflected at the surface by the 1040-mb. High in the vicinity of Ship "P" (50° N., 145° W.) on April 22 (fig. 4d). A lobe of this High, extending southward along a northwest-southeast axis, dominated the surface picture for the remainder of the month in the area off the west coast of North America. Inland, the surface chart presented a rather nondescript collection of small Highs and Lows in the western United States.

As the 500-mb. trough, and its associated vorticity maximum, moved southeastward from Alaska, surface pressures began falling in the Pacific Northwest about 1800 GMT on the 21st. During the following 6 hours the isallobaric fall center moved southeastward to the Great

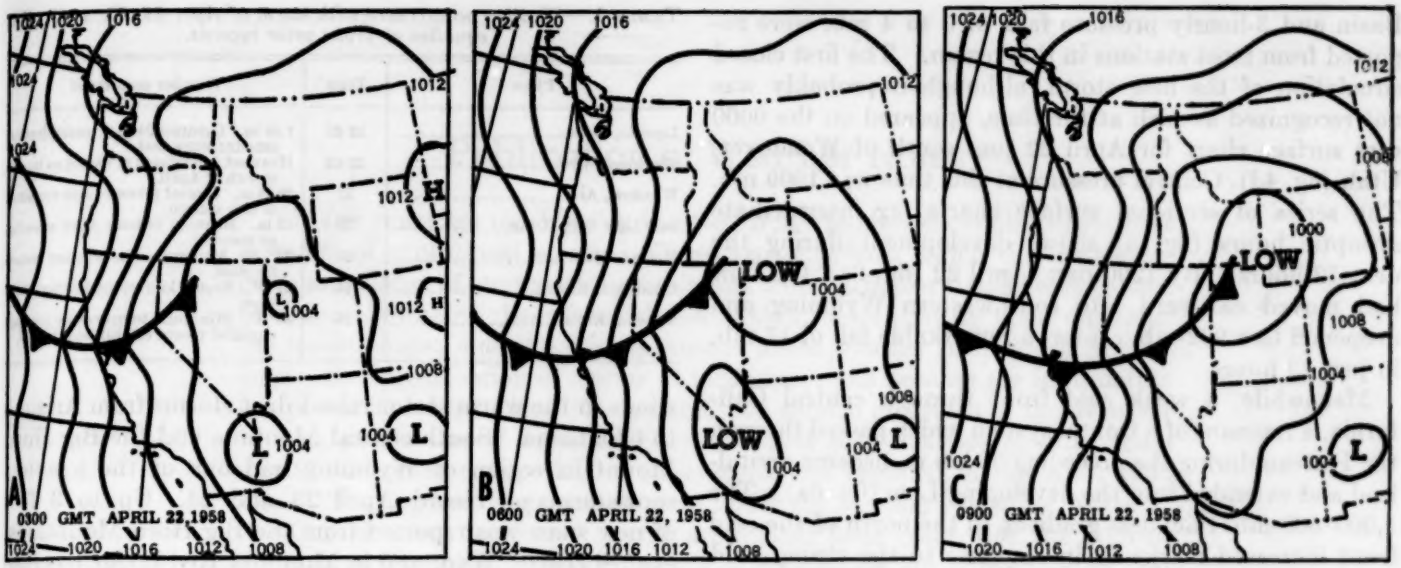

FIGURE 5.—Sectional surface synoptic charts. (a) 0300 GMT, April 22, (b) 0600 GMT, April 22, and (c) 0900 GMT, April 22, 1958.

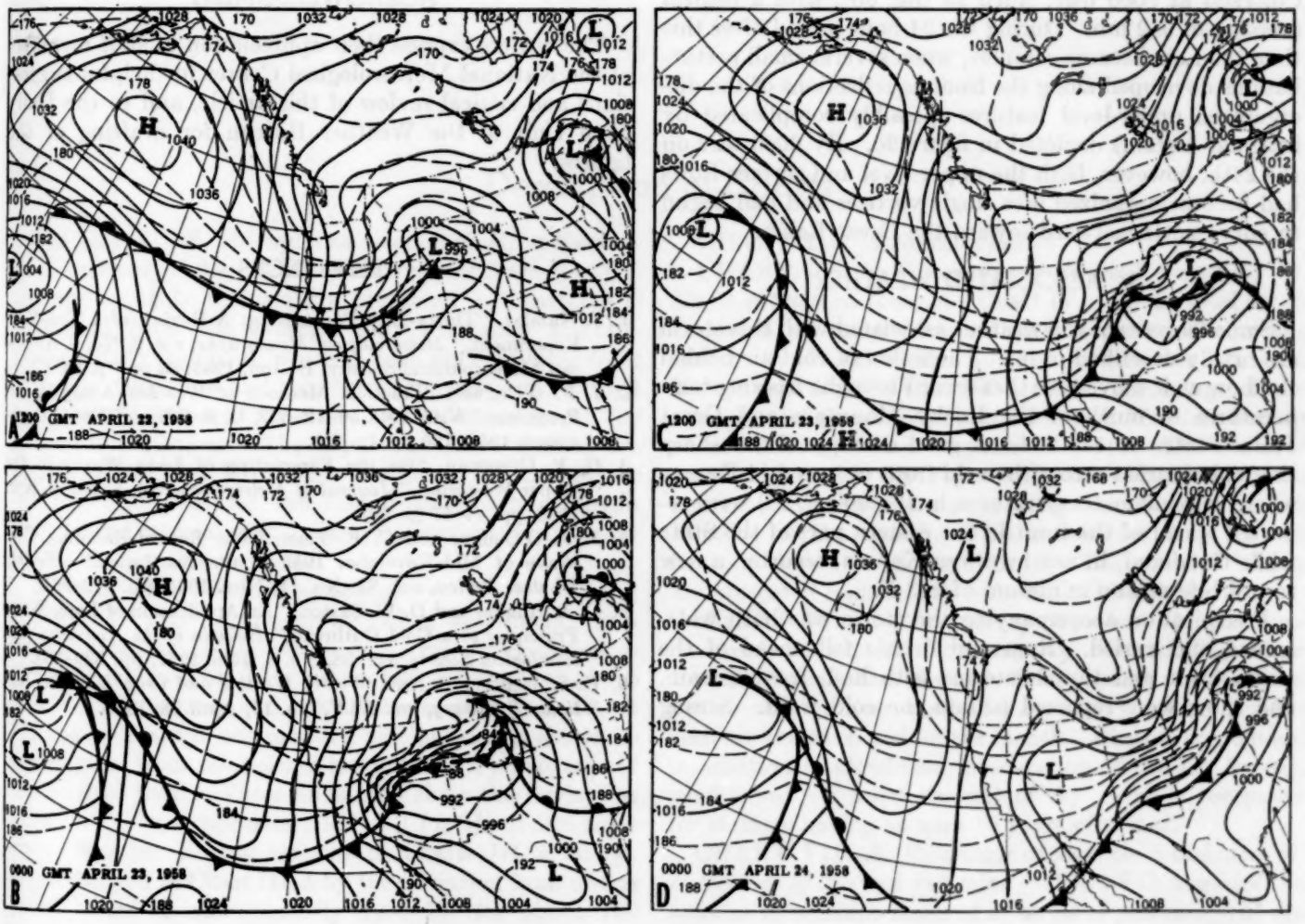

FIGURE 6.—Surface synoptic charts with 1000–500-mb. thickness lines (dashed). (a) 1200 GMT, April 22, (b) 0000 GMT, April 23, (c) 1200 GMT, April 23, and (d) 0000 GMT, April 24, 1958.

Basin and 3-hourly pressure falls of 3 to 4 mb. were reported from most stations in this region. The first closed circulation of the new storm, although it probably was not recognized as such at the time, appeared on the 0000 GMT surface chart for April 22 just south of Wendover, Utah (fig. 4d). Central pressure at this time was 1009 mb. The series of sectional surface charts for intermediate synoptic hours (fig. 5) shows development during the next 12 hours. By 1200 GMT, April 22 (fig. 6a), the Low had moved eastward into southwestern Wyoming and deepened to a 992-mb. center, a remarkable fall of 17 mb. in just 12 hours.

Meanwhile, a weak cold front through central California, a remnant of a frontal system which passed through the Plateau during the preceding 36 hours, became revitalized and extended into the developing Low (fig. 6a). The 1,000–500-mb. thickness gradient to the north of the cold front increased markedly in response to the strong cold air advection associated with the deepening upper trough. The sharp discontinuity of the thickness gradient across the front is shown very well in figures 6a-d.

The storm attained its greatest development in eastern Colorado at 0000 GMT, April 23 (fig. 6b), with a central pressure of 982 mb. During the 24-hour period after this time the Low became complex, when several small perturbations developed along the front as reflections of the disorganized upper-level features (possibly complicated by irregular terrain) depicted in figure 2c. By 0000 GMT on the 24th, however, both the upper-level and surface Lows had become organized into single vortices and had begun to curve northeastward toward the Great Lakes.

5. ASSOCIATED WEATHER

Some features of the weather associated with this storm are briefly described in [6]. The influx of cold air behind the Low as it moved northeastward brought freezing temperatures to much of the Rocky Mountain and Great Plains States on the 23d. A good example of the sharp thermal contrast across the cold front occurred in Kansas where maximum temperatures in the 90's (° F.) were reported ahead of the front in the eastern part of the State while Goodland, in northwestern Kansas, reported a new record late season minimum of 21° F.

Precipitation accompanying the storm was both widespread and varied. Rain and drizzle fell ahead of the warm front and thunderstorms with hail, freezing rain, and snow were reported behind the cold front. Strong winds in the warm sector raised dust storms from Arizona to Oklahoma. South-central Montana and the Big Horn Mountain region of Wyoming had one of the heaviest snowstorms on record April 23 and 24. Up to 3 feet of new snow was reported from the Big Horn Mountains, near Sheridan, Wyo., and in Montana, Red Lodge received 55 inches, and Nye and Mouat Mine 60 inches.

TABLE 1.—*Weather occurrences with storm of Apr. 22–23, 1958, that equalled or broke prior records.*

Place	Date	Weather occurrence
Lincoln, Nebr.	22–23	1.38 in. Greatest 24-hour precipitation amount since 1944.
Sheridan, Wyo.	22–23	Heaviest snowstorm of record so late in month of April.
Winslow, Ariz.	23	29.19 in. Lowest pressure ever recorded at this station.
Salt Lake City, Utah.	23	15 in. Heaviest 24-hour April snowfall on record.
Helena, Mont.	24	20° F. Minimum temperature record for date.
Goodland, Kans.	24	21° F. Record late season low temperature.
Topeka, Kans.	25	36° F. Minimum temperature for date equalled record established in 1907.

Table 1 lists weather occurrences with this storm that equalled or broke prior records.

ACKNOWLEDGMENT

The writers express their appreciation to staff members of the National Meteorological Center for helpful suggestions and critical review of this article, and to the Daily Map Unit of the Weather Bureau for drafting of the figures.

REFERENCES

1. J. Namias, "Thirty-Day Forecasting: A Review of a Ten-Year Experiment," *Meteorological Monographs*, vol. 2, No. 6, American Meteorological Society, Boston, 1953, 83 pp. (p. 61–62).
2. J. F. O'Connor, "Practical Methods of Weather Analysis and Prognosis," *NAVAER* 50–1P–502, U. S. Office of Naval Operations, 1952, 126 pp. (p. 81).
3. G. P. Cressman, "On the Forecasting of Long Waves in the Upper Westerlies," *Journal of Meteorology*, vol. 5, No. 2, Apr. 1948, pp. 44–57 (p. 53).
4. J. F. O'Connor and C. R. Fean, "The Record-Breaking Cold Wave of Mid-November 1955 in the Northwest," *Monthly Weather Review*, vol. 83, No. 11, Nov. 1955, pp. 279–291.
5. L. A. Hughes and D. W. Saxton, "An Application of Long-Wave Principles to a Cold Outbreak," *Bulletin of the American Meteorological Society*, vol. 38, No. 6, June 1957, pp. 329–334.
6. U. S. Weather Bureau, *Weekly Weather and Crop Bulletin, National Summary*, vol. XLV, No. 17, April 28, 1958.

Publication of Weather Notes

Many years ago the *Monthly Weather Review* published detailed eyewitness accounts of exceptional storms. These accounts both enrich the meteorologist's knowledge of storms and provide him with particular details that cannot be found elsewhere. Because such information bears directly upon questions the meteorologist must attempt to answer about weather phenomena (for example, the identification of storms as tornadoes), and because the information has potential value in both the research and service programs of the Weather Bureau, publication of eyewitness accounts and brief analyses of exceptional storms and other meteorological phenomena was resumed in the April 1955 issue. They appear from time to time under the heading "Weather Notes."

Contributions to these "Notes" are invited from readers of the *Review*. There is no limitation placed on length of description but it is expected that most will be short accounts. Any weather peculiarities, whether storms or other phenomena, are acceptable subject matter. Material should be addressed to Editor, Monthly Weather Review, U. S. Weather Bureau, Washington 25, D. C.

Description of Charts

CHART I. *A. Average Temperature (° F.) at Surface. B. Departure of Average Temperature from Normal.*—The average monthly temperature presented in Chart I-A is computed from the average daily maximum and the average daily minimum which in turn are computed from the daily maximum and minimum temperatures reported by some 225 first-order Weather Bureau stations and 700 cooperative stations. The departures from normal are presented in Chart I-B. They are based on the 30-year normals (1921–50) for the first-order Weather Bureau stations and on means of 25 years or more (mostly 1931–55) for the cooperative stations.

CHART II. *Total Precipitation.*—

CHART III. *A. Departure of Precipitation from Normal (inches). B. Percentage of Normal Precipitation.*—Chart II is based on daily precipitation records at about 800 Weather Bureau and cooperative stations. In Chart III the anomaly in the month's precipitation is shown as a departure from the normal total and as a percentage of the normal total. These anomalies show the deviations from the 30-year normals (1921–50) for about 225 first-order Weather Bureau stations in Charts III A and B, supplemented in Chart III-A by the deviation from means of 25 years or more (mostly 1931–55) for about 700 cooperative stations.

CHART IV. *Total Snowfall.*—

CHART V. *A. Percentage of Normal Snowfall. B. Depth of Snow on Ground.*—Chart IV gives the total depth in inches of unmelted snowfall as reported during the month by Weather Bureau and cooperative stations. This is converted in Chart V-A into a percentage of the normal total amount computed for each Weather Bureau station having at least 10 years of record. The depth of snow on ground is that reported by both Weather Bureau and cooperative stations as of 7:00 a. m. EST on the last Monday of the month. This is reported only for the months December through April. The snowfall charts are presented each month November through April.

CHART VI. *A. Percentage of Sky Cover Between Sunrise and Sunset. B. Percentage of Normal Sky Cover Between Sunrise and Sunset.*—These charts are based on visual observations made hourly at Weather Bureau stations and averaged for the month. Sky cover includes, in addition to cloudiness, obscuration of the sky by fog, smoke, etc. Normal amount of sky cover is computed for stations having at least 10 years of record.

CHART VII. *A. Percentage of Possible Sunshine. B. Percentage of Normal Sunshine.*—Chart VII-A shows the amount of sunshine received in terms of percentage of the total hours of sunshine possible during the month. In

Chart VII-B this is shown as a percentage of the normal number of hours of sunshine received; normals are computed for Weather Bureau stations having at least 10 years of record.

CHART VIII. *Average Daily Values of Solar Radiation, Direct and Diffuse.*—Plotted on the chart are the monthly means of daily total solar radiation, both direct and diffuse, in langleys (gm. cal. $cm.^{-1}$) for all Weather Bureau stations which record this element. Supplementary data, for which limits of accuracy are wider than for those data shown, are drawn upon in making the analysis. The inset shows the percentages of the mean based on the period 1951–55.

CHART IX. *Tracks of Centers of Anticyclones at Sea Level.*—

CHART X. *Tracks of Centers of Cyclones at Sea Level.*—Centers which can be identified for 24 hours or more are tracked in these charts. Semi-permanent features such as the Great Basin and Pacific Highs and Colorado and Mexico Lows are not shown. The 7:00 a.m. EST positions are shown by open circles, with the intermediate positions at 6-hour intervals shown by solid dots. The date is given above the circle and the central pressure to whole millibars below. A dashed track indicates a regeneration rather than actual movement to the next position. Solid square indicates position of stationary center for period shown beside it.

CHART XI. *Average Sea Level Pressure (mb.) and Surface Windroses.*—The average monthly sea level pressure is obtained from the averages of the 7:00 a.m. and 7:00 p.m. EST pressures reported at Weather Bureau stations. Windroses are based on the hourly wind directions (to 16 points of the compass) reported by Weather Bureau stations, each circle or arc indicating 5 percent of the time. The inset shows the departure of the average pressure from the normal average computed for each station having at least 10 years record and for each 10° intersection in a diamond grid over the oceans from interpolated values read from the Historical Weather Maps for the 20 years of best coverage prior to 1940.

CHARTS XII–XVII. *Average Height, Temperature, and Resultant Winds, 850, 700, 500, 300, 200, and 100 mb.*—Height is given in geopotential meters and temperature in degrees Celsius. These are the averages of the 1200 GMT radiosonde reports. Wind speeds are given in knots; flag represents 50 knots, full feather 10 knots, and half feather 5 knots. Directions are shown to 360° of the compass. Winds are based on rawins at 1200 GMT.

NOTE. Tabulations of exact values of most of these charted elements for Weather Bureau stations are printed each month in *Climatological Data—National Summary*, and annual averages are presented in the Annual Issue of that publication each year.

U. S. GOVERNMENT PRINTING OFFICE: 1958

Chart I. A. Average Temperature (°F.) at Surface, April 1958.

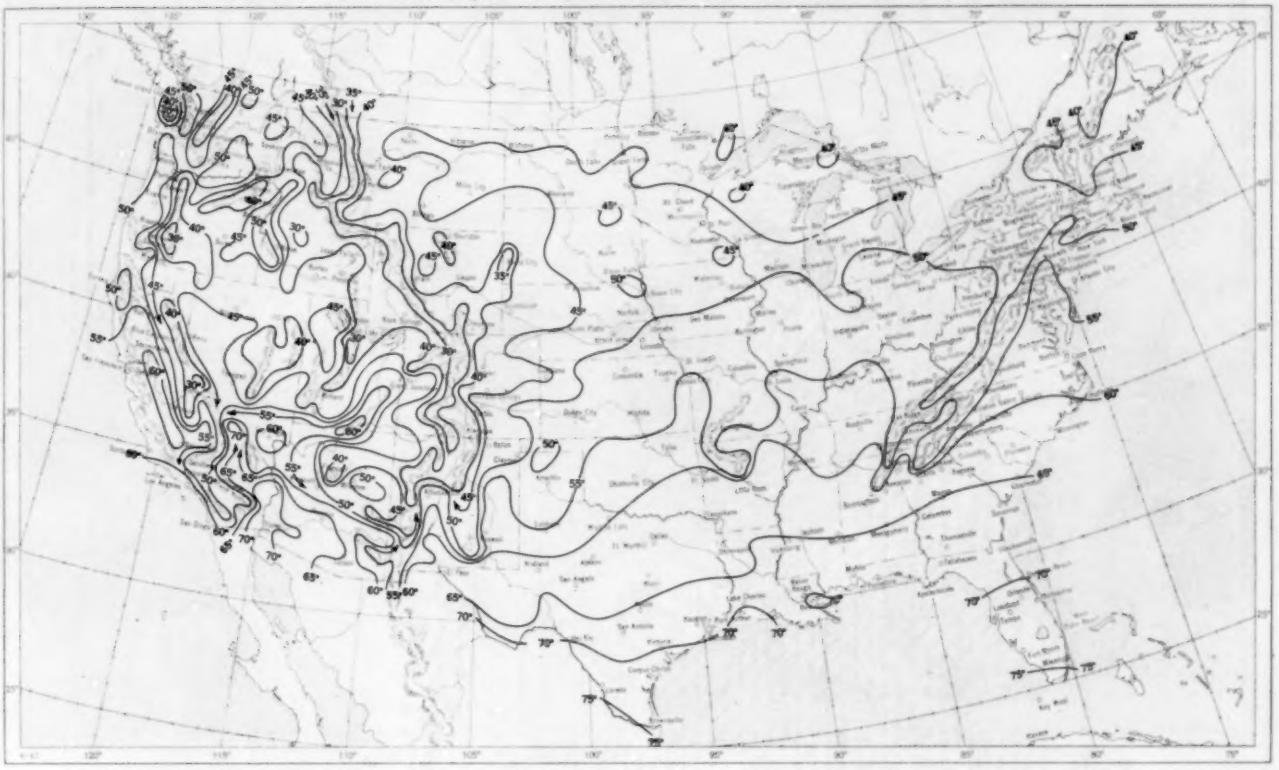

B. Departure of Average Temperature from Normal (°F.), April 1958.

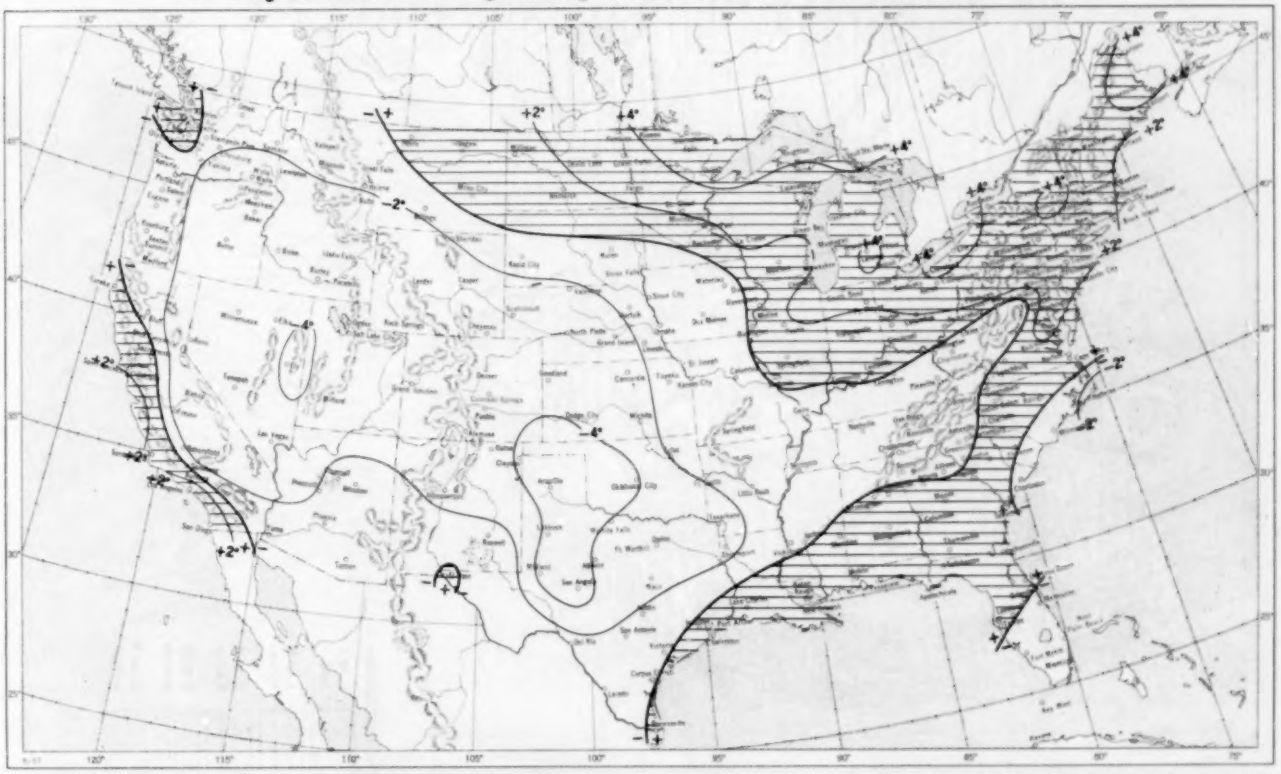

A. Based on reports from over 900 Weather Bureau and cooperative stations. The monthly average is half the sum of the monthly average maximum and monthly average minimum, which are the average of the daily maxima and daily minima, respectively.

B. Departures from normal are based on the 30-yr. normals (1921-50) for Weather Bureau stations and on means of 25 years or more (mostly 1931-55) for cooperative stations.

Chart II. Total Precipitation (Inches), April 1958.

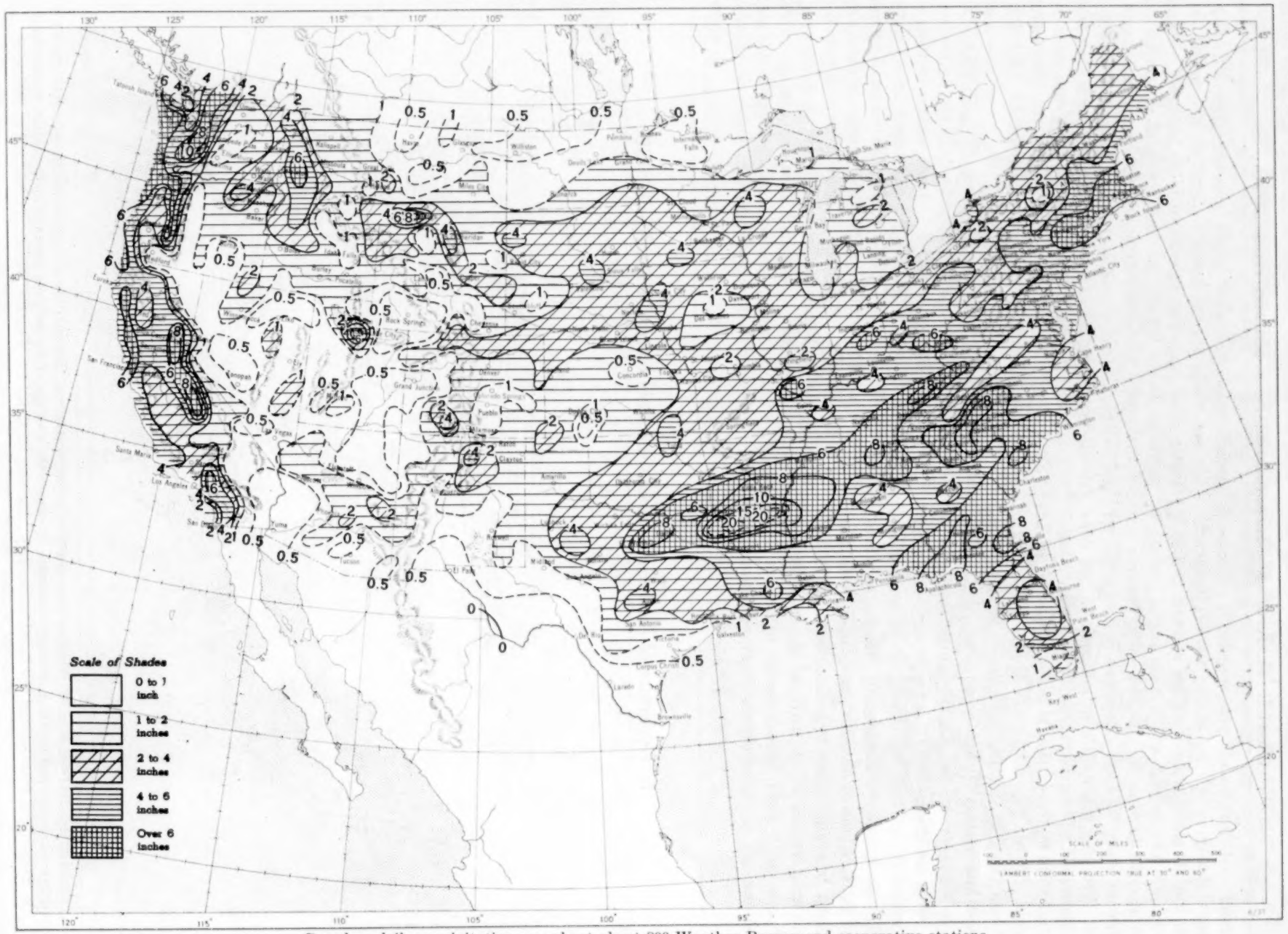
Scale of Shades
0 to 1 inch
1 to 2 inches
2 to 4 inches
4 to 6 inches
Over 6 inches
SCALE OF MILES
LAMBERT CONFORMAL PROJECTION, TRUE AT 30° AND 60°

Based on daily precipitation records at about 800 Weather Bureau and cooperative stations.

Chart III. A. Departure of Precipitation from Normal (Inches), April 1958.

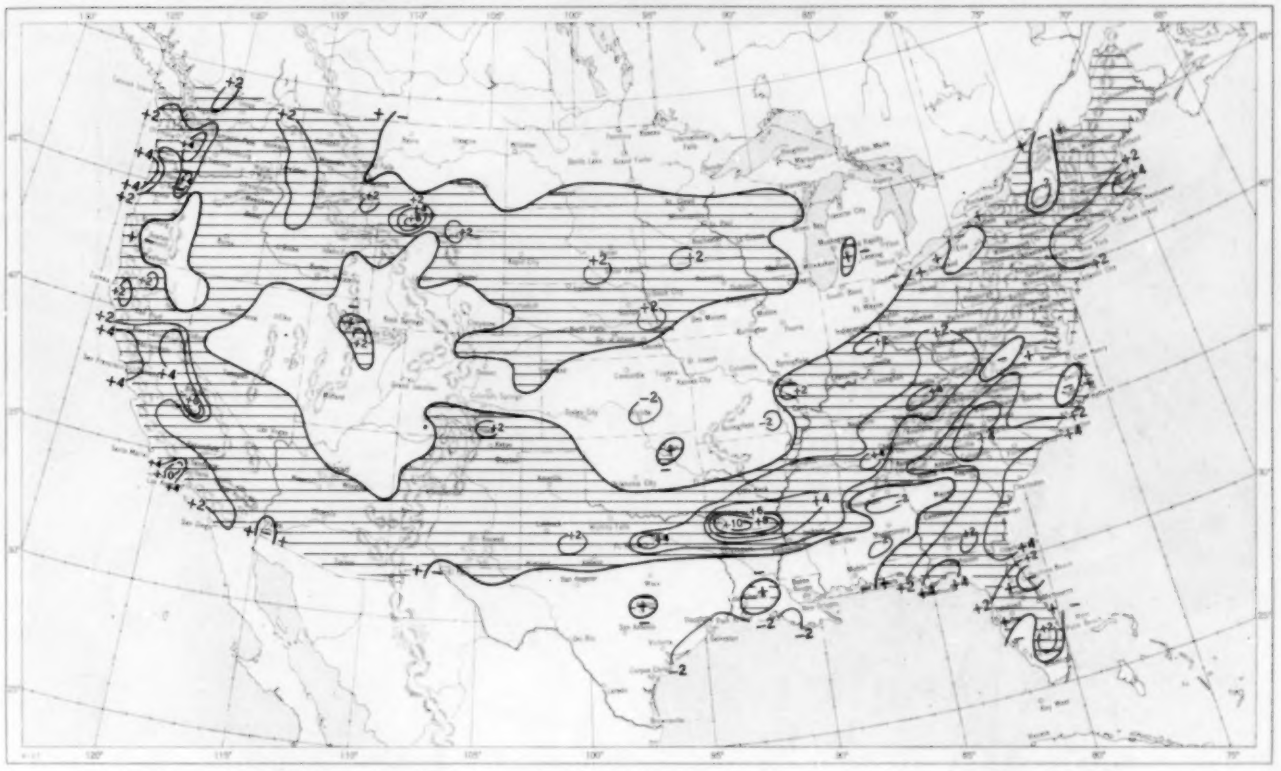

B. Percentage of Normal Precipitation, April 1958.

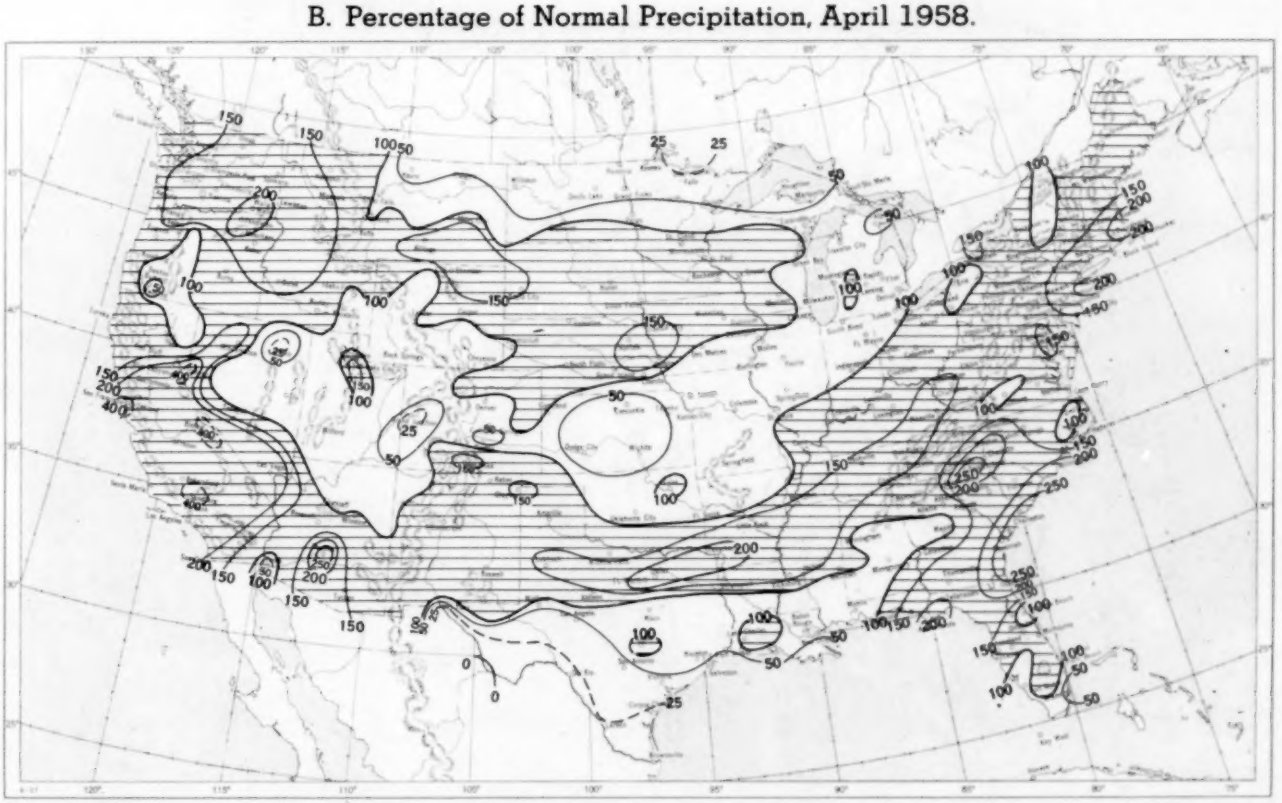

Normal monthly precipitation amounts are computed from the records for 1921-50 for Weather Bureau stations and from records of 25 years or more (mostly 1931-55) for cooperative stations.

Chart IV. Total Snowfall (Inches), April 1958.

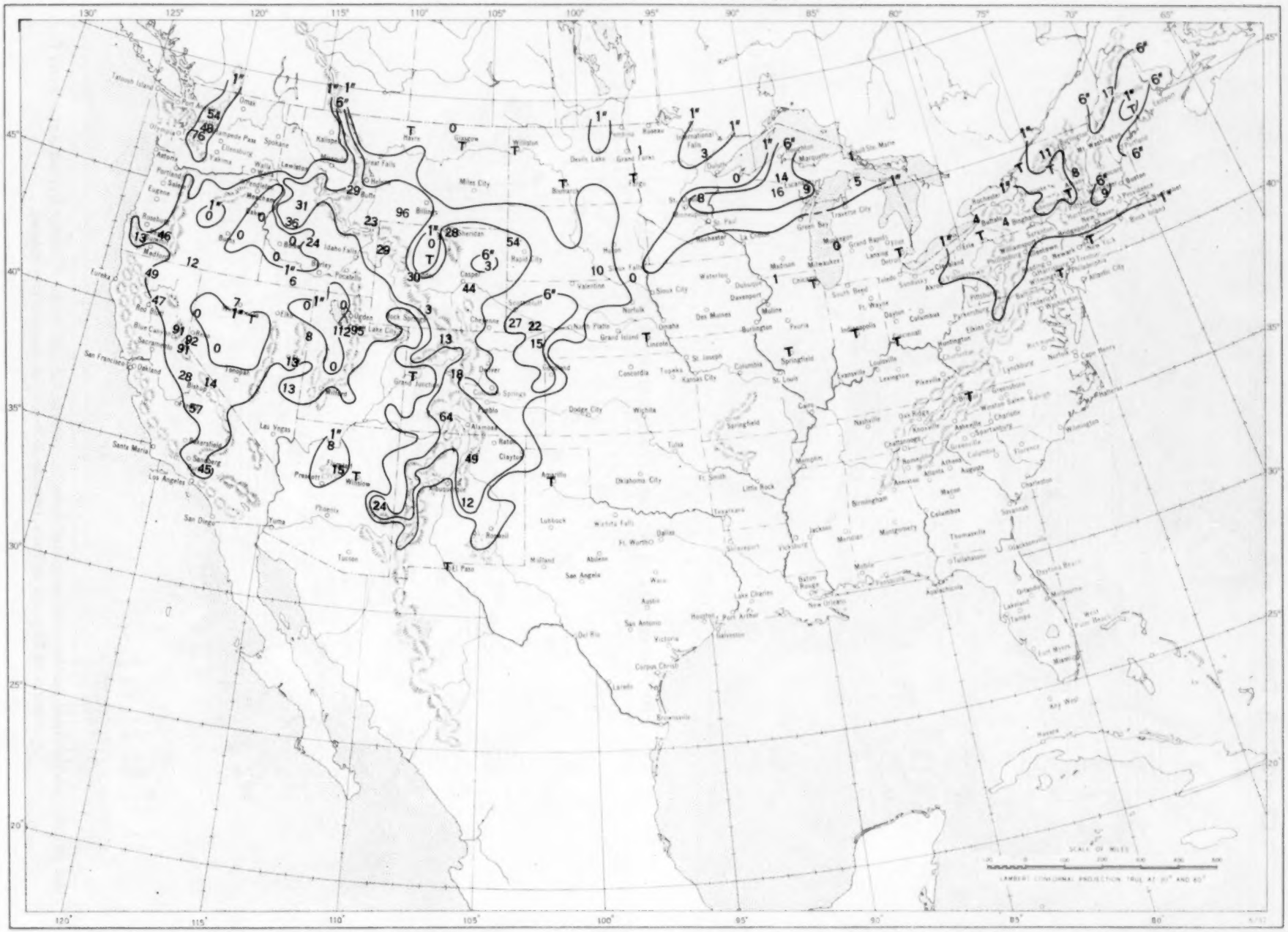

This is the total of unmelted snowfall recorded during the month at Weather Bureau and cooperative stations. This chart and Chart V are published only for the months of November through April although of course there is some snow at higher elevations, particularly in the far West, earlier and later in the year.

Chart V. A. Percentage of Normal Snowfall, April 1958.

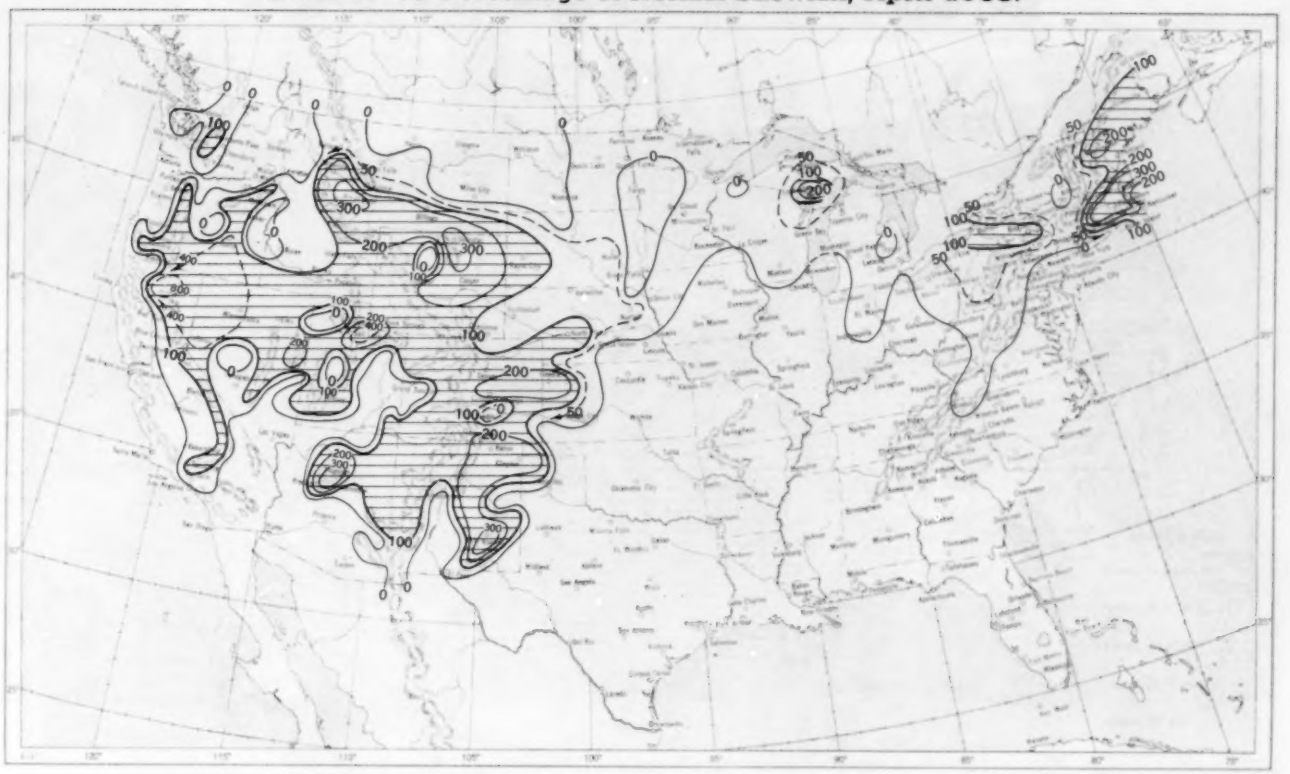

B. Depth of Snow on Ground (Inches)

A. Amount of normal monthly snowfall is computed for Weather Bureau stations having at least 10 years of record.
B. Shows depth currently on ground at 7:00 a.m. E.S.T., of the Monday nearest the end of the month. It is based on reports from Weather Bureau and cooperative stations. Dashed line shows greatest southern extent of snowcover during month.

Chart VI. A. Percentage of Sky Cover Between Sunrise and Sunset, April 1958.

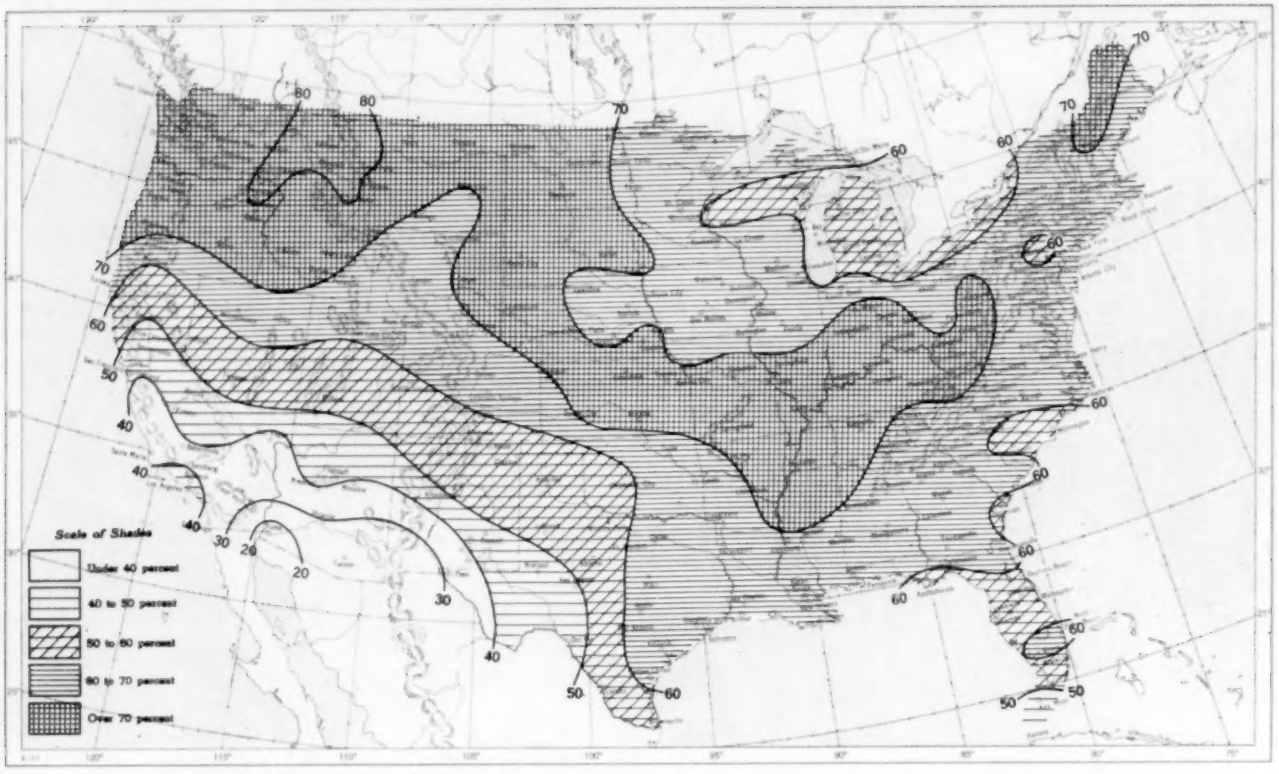

B. Percentage of Normal Sky Cover Between Sunrise and Sunset, April 1958.

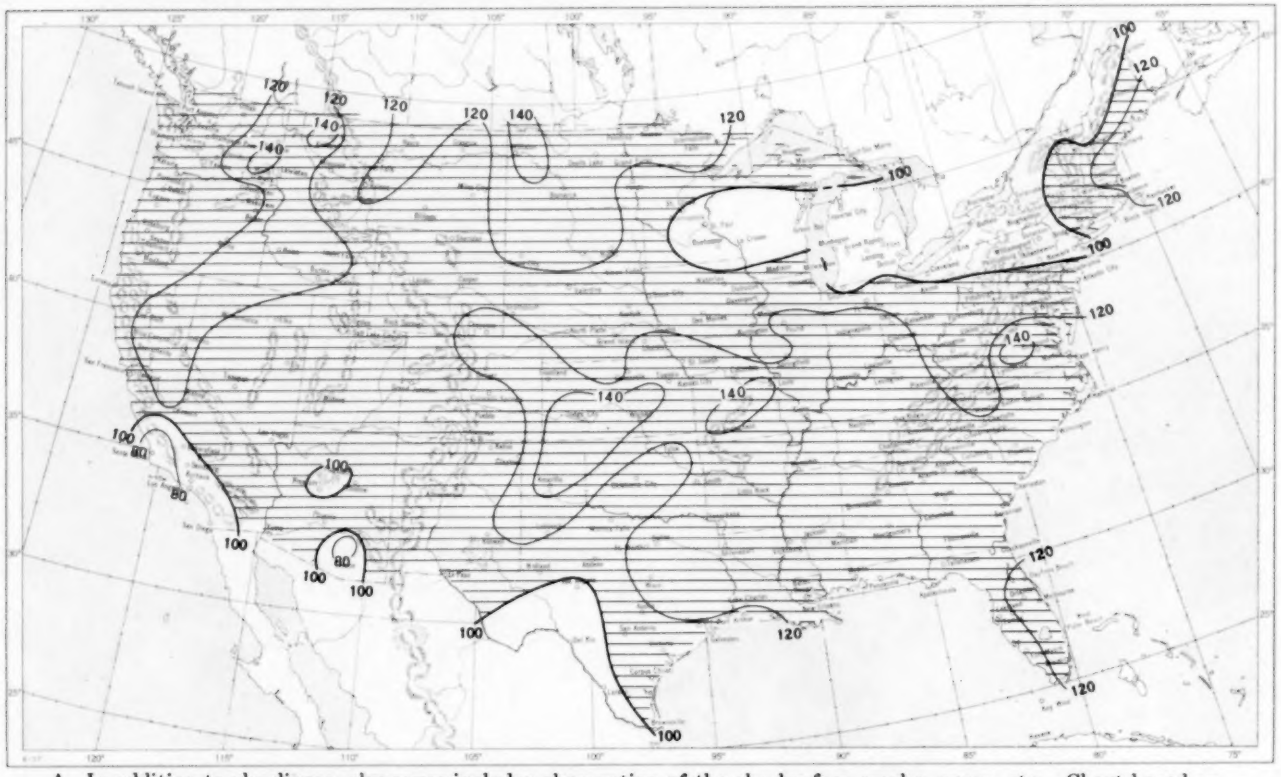

A. In addition to cloudiness, sky cover includes obscuration of the sky by fog, smoke, snow, etc. Chart based on visual observations made hourly at Weather Bureau stations and averaged over the month. B. Computations of normal amount of sky cover are made for stations having at least 10 years of record.

Chart VII. A. Percentage of Possible Sunshine, April 1958.

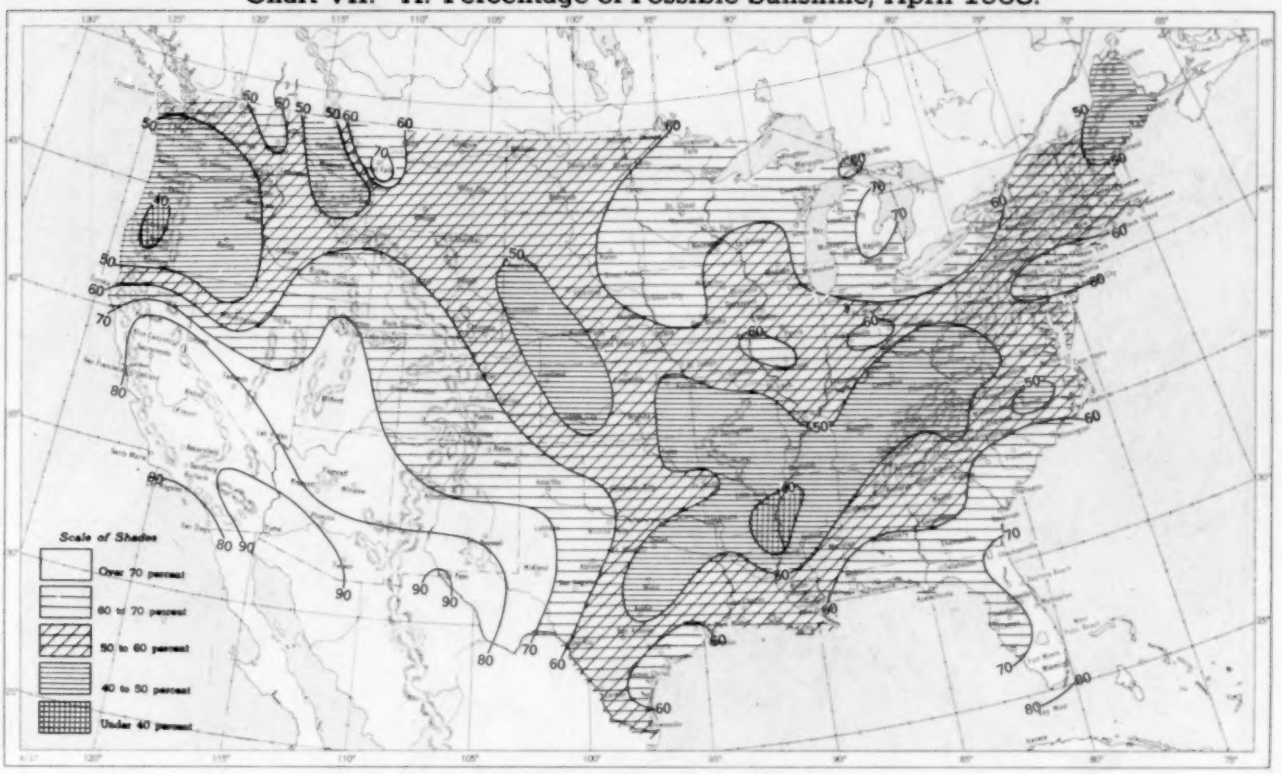

B. Percentage of Normal Sunshine, April 1958.

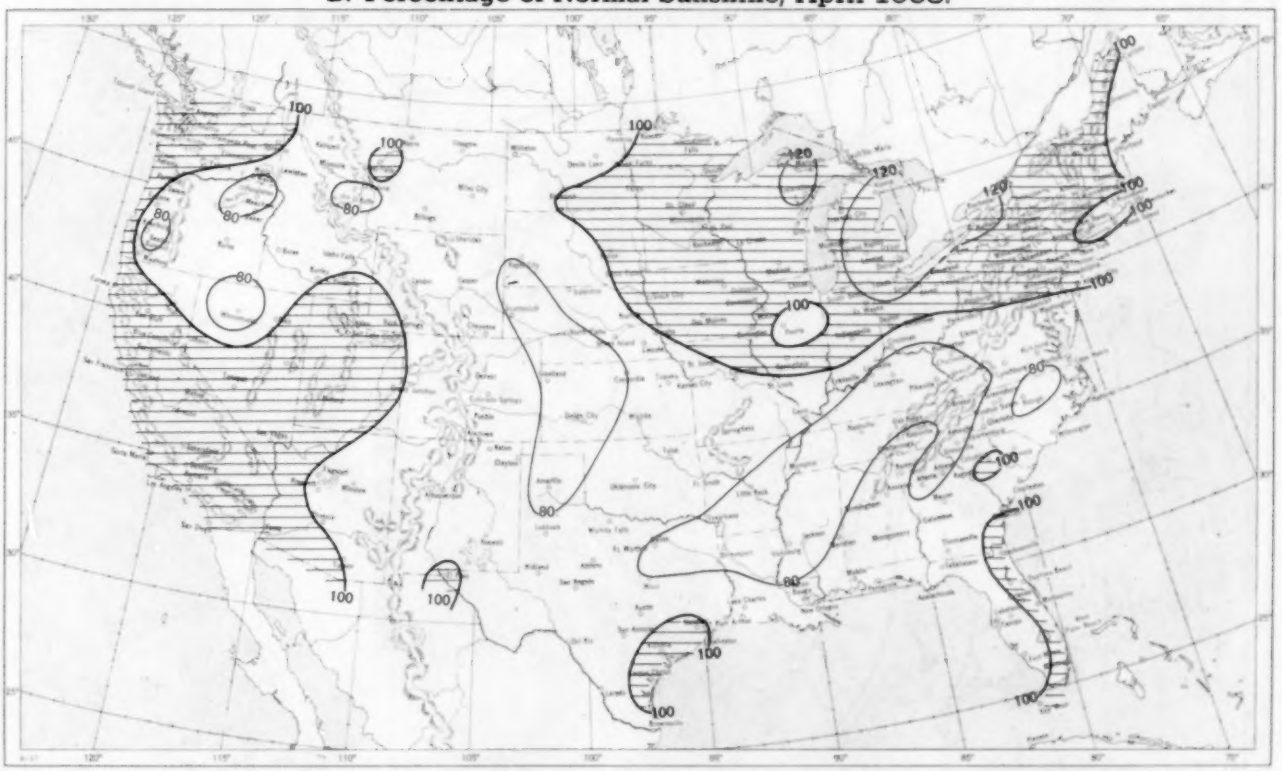

A. Computed from total number of hours of observed sunshine in relation to total number of possible hours of sunshine during month. B. Normals are computed for stations having at least 10 years of record.

Chart VIII. Average Daily Values of Solar Radiation, Direct + Diffuse, April 1958. Inset: Percentage of Mean Daily Solar Radiation, April 1958. (Mean based on period 1951-55.)

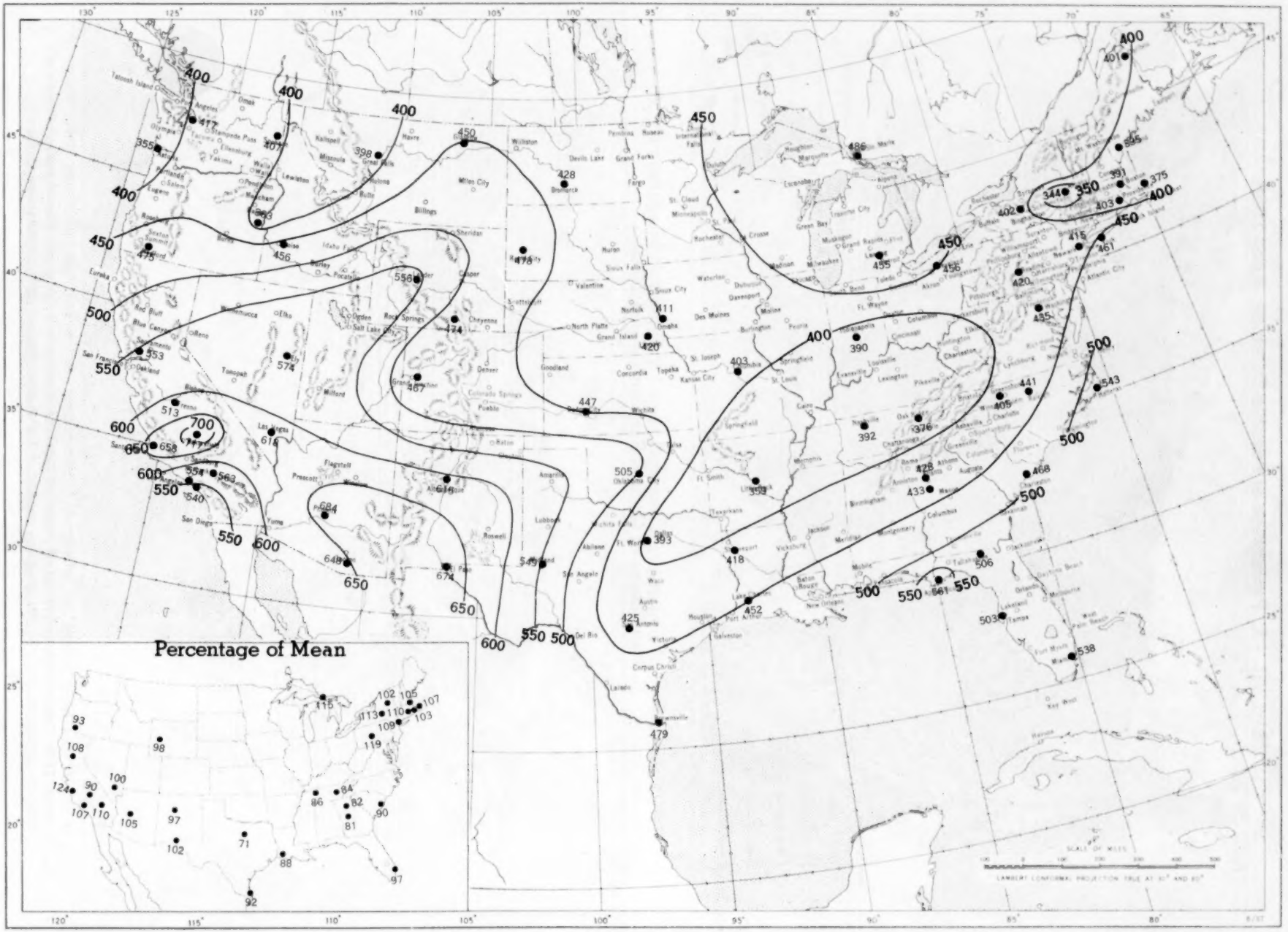

Chart shows mean daily solar radiation, direct + diffuse, received on a horizontal surface in langleys (1 langley = 1 gm. cal. cm. $^{-2}$). Basic data for isolines are shown on chart. Further estimates are obtained from supplementary data for which limits of accuracy are wider than for those data shown. The inset shows the percentage of the mean based on the period 1951-55.

Chart IX. Tracks of Centers of Anticyclones at Sea Level, April 1958.

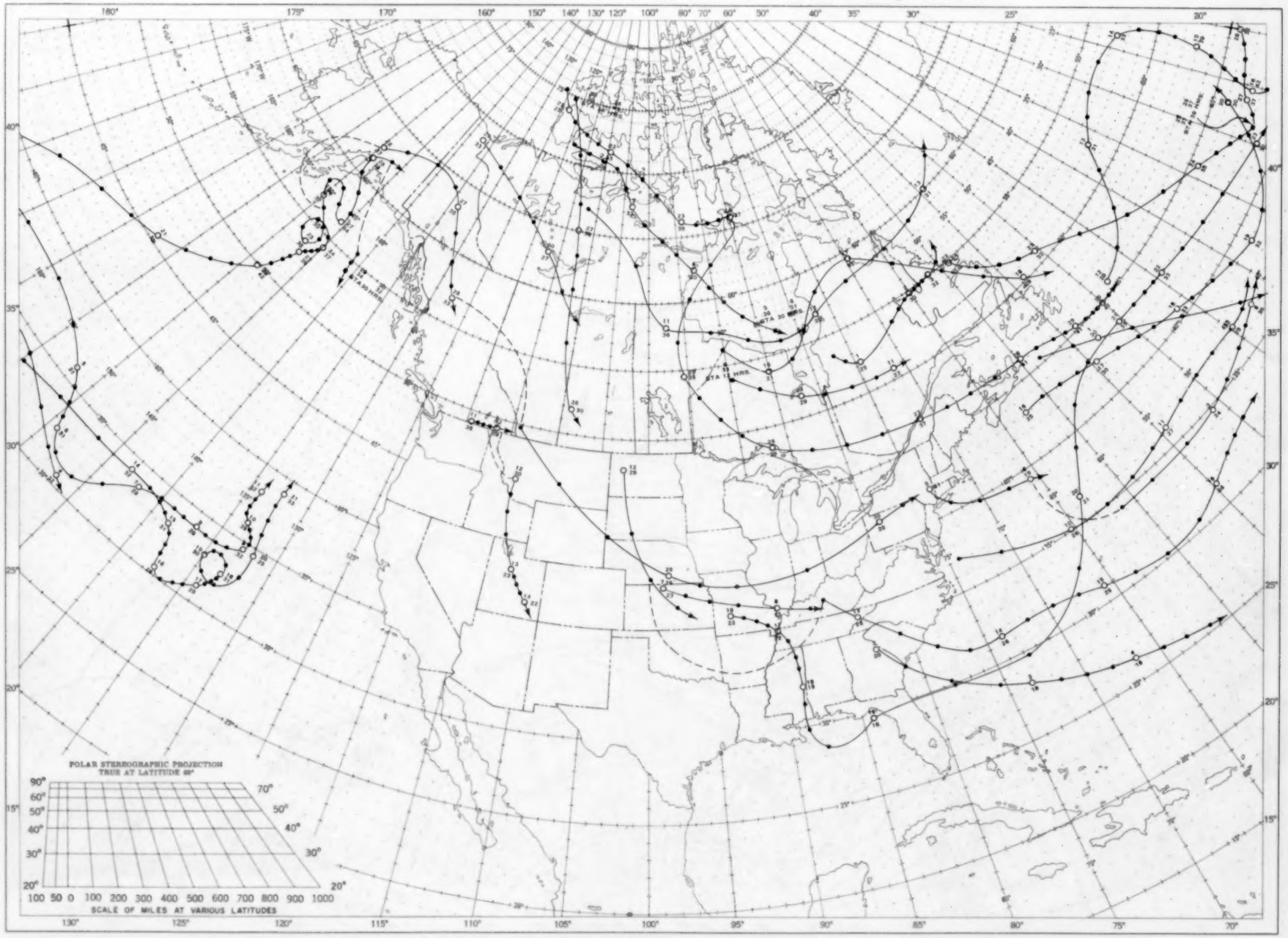
POLAR STEREOGRAPHIC PROJECTION
TRUE AT LATITUDE 60°
90° 60° 50° 40° 30° 20°
70° 50° 40° 30° 20°
100 50 0 100 200 300 400 500 600 700 800 900 1000
SCALE OF MILES AT VARIOUS LATITUDES

Circle indicates position of center at 7:00 a. m. E. S. T. Figure above circle indicates date, figure below, pressure to nearest millibar. Dots indicate intervening 6-hourly positions. Squares indicate position of stationary center for period shown. Dashed line in track indicates reformation at new position. Only those centers which could be identified for 24 hours or more are included.

Chart X. Tracks of Centers of Cyclones at Sea Level, April 1958.

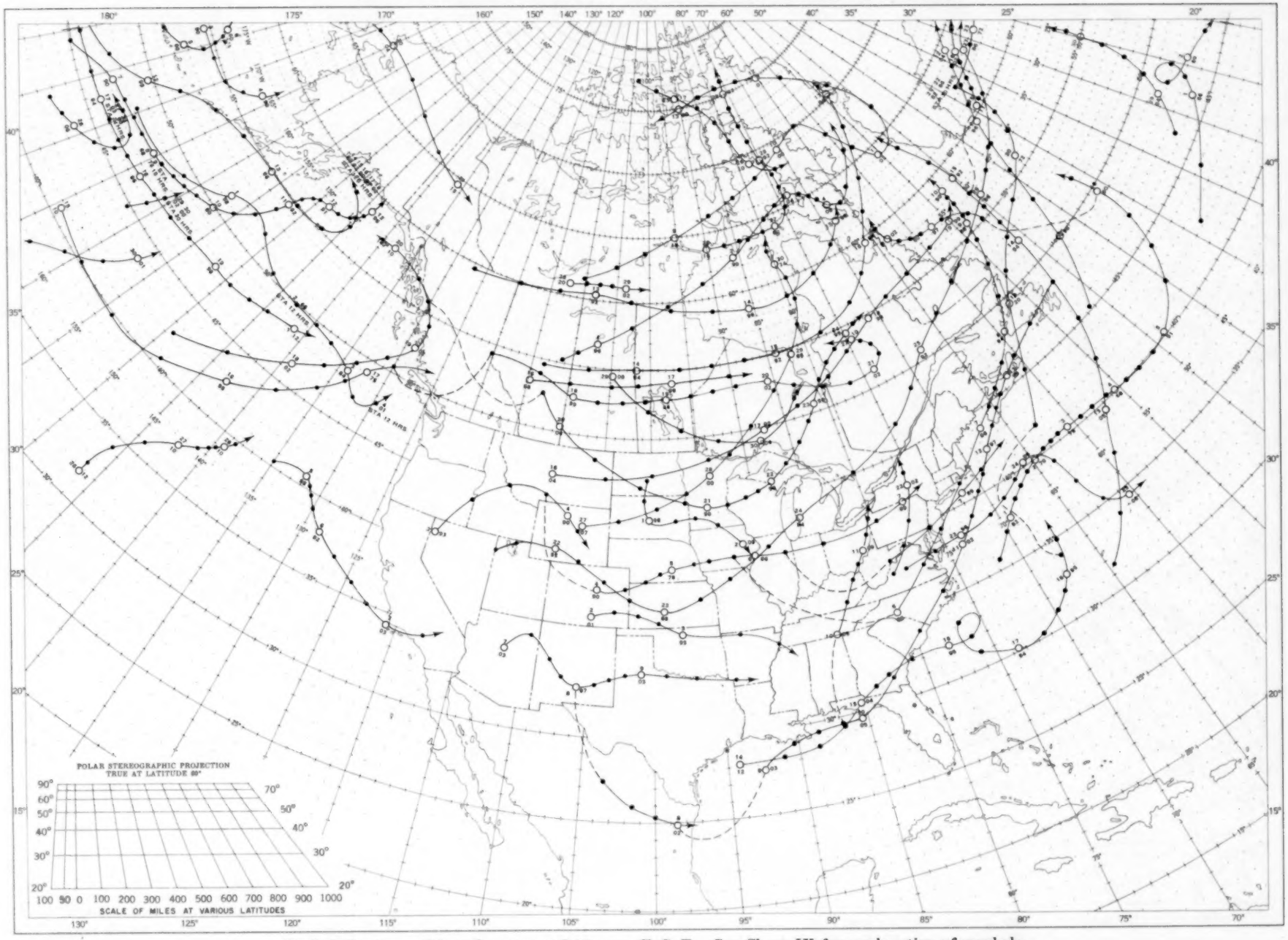

Circle indicates position of center at 7:00 a. m. E. S. T. See Chart IX for explanation of symbols.

Chart IX. Tracks of Centers of Anticyclones at Sea Level, April 1958.

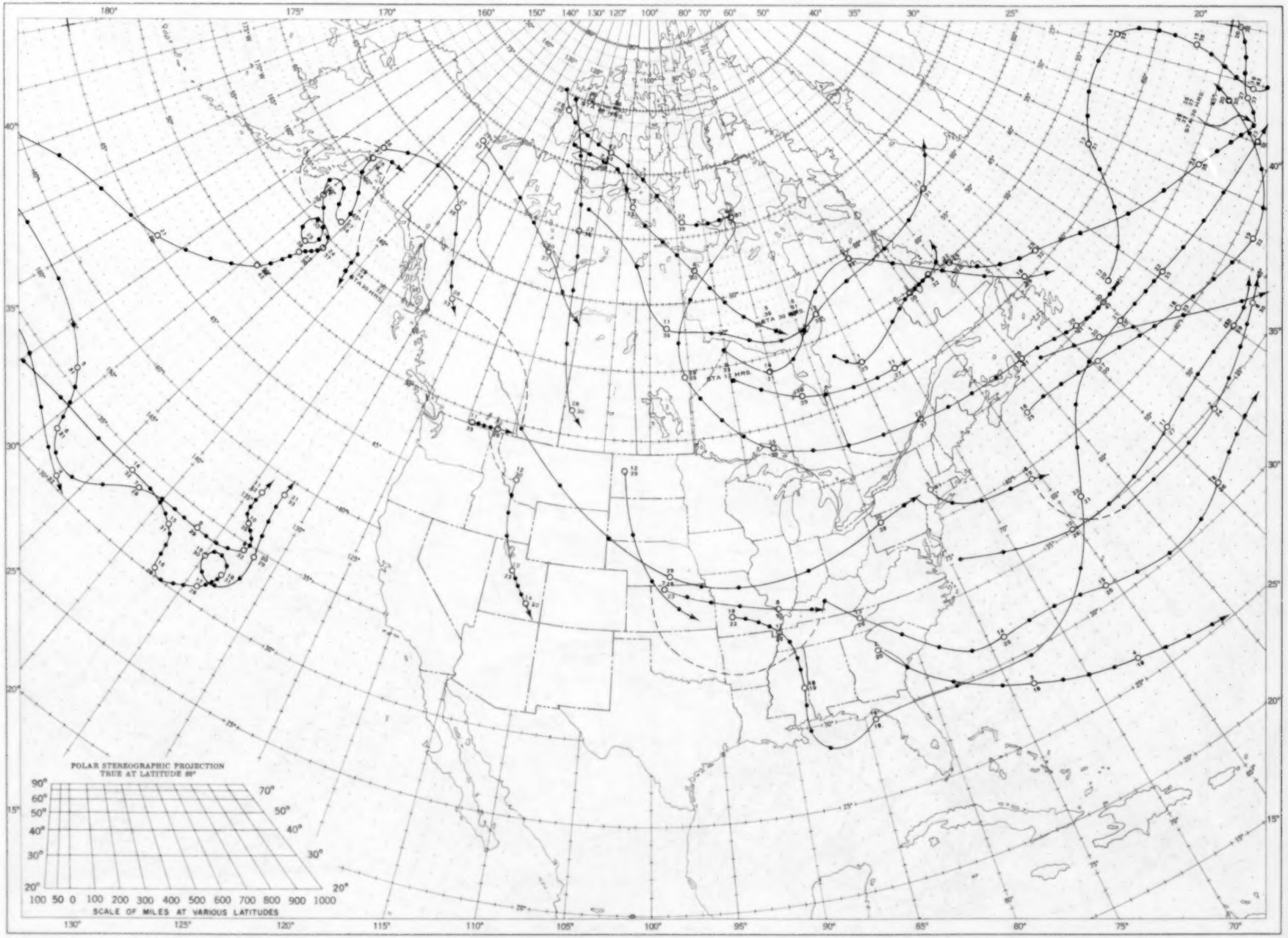
POLAR STEREOGRAPHIC PROJECTION
TRUE AT LATITUDE 60°
90° 60° 50° 40° 30° 20°
70° 50° 40° 30° 20°
100 50 0 100 200 300 400 500 600 700 800 900 1000
SCALE OF MILES AT VARIOUS LATITUDES

Circle indicates position of center at 7:00 a. m. E. S. T. Figure above circle indicates date, figure below, pressure to nearest millibar. Dots indicate intervening 6-hourly positions. Squares indicate position of stationary center for period shown. Dashed line in track indicates reformation at new position. Only those centers which could be identified for 24 hours or more are included.

Chart X. Tracks of Centers of Cyclones at Sea Level, April 1958.

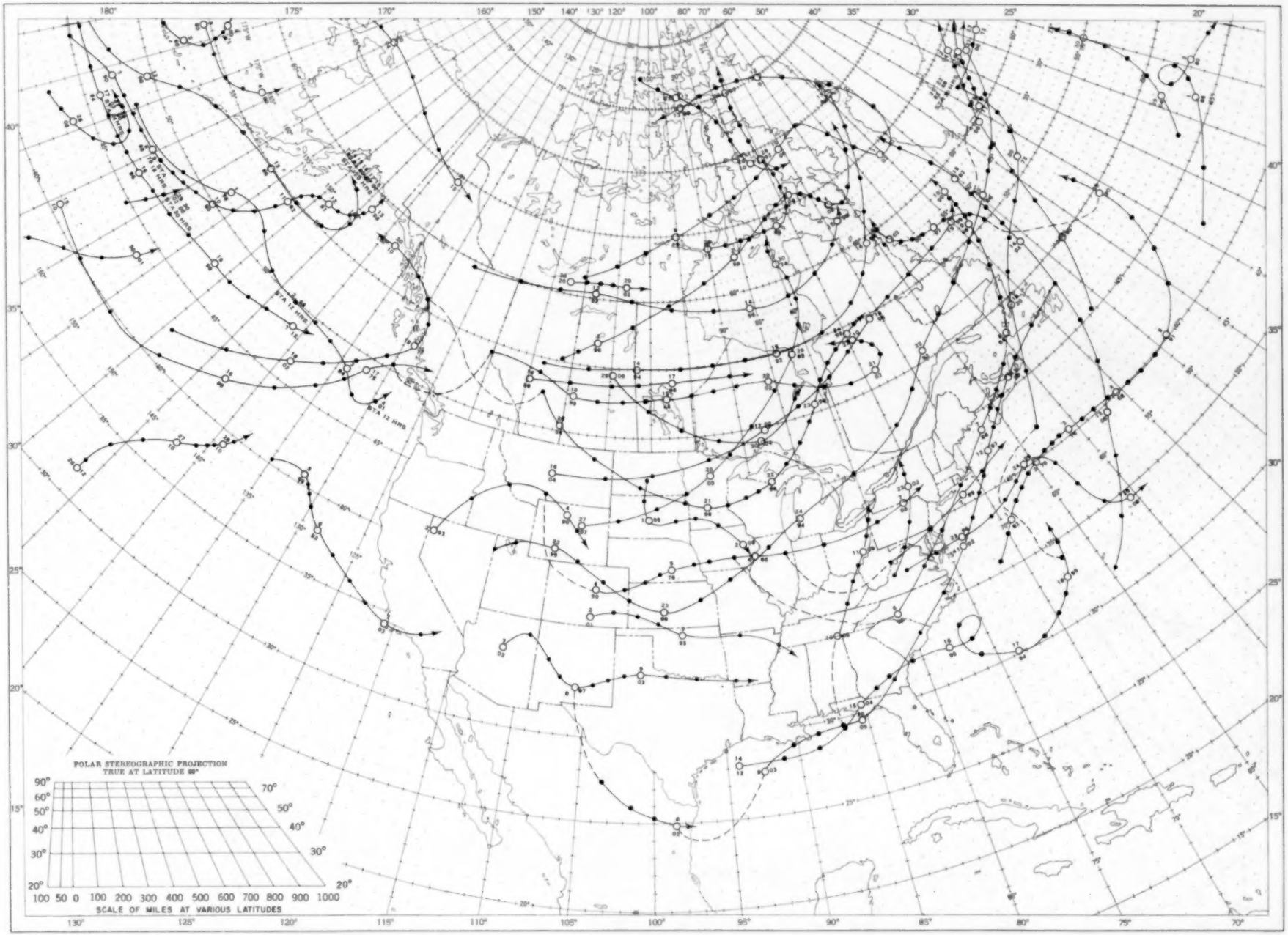
POLAR STEREOGRAPHIC PROJECTION
TRUE AT LATITUDE 60°
90° 60° 50° 40° 30° 20°
70° 50° 40° 30° 20°
100 50 0 100 200 300 400 500 600 700 800 900 1000
SCALE OF MILES AT VARIOUS LATITUDES

Circle indicates position of center at 7:00 a. m. E. S. T. See Chart IX for explanation of symbols.

Chart XI. Average Sea Level Pressure (mb.) and Surface Windroses, April 1958. Inset: Departure of Average Pressure (mb.) from Normal, April 1958.

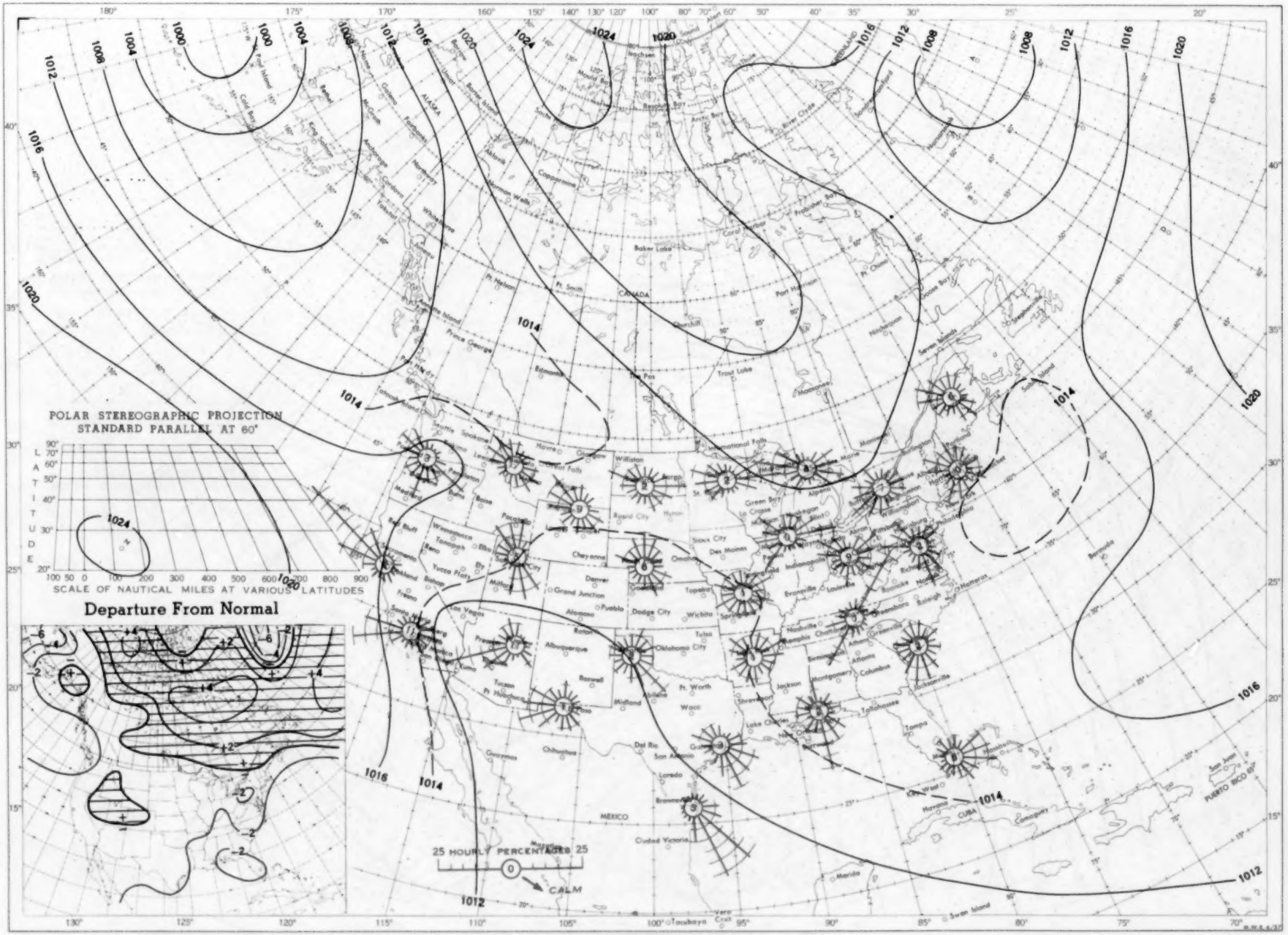

Average sea level pressures are obtained from the averages of the 7:00 a. m. and 7:00 p. m. E. S. T. readings. Windroses show percentage of time wind blew from 16 compass points or was calm during the month. Pressure normals are computed for stations having at least 10 years of record and for 10° intersections in a diamond grid based on readings from the Historical Weather Maps (1899-1939) for the 20 years of most complete data coverage prior to 1940.

Chart XII. 850-mb. Surface, 1200 GMT, April 1958. Average Height and Temperature, and Resultant Winds.

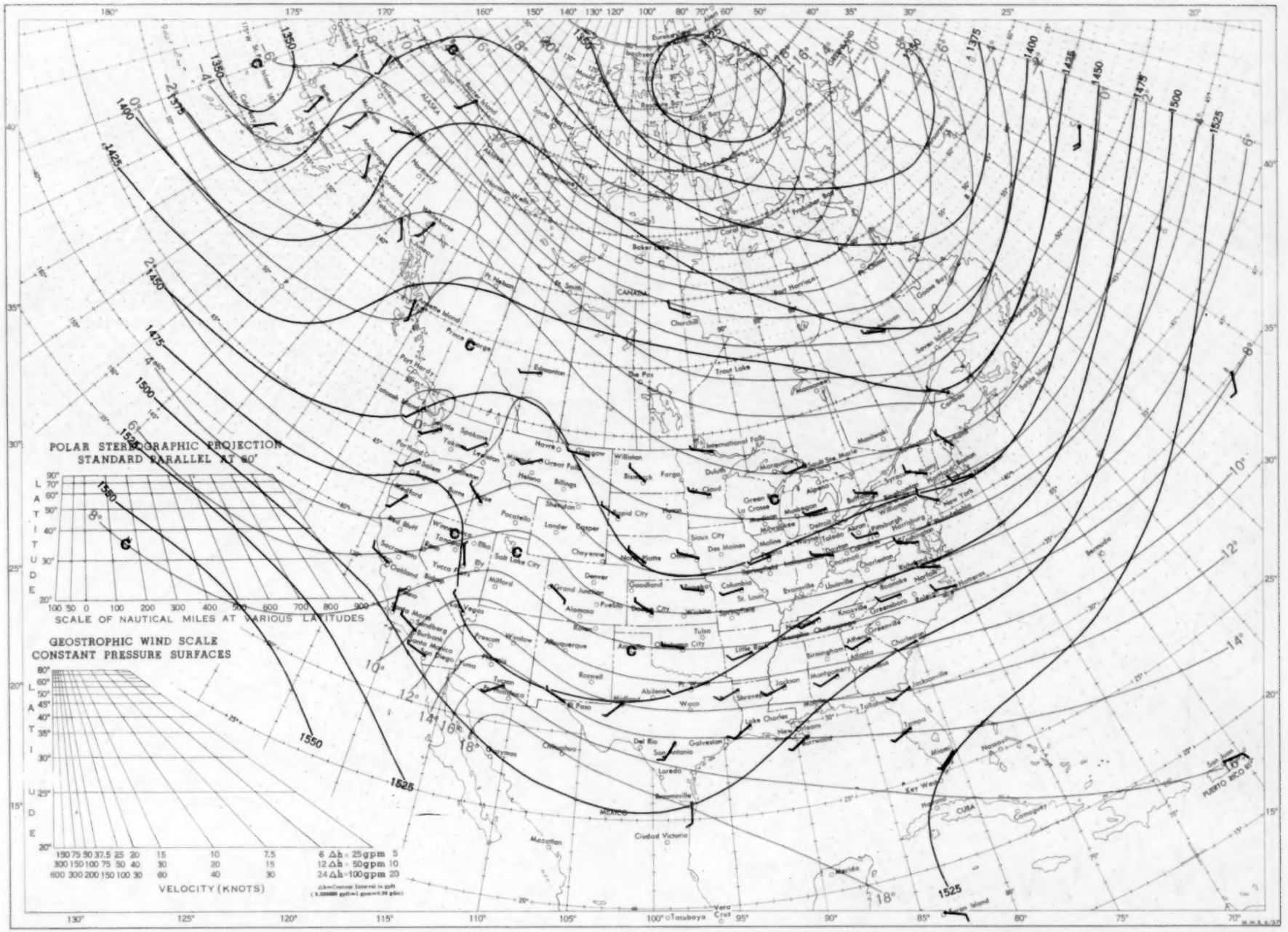
POLAR STEREOGRAPHIC PROJECTION
STANDARD PARALLEL AT 60°
SCALE OF NAUTICAL MILES AT VARIOUS LATITUDES
GEOSTROPHIC WIND SCALE
CONSTANT PRESSURE SURFACES
VELOCITY (KNOTS)
6 Δh = 25gpm 5
12 Δh = 50gpm 10
24 Δh = 100gpm 20

Height in geopotential meters (1 g.p.m. = 0.98 dynamic meters). Temperature in °C. Wind speed in knots; flag represents 50 knots, full feather 10 knots, and half feather 5 knots. All wind data are based on rawin observations.

Chart XIII. 700-mb. Surface, 1200 GMT, April 1958. Average Height and Temperature, and Resultant Winds.

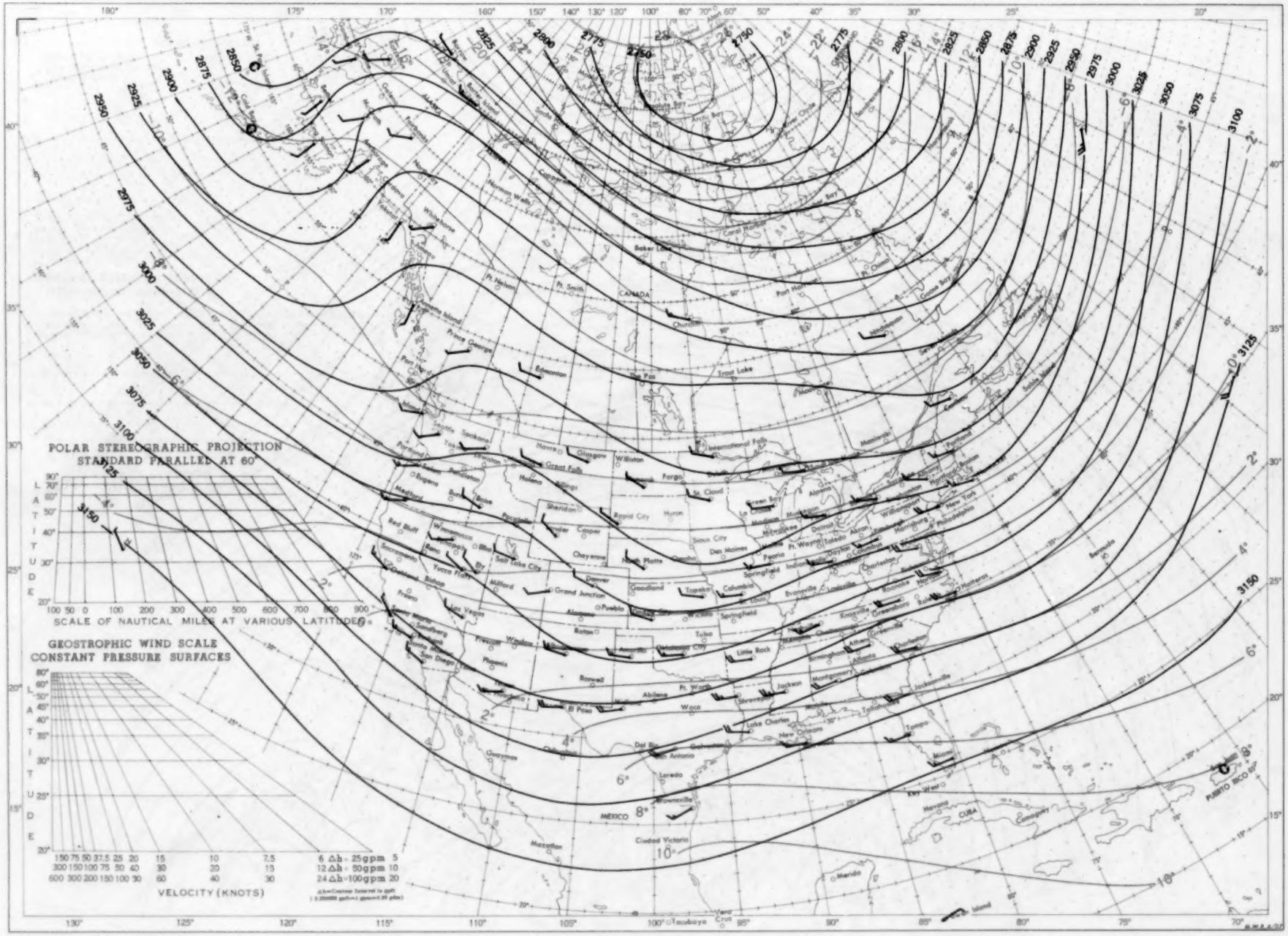

See Chart XII for explanation of map.

Chart XIV. 500-mb. Surface, 1200 GMT, April 1958. Average Height and Temperature, and Resultant Winds.

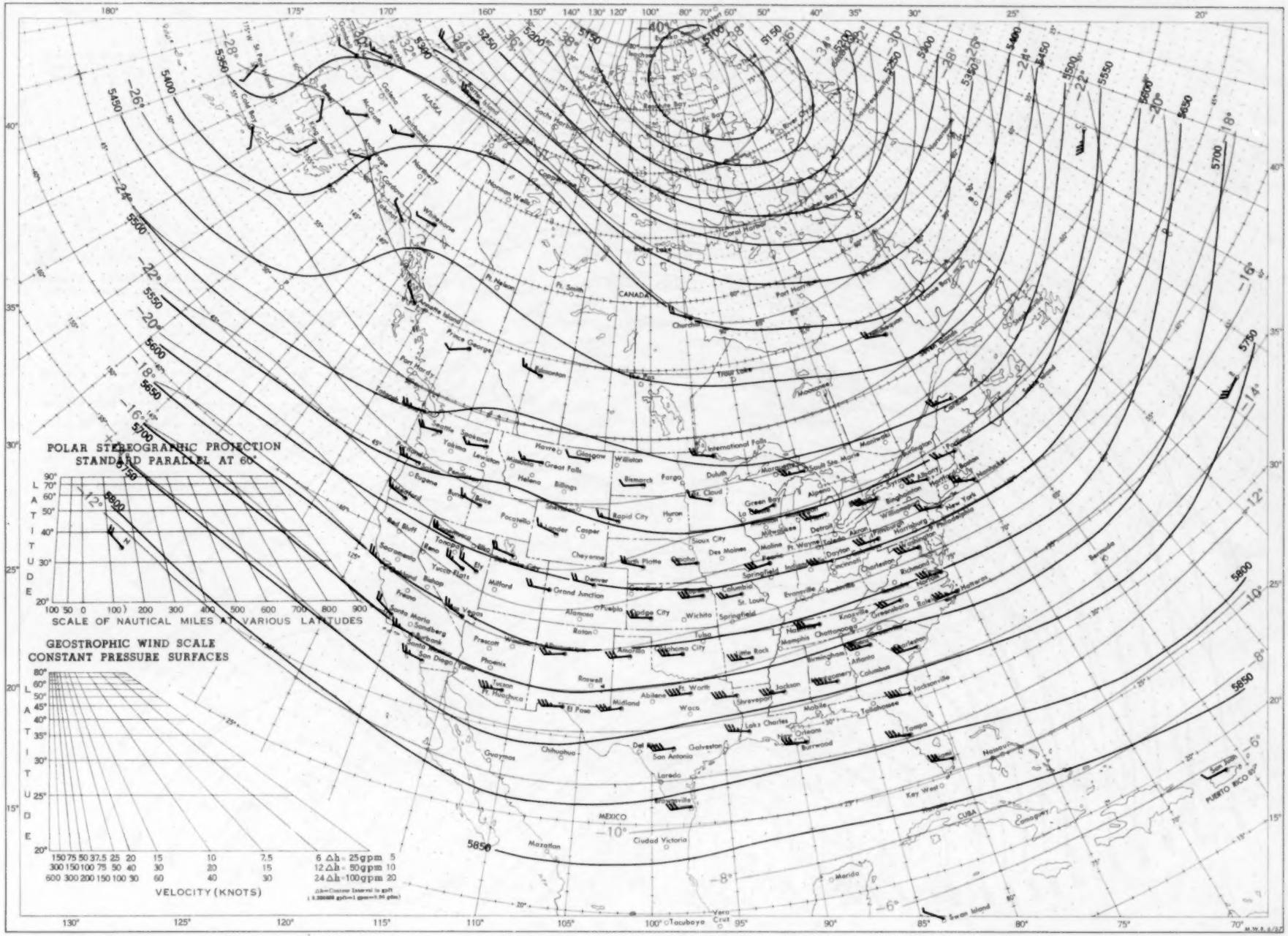

See Chart XII for explanation of map.

Chart XV. 300-mb. Surface, 1200 GMT, April 1958. Average Height and Temperature, and Resultant Winds.

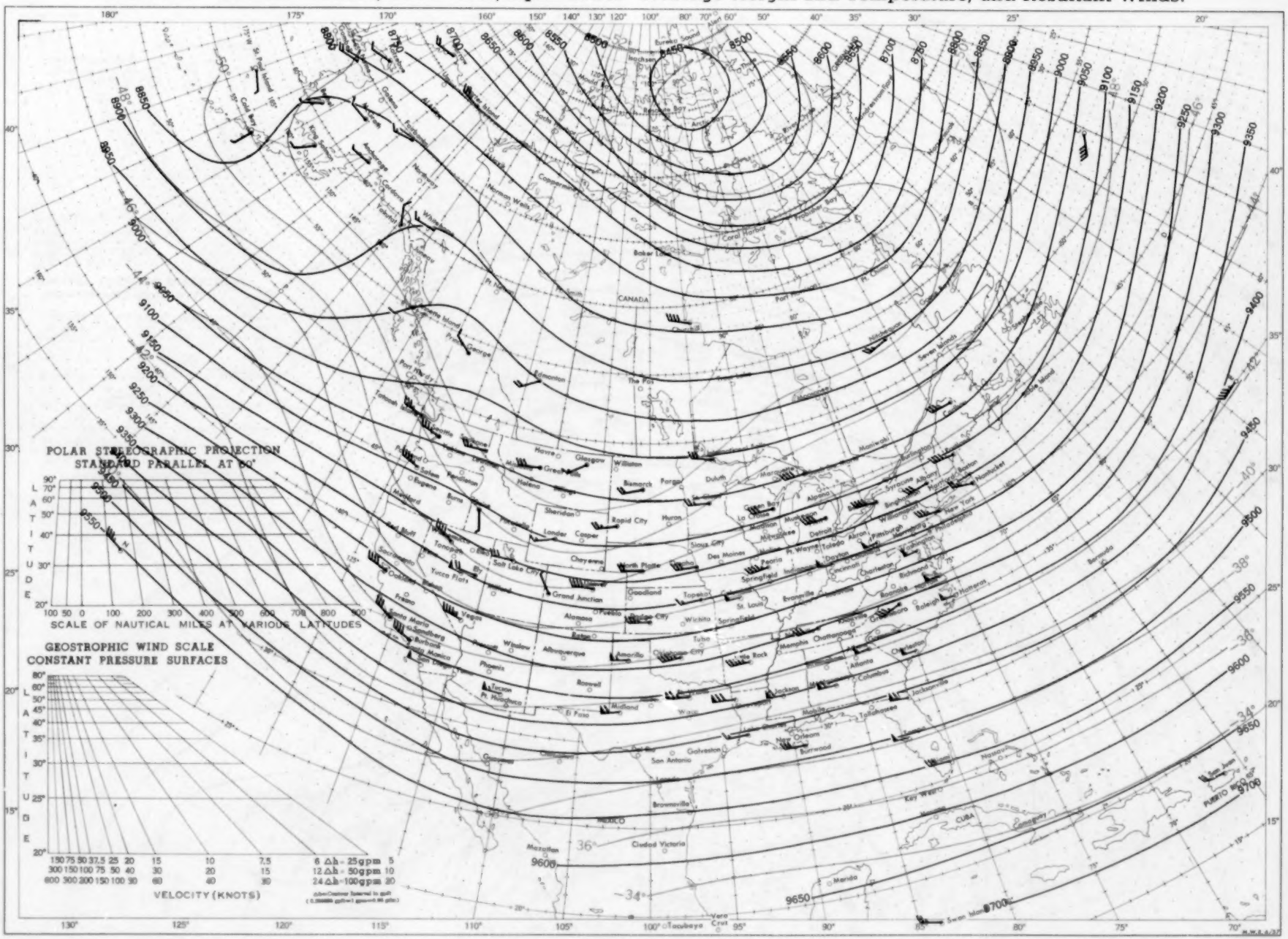

See Chart XII for explanation of map.

Chart XVI. 200-mb. Surface, 1200 GMT, April 1958. Average Height and Temperature, and Resultant Winds.

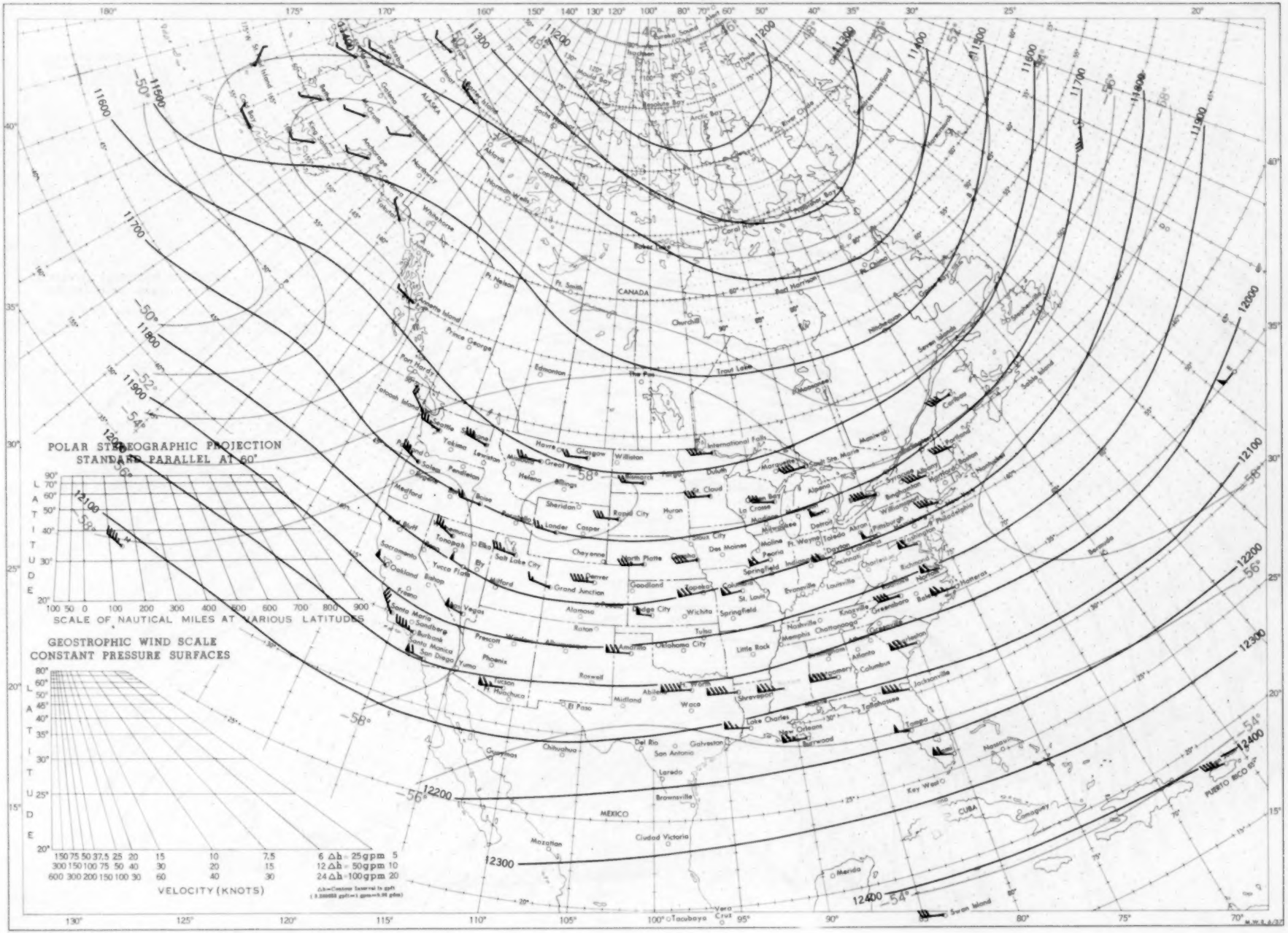

See Chart XII for explanation of map.

Chart XVII. 100-mb. Surface, 1200 GMT, April 1958. Average Height and Temperature, and Resultant Winds.

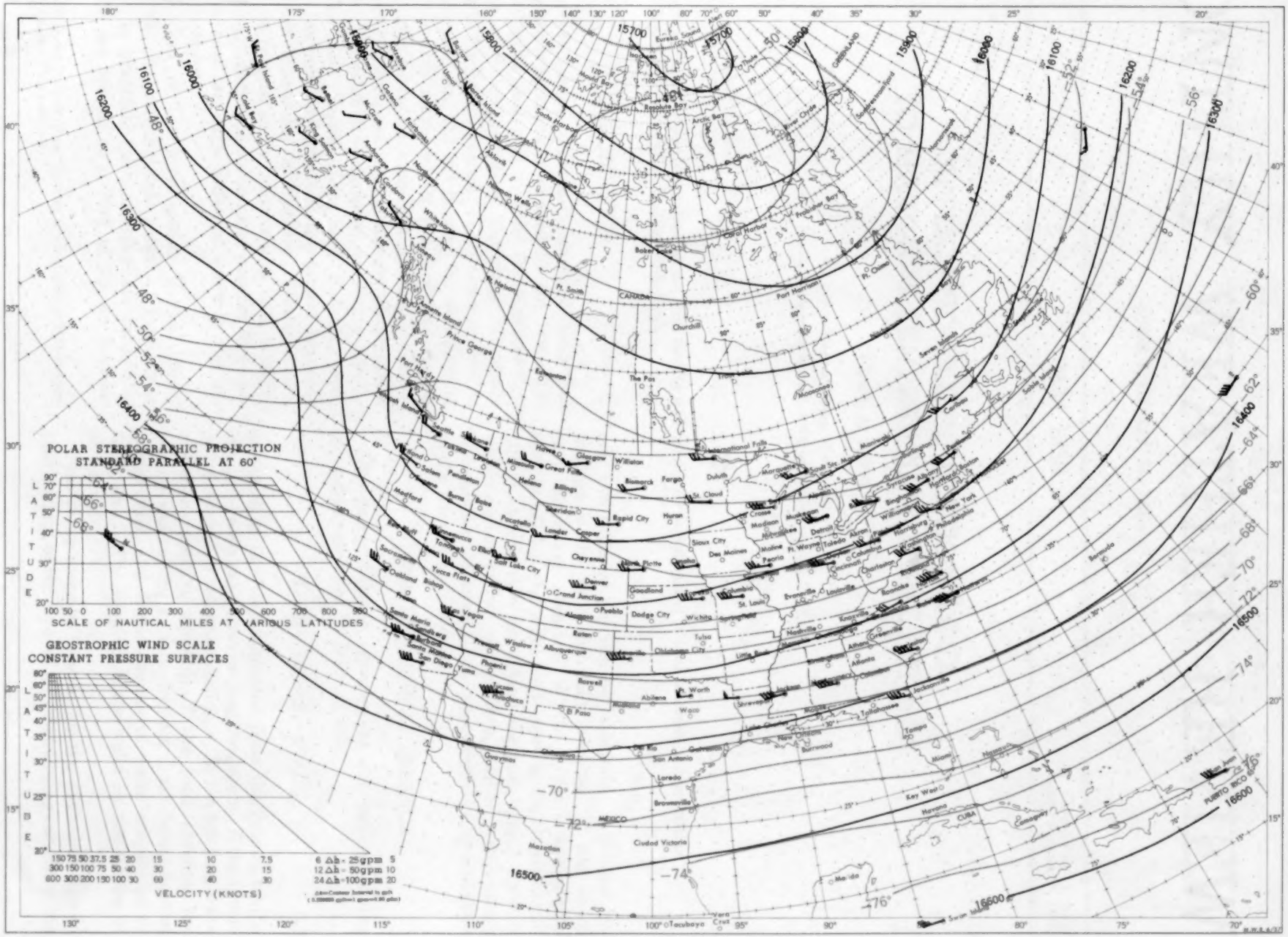

See Chart XII for explanation of map.